POWER SYSTEM TRANSMISSION LINE OUTAGE DETECTION AND IDENTIFICATION: A PHYSICS-INFORMED DATA-DRIVEN APPROACH

by

YANG XIAOZHOU

(B.Eng. (Hons.), National University of Singapore)

A THESIS SUBMITTED FOR THE DEGREE OF

DOCTOR OF PHILOSOPHY

in the

DEPARTMENT OF INDUSTRIAL SYSTEMS ENGINEERING AND MANAGEMENT

NATIONAL UNIVERSITY OF SINGAPORE

2021

Supervisor:
Associate Professor Chen Nan

Examiners:
Associate Professor Poh Kim Leng
Dr Liu Yang

Declaration

I hereby declare that this thesis is my original work and it has been written by me in its entirety. I have duly acknowledged all the sources of information which have been used in the thesis.

This thesis has also not been submitted for any degree in any university previously.

Yang Xiaozhou

Aug 2021

Acknowledgments

I would like to acknowledge the contribution of many people to the development of this thesis and my Ph.D. journey. Without them, this work would not have been possible, and I would not be the same.

I am most grateful to my Ph.D. advisor, Prof. Chen Nan, who has greatly influenced my professional and personal development over the last four years. His insistence on integrating domain knowledge and meticulous approach to contribution justification shaped my thinking of each research problem. He has provided a liberal and safe environment where I could learn continuously, form opinions, and discover insights every day. He has encouraged me on numerous occasions to think differently, dare answer a more difficult question, and step into new territories. The guidance from him has helped me become a better researcher and a better person. For that, I will be forever grateful.

I would also like to thank my collaborator, Prof. Zhai Chao. He provided much assistance and knowledge throughout the development of this thesis. In particular, his knowledge of power systems helped me tremendously during the early phase of my Ph.D. journey. I am fortunate to be among a group of motivated and supportive group mates. They are Shi Yuchen, Zhu Jun, Wang Rui, and Liang Hongde. They have always generously offered me words of encouragement and ideas from different perspectives.

I thank the Singapore-ETH Centre and Singapore's National Research Foundation for the financial support of my Ph.D. study. I also benefited significantly by working with colleagues from the Future Resilient Systems program at the SEC. They provided a comfortable and stimulating research environment for me.

Finally, I would like to thank my parents, Zhou Yonghong and Yang Zhenglu, my grandmother, Huang Bizhi, and my partner, Chen Linye, for their unwavering love and support. This thesis is dedicated to you all.

Contents

List of Figures

List of Tables

Chapter 1

Introduction

Critical infrastructures (CIs) are essential to lives, livelihoods, and the proper functioning of societies. CIs are networks of inter- or independent manufactured systems and processes that produce and distribute a continuous flow of essential goods and services [1]. Five main types of CIs are electrical power systems, gas networks, water networks, transportation networks, and telecommunication systems. They have many common characteristics. For example, they are networks with many nodes and links, span extensively in geographical scale, and have developed capabilities for near real-time monitoring [2].

The central theme of this thesis revolves around electrical power systems, in particular, novel methods for their protection. Electricity is needed in almost every aspect of modern society. It is particularly critical as other CIs are increasingly reliant on it as an input. Traditional power systems consist of three functional parts: generation, transmission, and distribution. The first part generates electrical power to meet the overall demand. Power is then delivered through loss-minimizing transmission lines to downstream areas. Finally, end consumers such as residential and office buildings receive usable power supply via distribution systems.

To ensure a continuous supply of high-quality electricity, power system operators work around the clock to keep the system running smoothly. However, this is not an easy feat. Power systems are highly complex because of the extensive geographical scale, fast dynamics, and high operational standards. A real-world power system typically spans across multiple states in the United States or cities

and countries in Europe's case. Within such a system, a plethora of dynamics are always in play. Thousands of power generators, transformers, electric lines, and other components could be interacting with each other at any moment. Three major power grids of the United States consist of 275,000 kilometers of high-voltage transmission lines and over nine million kilometers of low-voltage distribution lines; in Europe, four major grids are comprised of four million transformers and ten million kilometers of distribution lines. At the same time, the integration of distributed energy resources, smaller power sources such as batteries and renewable energy sources, introduces increasing volatility to modern power systems [3].

1.1 Motivation

Ensuring a reliable electricity supply is a challenging task. Fast and accurate abnormal event detection and identification (D&I) is necessary to contain system failures in time and minimize the impact of such events. Abnormal events in power systems create disturbances that are different from a normal operating condition. Depending on the cause and duration, such disruptions may or may not lead to acute or cascading failures. Given the complexity of the system, there are many types of disturbances that could happen [4]. Among them, power transmission line outage receives a significant amount of attention from both the research community and the industry. Power line outages can frequently occur due to adverse weather conditions, component wear and tear, vandalism, or other reasons. The increased research activities in power line outage D&I can be attributed to two reasons. One is the urgent need to improve system operators' real-time situational awareness. On the other hand, the emergence of phasor measurement unit (PMU) technology makes numerous real-time monitoring and control applications possible.

1.1.1 Real-time Situational Awareness

Real-time situational awareness about the system, e.g., changes in operating conditions and external system contingencies, enables system operators to identify

and respond to abnormal events promptly [5]. From a contingency point of view, delayed information regarding system faults might allow localized faults to cascade into large-scale blackouts [6]. For example, one of the common contributing factors of the 2003 Northeast and 2011 Southwest blackout was that the operators were not alerted in time about external outage contingencies, e.g., a critical transmission line tripping [7]. One of the challenges about real-time monitoring is that line outage dynamics can manifest in a time scale of milliseconds [8]. The traditional supervisory control and data acquisition (SCADA) system cannot capture these dynamics since it reports at a rate of one measurement every several seconds [9].

1.1.2 Emergence of Phasor Technology

Synchrophasors are time-synchronized numbers representing both the magnitude and phase angle of the sine waves found in electricity, e.g., voltage phasor or current phasor. PMUs are devices capable of recording such synchrophasor samples when installed across the power grid with high precision, high fidelity, and GPS time stamps [6]. An industry-grade PMU can measure voltage phasors on the bus with a total vector error of less than 1% and report 30 to 60 samples per second. The rising prevalence of PMUs makes numerous real-time monitoring, protection, and control applications possible since they can measure system states at a much higher frequency than traditional SCADA systems. As a result, many consider PMU technology as the key to grid modernization. This is also in line with the smart grid vision that calls for better observability, controllability, and operational flexibility [10].

Consequently, there is a large body of research works on PMU and their application in power systems. PMU technologies are actively studied for power oscillation monitoring, abnormal event detection, and dynamic state and parameter estimation. According to the excellent review paper [6], in their nine categories of PMU-related power system research, there are about 500 papers published in Institute of Electrical and Electronics Engineers (IEEE) and Institution of Engineering and Technology (IET) journals over the 30 years before 2014. The number is seen growing at an exponential rate recently. Readers can refer to [6]

for a comprehensive review of PMU applications in power systems.

1.2 Challenges

However, several challenges need to be addressed before realizing the full potential of PMU technology for line outage D&I. One is the real-time computational challenge. As mentioned, outage D&I is most wanted for enhancing operators' real-time awareness. Consequently, a common goal for any D&I scheme is to keep computational cost low enough for real-time processing and extracted information useful enough for analytics. In particular, PMU's high sampling rate means that data processing has to be fast. Furthermore, a realistic power system usually contains hundreds of lines and substations. Therefore, the proposed D&I scheme must be efficient to handle real-time processing of fast streaming data and scalable to large dimensions.

Also, a specific challenge for outage line identification is the inherent combinatorial nature of potential outage locations. An outage can happen at one or multiple transmission lines; the total number is in general not known a priori. For example, for a system with L transmission lines, the solution space for identification consists of 2^L location combinations. An exhaustive search is only possible for small systems. The proposed scheme has to overcome this challenge for any realistic power system implementation.

Another challenge for line outage D&I is that sensor deployment is limited in number. PMU is the foundation for many D&I schemes. However, PMUs are only progressively adopted by energy companies. Installing PMUs also means the whole data communication, processing, and storage infrastructure behind the technology, which is expensive. Separately, there have been many research works suggesting a full PMU deployment is not needed for many applications [11]. Therefore, when designing a D&I scheme, one must consider a limited PMU deployment in the system, i.e., some parts are not observable.

Therefore, a limited PMU deployment, in terms of the number and location, impacts the outage detection scheme's effectiveness. In particular, line outages that happen far away from buses with PMUs would register mild signals in the

data, leading to a longer detection delay or missed detection [12]. It remains a challenge to design a detection scheme robust to the location of the PMUs and outages.

On the other hand, a limited coverage also leads to increased identification difficulty. Pre- and post-outage states at different parts of the system are needed to discriminate outages of one location from another. Having unobserved buses might lead to the signatures of some outages being missed out. This loss of information might lead to some outages of different locations being indistinguishable from one another [13–15]. Hence, an effective outage identification scheme must overcome the ambiguity issue caused by a limited PMU deployment.

1.3 Thesis Organization

This thesis is devoted to developing novel power system line outage D&I methods by addressing existing challenges and research gaps. In particular, the rest of this thesis is organized as follows.

Chapter 2 surveys the state of the art in the domain of sensor data-driven real-time power system line outage detection and identification. Existing research works are reviewed and gaps are identified in two directions: outage detection, that concerns with the problem of detecting an outage as fast as possible, and outage identification, that concerns with the problem of accurately locating the actual tripped line(s).

Chapter 3 gives background information on how power systems as complex networks could be modeled and simulated. This information will be repeatedly referenced in the rest of this thesis. Specifically, the section introduces the AC power flow model that describes system algebraic states and relevant power system physical quantities. Then, the dynamic simulation procedure of power systems and the open-source software package used to do it are introduced. These describe how line outage data are simulated and obtained using standard IEEE test power systems.

Chapter 4 describes a novel real-time dynamic outage detection scheme based on the AC power flow model and statistical change detection theory, using voltage

phase angle data collected from a limited number of PMUs. The proposed method can capture system dynamics since it retains the time-variant and nonlinear nature of the power system. The method is computationally efficient and scales to large and realistic networks. Extensive simulation studies on IEEE 39-bus and 2383-bus systems demonstrated the effectiveness of the proposed method.

In Chapter 5, a unified detection framework that utilizes both generator dynamic states and nodal voltage information is proposed. The inclusion of generator dynamics makes detection faster and more robust to a priori unknown outage locations. The superior performance is demonstrated using the IEEE 39-bus test system. In particular, the scheme achieves an over 80% detection rate for 80% of the lines, and most outages are detected within 0.2 seconds. The new approach could be implemented to improve system operators' real-time situational awareness by detecting outages faster and providing a breakdown of outage signals for diagnostic purposes.

Chapter 6 describes a new framework of multiple-line outage identification using partial nodal voltage measurements. Using the AC power flow model, voltage phase angle signatures of outages are extracted and used to group lines into minimal diagnosable clusters. Identification is then formulated into an underdetermined sparse regression problem solved by lasso. Tested on IEEE 39-bus system with 25% and 50% PMU coverage, the proposed identification method is 93% and 80% accurate for single- and double-line outages. This study suggests that the AC power flow is better at capturing outage patterns, and sacrificing a moderate amount of precision could yield substantial improvement in identification accuracy. These findings could contribute to developing future control schemes that help power systems resist and recover from outage disruptions in real-time.

Chapter 7 concludes this thesis and discusses future research directions.

Chapter 2

Literature Review

The state-of-the-art research works in power system real-time line outage detection and identification using PMU data are reviewed in this section.

2.1 Outage Detection

Research that deals with detecting a line outage as fast as possible after it happened can be summarized from two aspects: the approach and the type of system dynamics considered. Outage detection research by their approach is first reviewed. Then, from the perspective of system dynamics, current work is examined for further research gaps. Finally, research work that focuses on outage line identification is reviewed.

2.1.1 By Approach

Most works of line outage detection using PMU data can be classified by the two approaches taken. One is a data-driven approach where no or very little physical knowledge about the system is required [16–18]. On the other hand, many take a hybrid approach where first-principle models are incorporated with data-driven methods [19–27].

2.1.1.1 Data-driven Approach

Authors in [16] focus on analyzing the underlying dimensionality of the raw PMU data obtained. Using projection by principal component analysis (PCA), they then build a lower-dimensional representation of observable bus states from

available PMU data under an outage-free condition [16]. An event indicator is constructed based on the reconstruction error between the representation and the actual measurements. Similarly, using a moving-window PCA on normal condition system-wide frequency data, Rafferty *et al.* design a Hotelling's T^2 control chart to detect and classify multiple types of abnormal frequency events [17]. While many works focus on the detection of a single event, this work considers detecting cascading failures where a series of disruptive events happen in a short time window. They investigated the ability of the proposed method to identify both simulated and real cascading events such as generation dip followed by a loss of load, multiple islanding from line tripping events, and short circuit event followed by an islanding event.

Hosur and Duan proposed constructing an observation matrix based on the frequency difference between buses under a normal condition by modeling the network as a linear time-invariant (LTI) system [18]. An alarm is raised whenever the underlying null space of the observation matrix changes due to different types of events, such as topology change or forced oscillation. The method is not limited to line outages but requires a window of samples to reflect a null space change.

Without a model for the power system based on physical laws, these data-driven schemes are flexible enough to detect both outages and other abnormal events. However, they often face difficulties when the events have a low signal-to-noise ratio, e.g., outages with mild phase angle disturbances. On the other hand, the hybrid approach augments PMU data with physical system information to improve the detection performance under such conditions.

2.1.1.2 Hybrid Approach

One group of work that takes a hybrid approach to outage detection makes use of the Ohm's law, which relates voltage, current, and line admittance. Jamei *et al.* show that the correlation matrix between voltage and current measurements of a pair of buses has rank one under normal conditions [19, 20]. A cumulative sum (CUSUM) control chart is then set up to monitor the approximation error based on the rank-1 assumption. An outage alarm is raised once the error deviates significantly from zero. The authors devised both a local and central rule for

abnormal event detection. The formulation also considers the unique condition of unbalanced phases in a distribution grid. However, currents and voltages at both ends of the line are assumed to be known. Also, the focus of the detection scheme is on deriving the signal without a systematic approach to designing a monitoring scheme that balances detection speed and false alarm rate. Also based on Ohm's law, Ardakanian *et al.* focus on monitoring the discrepancy between measured and computed quasi-steady-state current phasors using the recovered admittance matrix [21, 22]. The post-outage system admittance matrix is recovered from PMU data by solving an inverse power flow and system identification problem. Since the method is based on the admittance matrix, it has the potential to be extended to detecting other disruptive events which induce a change in the matrix.

A separate line of work makes use of the direct current (DC) power flow model, which describes the relationship between substation power injections, voltage, and line admittance [26, 28]. In general, they focus on monitoring the pre- and post-outage steady-state voltage phase angle difference. Outage detection is then formulated as a quickest change detection problem. The detection is done by sequential likelihood ratio testing. This line of work does not require all buses to be monitored by a PMU. However, the steady-state approximation would not be sufficient at describing the actual system dynamic behavior following an outage.

Therefore, existing methods do not consider the transient dynamics following an outage or require a full PMU deployment. There is minimal work on detection schemes that consider unobserved buses and exploit the system's transient response to an outage for faster detection.

2.1.2 By System Dynamics

In addition to the usage of physical system models, most state-of-the-art works on outage detection can also be categorized by the type of power system transient dynamics, the evolution of system states following a disturbance, considered in their problem formulation. A review from this perspective allows new research direction to be discovered.

2.1.2.1 Steady State

The first group models power systems based on the quasi-steady-state assumption where no transient dynamics are considered [21–24, 26, 29]. Their detection methods assume that the system is in a quasi-steady-state both before and after the outage. Under this assumption, the DC power flow model, which simplifies many details of the system, is usually used as the starting point for detection scheme design. However, transient dynamics can often last up to several seconds and are non-negligible in real-time operations [30]. Therefore, this approach may not be adequate at describing the actual system behavior.

2.1.2.2 Approximate Dynamics

The second group relaxes the quasi-steady-state assumption and attempts to account for the post-outage transient dynamics. That means the voltage and current profiles of buses and transmission lines are assumed to be time-variant rather than static, especially after an outage.

Building on the sequential likelihood ratio testing approach in [26], Rovatsos *et al.* modeled the dynamic evolution of post-outage voltage phase angles using a series of time-dependent participation factor matrices. The matrices quantify the impact of an outage on system bus voltage phase angles based on topology and current operating states [27]. However, it is not clear how each of the matrices could be obtained given a new system design and further investigation is needed. Similarly, using voltage angles, a generalized likelihood ratio-based detection scheme is developed using the AC power flow model in Chapter 4 of this thesis.

Separately, monitoring is also done on low-dimensional subspaces derived from PMU measurements that capture post-outage transient dynamics. Methods such as principal component analysis (PCA) [16], moving-window PCA [17], and hidden Markov model (HMM) [31] are used. Jamei *et al.* proposed to monitor the correlation matrix obtained from adjacent bus voltage and current phasors [20]; Hosur and Duan proposed to monitor that of the observation matrix obtained during outage-free operation [18].

Overall, these methods can capture post-outage system dynamics in a more realistic way than those assuming quasi-steady-state operations. However, all of

them rely on system algebraic variables, e.g., bus voltage and current phasors to model the dynamics. System transient dynamics after an outage come from power generators [30]. Therefore, power generator state variables can better characterize the system's transient response to the power imbalance created by the outage.

2.1.2.3 Generator Dynamics

Based on the generator dynamics insight, the third group models the power system as a dynamic system, utilizing both the measurable algebraic variables and hidden generator state variables. The hope is that the addition of generator information could help better identify line outages. Using the swing equation, a second-order differential equation describing the dynamics of generators, Pan *et al.* formulated outage diagnosis as a sparse recovery problem solved by an optimization algorithm [32]. Similarly, a visual observer network is constructed using the swing equation to monitor line admittance changes by a parameter identification method [33]. However, both of these works focus on the outage diagnosis problem, i.e., outage line identification and post-outage parameter estimation. However, a systematic detection scheme is the prerequisite for such tasks and needs to be developed.

Therefore, there is limited work on systematic line outage detection considering generator dynamics in a partially observed network. No work has been done to integrate generator information and power flow algebraic variable information for faster and more reliable outage detection.

2.2 Outage Identification

Early detection of line outage may not lead to better system protection if the location of the outage line(s) are not known. Research on outage lines identification has also thrived in the past twenty years, mainly taking three directions. Research work that focuses on identifying outage lines by estimating post-outage line parameters is reviewed first. Then, those with a machine learning approach and expected phase angle change approach are reviewed.

2.2.1 Parameter Recovery Approach

Line outage identification, in general, can be formulated as a parameter change identification problem. An outage of line ℓ corresponds to the change when the line admittance of ℓ drops to zero. When post-outage system parameters are estimated, a comparison with pre-outage baseline information could reveal outage locations. Some attempted to solve this problem by recovering changed line parameters. Yu *et al.* use the power flow equations to formulate line parameters as unknown regression coefficients and recover them via the total least squares method in [34] and considering changing baseline conditions [35]. Another approach focuses on the system admittance matrix, which depends on line-bus connection information, and recovers the matrix elements via matrix decomposition and adaptive lasso [22, 28].

These methods can both locate multiple line outages and recover post-outage system parameters. However, they either require a full PMU deployment or smart meter measurements, e.g., power injection and voltage measurements for the power flow approach, current and voltage measurements for the admittance matrix approach at all buses.

2.2.2 Machine Learning Approach

However, it is more realistic to assume only part of the system is observable by PMUs or smart meters, as mentioned in the challenge section. Under this assumption, researchers mainly seek to solve line outage identification problems, i.e., locate outage lines. Two main approaches are taken. The first, machine learning-based approach, is reviewed here. This line of work leverages easily accessible simulated power system outage data, extracts valuable information from them, and trains an outage classifier in a supervised learning setting. The classifier then identifies the most likely outage locations when given a new set of system data. Classical supervised learning techniques such as multinomial logistic regression classifiers are used [36, 37]. Recently, convolutional and Bayesian neural networks, a family of versatile machine learning techniques, are proposed to identify tripped lines [38, 39].

The machine learning-based approach exploits the ability of these algorithms to learn an excellent representation of line outages. They are powerful at locating multiple line outages with limited PMUs. However, their performance depends on the avaibility of generalizable and usually massive training data.

2.2.3 Expected Angle Change Approach

The second approach that does not demand a full PMU deployment on the power system is the expected voltage phase angle change formulation. Different from the machine learning approach, this line of work does not depend on training data. Instead, well-known physical laws governing power systems are utilized to construct a "dictionary" of how voltage phase angles might change following any outage. That knowledge is then used to decide where outages might have happened after collecting post-outage system data. This dictionary of patterns of angle change is usually based on either the DC power flow model [13, 23, 24, 40–42] or the AC model [14]. Outage line identification is then formulated into an unknown sparse vector recovery problem or a pattern-matching problem. For example, the outage status of all lines is formulated as an unknown vector recovered by optimization methods such as orthogonal matching pursuit, mixed-integer programming, cross-entropy optimization, and matrix decomposition [13, 40–42]. Also, Tate and Overbye and Enriquez *et al.* used the correlation between measurement data and expected phase angle data to identify the most likely outage locations [14, 23].

However, the usage of the DC power flow model potentially creates system representations with fidelity inadequate for accurate single- and multiple-line outage identification. All but Enriquez *et al.* consider the AC power flow model. However, their approach requires both voltage and current information. Overall, despite demonstrated effectiveness by the above works, the identification performance degrades significantly when a limited number of PMUs are available or when multiple-line outages are considered.

Therefore, given an outage detection timestamp, multiple-line outage identification problem remains difficult when (1) massive generalizable training data

is not available or feasible, (2) only a portion of the system buses are equipped with PMUs, (3) and only bus voltage phasor information is used.

Chapter 3

Power System Background

This chapter provides brief background information on power system modeling and simulation. In particular, relevant physical quantities and physical laws governing power systems are introduced in Section 3.1. Power system simulation and PMU data collection are presented in Section 3.2.

3.1 Power System Model

Sinusoidal physical quantities in power systems at constant frequency are phasors characterized by their maximum value and phase angle. For example, voltage phasor can be represented by

$$v(t) = \mathrm{V}_{\max} e^{j\theta}\,, \tag{3.1}$$

where $\mathrm{V}_{\max}$ is the maximum value and θ is voltage phase angle. The effective value, V, is

$$\mathrm{V} = \frac{\mathrm{V}_{\max}}{\sqrt{2}}\,, \tag{3.2}$$

and voltage phasor can also be written as

$$V = \mathrm{V}e^{j\theta} = \mathrm{V}\angle\theta = \mathrm{V}\cos\theta + j\mathrm{V}\sin\theta\,, \tag{3.3}$$

in the so-called exponential, polar, and rectangular form. The same can be written for current phasor I. The complex power in power systems can be obtained by multiplying the voltage and current phasor:

$$S = VI^* \tag{3.4}$$

$$= \mathrm{P} + j\mathrm{Q}\,, \tag{3.5}$$

where I^* is the complex conjugate of I. P is real (active) power and Q is reactive power.

A power system can be modeled as a network with N buses

$$\mathcal{N} = \{1, \ldots, N\},$$

connected by L transmission lines

$$\mathcal{L} = \{1, \ldots, L\}.$$

An example power system is illustrated in Figure 3.1. This is a well-known IEEE standard test system representing the power system of New England area of the United States. This system has 39 buses connected by 46 transmission lines. The flow of real and reactive power in the network can be characterized by a set of non-linear algebraic equations called the AC power flow model. This set of equations describes the relationship between net active power injection (P), net reactive power injection (Q), voltage magnitude (V), and voltage phase angle (θ) governed by Kirchhoff's circuit laws. They can be written as:

$$\mathrm{P}_m = \mathrm{V}_m \sum_{n=1}^{N} \mathrm{V}_n \mathrm{Y}_{mn} \cos(\theta_m - \theta_n - \alpha_{mn}), \tag{3.6a}$$

$$\mathrm{Q}_m = \mathrm{V}_m \sum_{n=1}^{N} \mathrm{V}_n \mathrm{Y}_{mn} \sin(\theta_m - \theta_n - \alpha_{mn}), \tag{3.6b}$$

for bus $m \in \mathcal{N}$ [30]. Y_{mn} is the magnitude of the $(m,n)_{th}$ element of the bus admittance matrix $\boldsymbol{Y}_{bus}$ when the complex admittance is written in the exponential form, i.e.,

$$\mathrm{Y}_{mn} e^{j\alpha_{mn}} = G_{mn} + jB_{mn}, \tag{3.7}$$

where G_{mn} and B_{mn} are the conductance and susceptance of line ℓ connecting bus m and bus n.

Elements of the bus admittance matrix corresponding to a baseline condition are usually known and this condition is also assumed for the rest of this thesis. For a large system, $\boldsymbol{Y}_{bus}$ is usually a sparse matrix since a single bus usually has a few incident buses, i.e., $\mathrm{Y}_{mn} = 0$ if bus m and n are not connected. Therefore, the topology of a power system is embedded in the admittance matrix, and in

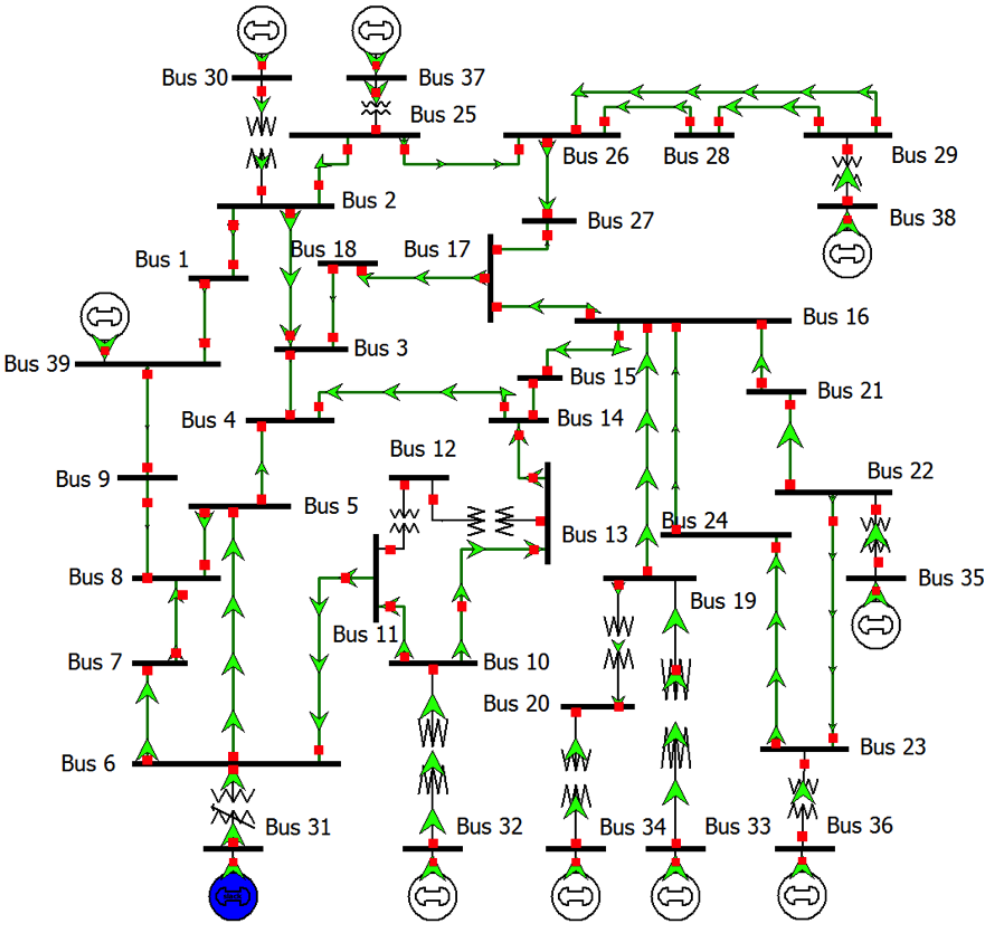

Figure 3.1: *10-machine New England power system. This IEEE test system has 39 buses including 10 generator buses and 29 load buses. Bus is represented by black horizontal bar and transmission line by green line with arrow.*

turn, in the AC power flow model. Let $A \in \{-1, 1\}^{N \times L}$ be the bus to branch incidence matrix with columns representing transmission lines and rows as buses. For line ℓ transferring power from bus m to bus n, the l_{th} column of the matrix A has 1 and -1 on the m_{th} and n_{th} position and 0 everywhere else. Also let $\mathbf{y}$ be the L-vector of individual line admittance. Then, the admittance matrix can be constructed by

$$\boldsymbol{Y}_{bus} = A \operatorname{diag}(\mathbf{y}) A^{\top} \tag{3.8}$$

where $\operatorname{diag}(\mathbf{y})$ is the diagonal matrix with individual line admittance on the diagonal and $A^{\top}$ is the transpose of A. The bus to branch incidence matrix and the bus admittance matrix of the IEEE 39-bus system are plotted in Figure 3.2

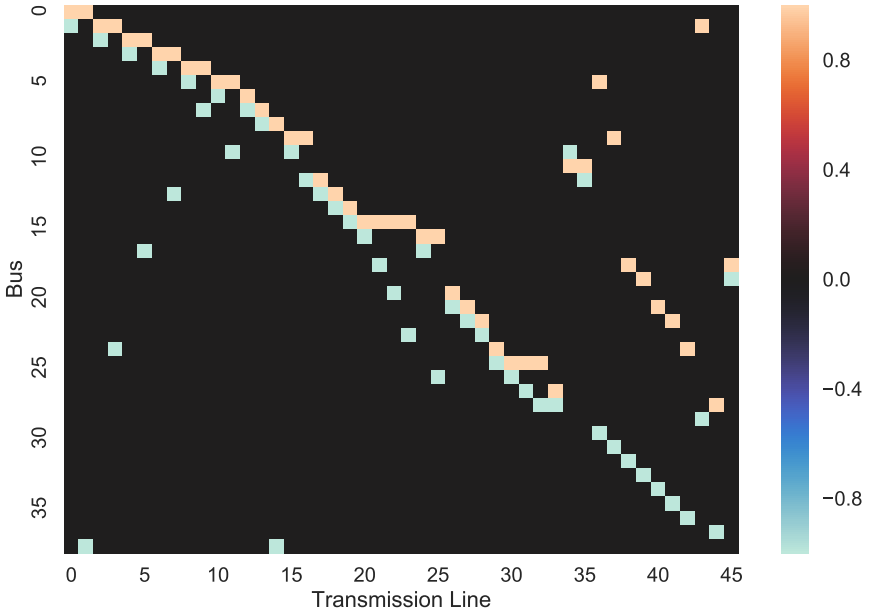

Figure 3.2: *Bus to branch incidence matrix of IEEE 39-bus system.*

and 3.3. From the figures, the sparsity structure of the matrices are clearly visible.

3.2 Power System Simulation

Dynamic simulation of power systems is an important area of research useful for tasks such as expansion planning, generator scheduling, and contingency studies. In this thesis, the open-source dynamic simulation package, the Cascading Outage Simulator with Multiprocess Integration Capabilities or COSMIC [43], is used to generate realistic power system dynamic data under the impact of line outages[1].

The simulation package builds a complete model of the power system using a set of differential-algebraic equations (DAEs). The dynamic components of the system, e.g., synchronous machines of generator bus, exciters, and governors, are modeled using differential equations. The associated nonlinear power flows

[1]The package is implemented in MATLAB and the source code is accessible at this GitHub repository.

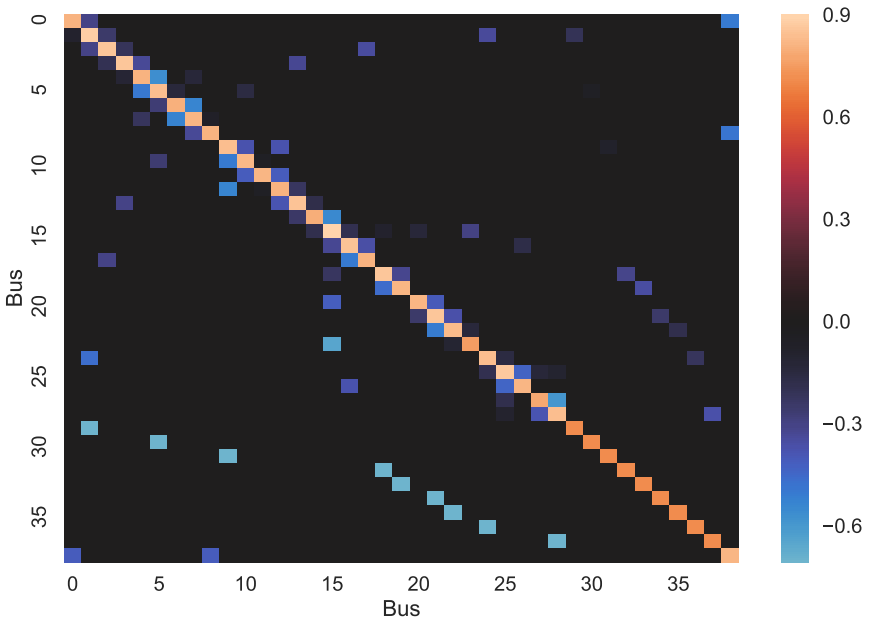

Figure 3.3: *Bus admittance matrix of IEEE 39-bus system.*

on power grids are modeled using the AC power flow equations of (3.6). In addition, for contingency studies, discrete changes to system configurations due to exogenous or endogenous factors are modeled using a set of discrete variable constraints. When any discrete variable changes during a simulation, e.g., a line outage has happened, the DAE solver stops temporarily to process the event, update the system's initial conditions, and resume solving the set of DAEs with the new system condition.

For all the simulation studies in this thesis, transmission line outages are simulated using COSMIC using a particular IEEE test system. The dynamic simulation is run for 10 seconds, and the outage is scheduled to happen at the third second. The outage is assumed to be persistent, i.e., they are not repaired throughout the simulation. Although system load models are fixed in advance, during each step of the DAE solver, 5% random perturbation of the real and reactive power is added to the system, representing stochastic fluctuations in short-term power demand. Lastly, for a bus equipped with PMU, V and θ are assumed to be measured and available from COSMIC.

Chapter 4

AC Power Flow Model-Based Outage Detection

4.1 Introduction

In this chapter, an outage detection scheme making use of approximate transient dynamics is proposed[1]. The scheme represents a novel hybrid approach to outage detection where a power system model is the building block for the statistical detection method. A time-variant small-signal relationship between net active power and nodal voltage phase angles is derived from the AC power flow model. Outage detection is then formulated as a statistical distribution change detection problem. A generalized likelihood ratio (GLR) detection scheme is implemented to detect the outage at a pre-specified false alarm rate.

The main contributions of this research work can be summarized in two aspects. Firstly, the power system model retains the non-linear and time-varying characteristics of the system transient response after the outage. The system is not assumed to be in a quasi-steady state immediately after the disruption like many existing methods. From the dynamic outage simulation, it is observed that the transient response could last over 10 seconds. Secondly, the proposed GLR detection scheme can deal with the trade-off between system-wide false alarm rate and detection delay. The ability to decide among different detection

[1]This chapter is based on the paper: X. Yang, N. Chen, and C. Zhai, "A control chart approach to power system line outage detection under transient dynamics", *IEEE Transactions on Power Systems*, vol. 36, no. 1, pp. 127–135, 2021.

thresholds gives operators the flexibility to cater to their system needs. The detection scheme is also computationally efficient, therefore, suitable for online implementation in a network of realistic size.

The remainder of this chapter is organized as follows. Section 4.2 describes the power system model and the statistical model used to characterize system behaviors before and after the outage. Then, a dynamic detection scheme is developed in Section 4.3. The effectiveness of the proposed scheme on simulation data of two test power systems is reported and discussed in Section 4.5. Section 4.6 concludes this work with two further research directions.

4.2 Problem Formulation

4.2.1 Approximate Transient Dynamics Model

Consider a power system with N buses connected by L transmission lines as mentioned in Section 3.1. Without the loss of generality, bus 1 is assumed to be the reference bus. This bus serves as the angular reference to all other buses, and its phase angle is set to 0°. The voltage magnitude at the reference bus is also set to 1.0 per unit (p.u.). Let $\mathbf{P}$, $\mathbf{Q}$, $\boldsymbol{\theta}$, and $\mathbf{V}$ represent the $(N-1)$-dimensional column vectors of net active power, net reactive power, voltage angles, and magnitudes, respectively, at all buses except the reference bus. Taking a derivative with respect to time t on both sides of the AC power flow model of (3.6), then

$$\begin{bmatrix} \frac{\partial \mathbf{P}}{\partial t} \\ \\ \frac{\partial \mathbf{Q}}{\partial t} \end{bmatrix} = \left[\begin{array}{c|c} J_1 & J_2 \\ \hline J_3 & J_4 \end{array}\right] \cdot \begin{bmatrix} \frac{\partial \boldsymbol{\theta}}{\partial t} \\ \\ \frac{\partial \mathbf{V}}{\partial t} \end{bmatrix}, \tag{4.1}$$

where $J_i, i = 1, \ldots, 4$ are the four submatrices of the AC power flow Jacobian with

$$J_1 = \frac{\partial \mathbf{P}}{\partial \boldsymbol{\theta}}, J_2 = \frac{\partial \mathbf{P}}{\partial \mathbf{V}}, J_3 = \frac{\partial \mathbf{Q}}{\partial \boldsymbol{\theta}}, J_4 = \frac{\partial \mathbf{Q}}{\partial \mathbf{V}}. \tag{4.2}$$

In the usual operating range of relatively small angles, real power systems exhibit much stronger interdependence between $\mathbf{P}$ and $\boldsymbol{\theta}$ and between $\mathbf{Q}$ and $\mathbf{V}$ than those between $\mathbf{P}$ and $\mathbf{V}$ and between $\mathbf{Q}$ and $\boldsymbol{\theta}$ [44]. By neglecting J_2 and J_3,

(4.1) reduces to the decoupled AC power flow equations where the changes in voltage angles and magnitudes are not coupled, i.e.,

$$J_2 = J_3 = \mathbf{0}.$$

Therefore, a small-signal time-variant model describing the relationship between active power mismatches and the changes in voltage angles is obtained:

$$\frac{\partial \mathbf{P}}{\partial t} \approx J_1(\boldsymbol{\theta}) \frac{\partial \boldsymbol{\theta}}{\partial t}\,. \tag{4.3}$$

From here onwards, the subscript 1 is dropped from J_1. The off-diagonal and diagonal elements of the J matrix can be derived from (3.6a) respectively:

$$\frac{\partial \mathrm{P}_m}{\partial \theta_n} = \mathrm{V}_m \mathrm{V}_n \mathrm{Y}_{mn} \sin\left(\theta_m - \theta_n - \alpha_{mn}\right)\,, m \neq n\,, \tag{4.4a}$$

$$\frac{\partial \mathrm{P}_m}{\partial \theta_m} = -\sum_{\substack{n=1 \\ n \neq m}}^{N} \mathrm{V}_m \mathrm{V}_n \mathrm{Y}_{mn} \sin\left(\theta_m - \theta_n - \alpha_{mn}\right)\,. \tag{4.4b}$$

Note that $t \in [0, \infty)$ is implicit in the continuous-time quantities $\mathbf{P}, \mathbf{V}$, and $\boldsymbol{\theta}$. Accordingly, their discrete counterparts are defined as $\mathbf{P}_k, \mathbf{V}_k$, and $\boldsymbol{\theta}_k$ at time t_k for $k = 1, 2, \ldots$. For PMU devices with a sampling frequency of 30 Hz,

$$\Delta t = t_k - t_{k-1} = 1/30\, s\,.$$

A first-order difference discretization by Euler's formula can approximate (4.3) by:

$$\Delta \mathbf{P}_k = J(\boldsymbol{\theta}_{k-1}) \Delta \boldsymbol{\theta}_k\,, \tag{4.5}$$

where

$$\Delta \mathbf{P}_k = \mathbf{P}_k - \mathbf{P}_{k-1}$$

and

$$\Delta \boldsymbol{\theta}_k = \boldsymbol{\theta}_k - \boldsymbol{\theta}_{k-1}\,,$$

i.e., the active power mismatch and difference between two consecutive angle measurements. A time-variant relationship between variations in phasor angles and net active power on buses is derived. The key feature of the proposed model lies in the J matrix in (4.5). The matrix changes with $\boldsymbol{\theta}$, which in turn changes

with time. Therefore, it retains the non-linear and dynamic nature of the AC power system.

Methods relying on a static relationship between $\Delta\mathbf{P}$ and $\Delta\boldsymbol{\theta}$ make three further assumptions about the system [23, 26]: (1) System operates with a flat voltage profile, i.e.,

$$\mathrm{V}_m \approx \mathrm{V}_n \approx 1.0\,\mathrm{p.u.}\,,$$

(2) and with approximately homogeneous bus angles across the network, i.e.,

$$\cos(\theta_m - \theta_n) \approx 1, \sin(\theta_m - \theta_n) \approx 0\,.$$

(3) The reactive property of a line is much more significant than its resistive property, i.e.,

$$B_{mn} \gg G_{mn}\,,$$

for $m, n \in \mathcal{N}$. Under these assumptions, (4.3) reduces to

$$\frac{\partial \mathbf{P}}{\partial t} \approx -\mathbf{B}\frac{\partial \boldsymbol{\theta}}{\partial t}\,, \tag{4.6}$$

where $\mathbf{B}$ is the imaginary component of $\boldsymbol{Y}_{bus}$. This is obtained by applying the assumptions and using (3.7) to write (4.4a) as

$$\begin{aligned}\frac{\partial \mathrm{P}_m}{\partial \theta_n} &= \mathrm{Y}_{mn}\left(\sin\theta_{mn}\cos\alpha_{mn} - \cos\theta_{mn}\sin\alpha_{mn}\right)\,,\\ &= G_{mn}\sin\theta_{mn} - B_{mn}\cos\theta_{mn}\,,\\ &\approx -B_{mn}\,,\end{aligned} \tag{4.7}$$

for $m \neq n$. Similarly,

$$\frac{\partial \mathrm{P}_m}{\partial \theta_m} \approx \sum_{n=1, n\neq m}^{N} B_{mn}\,. \tag{4.8}$$

Putting the elements in (4.7) and (4.8) together, the relationship (4.6) is obtained. While line resistances in transmission systems are generally one order of magnitude smaller than reactances, this is not usually the case for distribution systems [45]. Also, a static model may not be accurate enough to reflect the transient behavior after an outage since the homogeneous angles assumption might be violated [46]. This phenomenon is routinely encountered in dynamic simulation. For example, in Fig. 4.1, the balance between voltage angles is severely distorted following

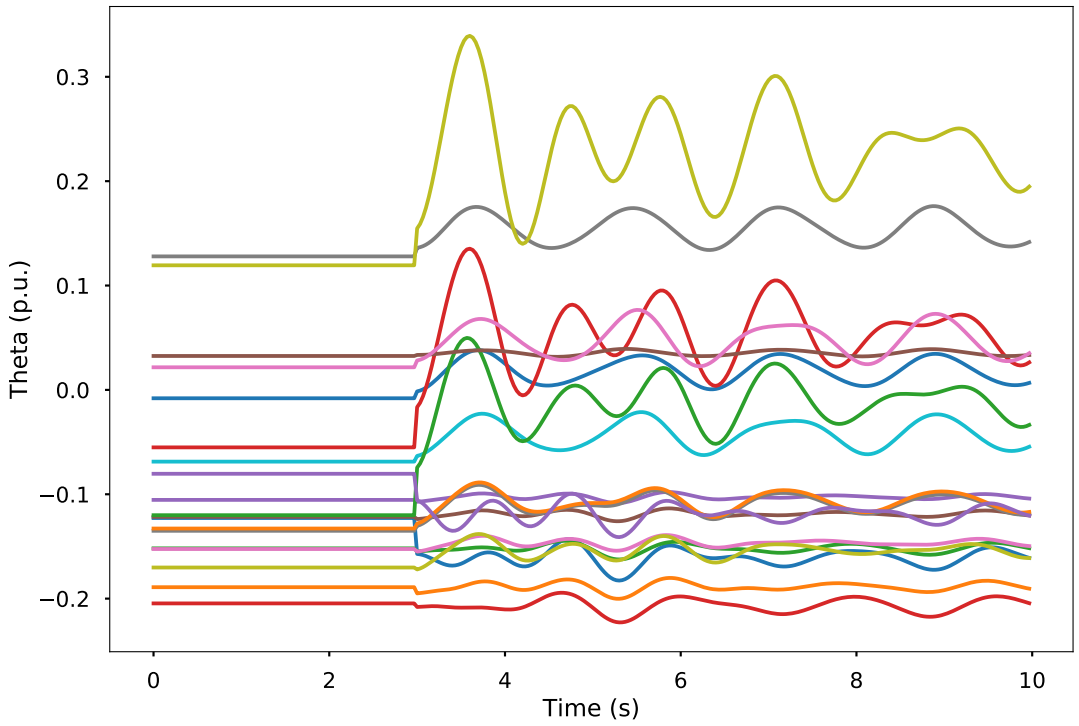

Figure 4.1: *The progression of selected bus voltage phase angles after an outage at $t = 3$ s, where each line corresponds to one bus. The steady-state bus angle balance is severely distorted during the transient response phase.*

an outage, e.g., at around $t = 3.75$ s. Furthermore, the duration of transient dynamics is non-negligible for real-time detection purposes. Therefore, to reflect the dynamic behavior in a timely and accurate manner, J matrix in (4.5) is updated by real-time streaming PMU data.

4.2.2 Line-specific Outage Statistical Model

For a balanced steady-state power system with no active power mismatch, it can be assumed $\mathbf{P}_0 = \mathbf{0}$. Within a short period of time, net active power fluctuates around zero as the generators respond to random changes in electricity demand. Therefore, the trajectory of $\mathbf{P}$ can be modeled as a Brownian motion with drift $\mathbf{0}$ and variance $\sigma^2 t\mathbf{I}$ which is a continuous-time stochastic process:

$$\{\mathbf{P}_t : t \in [0, \infty)\}.$$

σ^2 is pre-determined and $\mathbf{I}$ is an identity matrix of appropriate dimension. One of the implications of a Brownian motion is that their independent increment, i.e.,

$$\Delta \mathbf{P}_k = \mathbf{P}_{t_k} - \mathbf{P}_{t_{k-s}}\,,$$

follows a multivariate Gaussian distribution with mean $\mathbf{0}$ and variance $\sigma^2(t_k - t_{k-s})\mathbf{I}$ [47]. In particular, taking $s = 1$, then $t_k - t_{k-s} = \Delta t$ and

$$\Delta \mathbf{P}_k \sim \mathcal{N}(\mathbf{0}, \sigma^2 \Delta t \mathbf{I})\,. \tag{4.9}$$

Since σ^2 is pre-determined, $\sigma^2\Delta t$ can be replaced by σ^2 for notational simplicity. Rearranging the variables in (4.5) results in

$$\Delta \boldsymbol{\theta}_k = J(\boldsymbol{\theta}_{k-1})^{-1} \Delta \mathbf{P}_k\,. \tag{4.10}$$

Therefore, bus angle variations can be characterized by

$$\Delta \boldsymbol{\theta}_k \sim \mathcal{N}(\mathbf{0}, \sigma^2 (J(\boldsymbol{\theta}_{k-1})^T J(\boldsymbol{\theta}_{k-1}))^{-1})\,. \tag{4.11}$$

From (4.11), it can be seen that the angle variations at time k are characterized by the structure of J and the angle values at $t = k-1$. Let $\mathcal{L}_o$ represent the set of all possible combinations of outages, e.g., single-line outage, double-line outage. When an outage $\ell \in \mathcal{L}_o$ happens, the grid topology and the bus admittance matrix changes. The new bus admittance matrix $\boldsymbol{Y}_{bus,\ell}$ induces a new J_ℓ, and therefore, a new distribution of $\Delta\boldsymbol{\theta}_k$. There is a one-to-one correspondence between an outage scenario and a distribution of $\Delta\boldsymbol{\theta}_k$. Furthermore, the outage is assumed to be persistent, i.e., tripped lines are not restored in the time under consideration, and does not result in any islanding in the network, i.e., no part of the system is isolated from the main grid.

In light of the above characterization, a hypothesis testing framework is adopted to detect the distribution change in $\Delta\boldsymbol{\theta}_k$:

$$H_0 : \Delta\boldsymbol{\theta}[k] \sim N(\mathbf{0}, \sigma^2 (J_0^T J_0)^{-1})\,, \tag{4.12a}$$

$$H_1 : \Delta\boldsymbol{\theta}[k] \sim N(\mathbf{0}, \sigma^2 (J_\ell^T J_\ell)^{-1})\,, \ell \in \mathcal{L}_o\,, \tag{4.12b}$$

for $k = 1, 2, \ldots$. The null hypothesis is that there is no outage, and the corresponding Jacobian is J_0. The alternative hypothesis is that there is an outage

scenario ℓ, where the corresponding Jacobian is J_ℓ. If the null hypothesis is rejected at time τ, then the distribution of $\Delta\boldsymbol{\theta}[k]$ has changed, and the outage is detected. The detailed procedure of real-time detection under this framework is described in Section 4.3.

A common challenge for PMU applications is that not all buses are equipped with a PMU. Here the previous formulations to a limited PMU deployment is adapted. Suppose K PMUs are installed where $K < N$. Given a selection matrix $S \in \{0,1\}^{K\times N}$ that selects K observable buses from the complete set of N buses, observable bus angle data is

$$\boldsymbol{\theta}_k^o = S\boldsymbol{\theta}_k\,, \tag{4.13}$$

where S is a diagonal matrix of size $K \times N$ and entries equal to 0 or 1. The corresponding angle variations and Jacobian matrix are

$$\Delta\boldsymbol{\theta}_k^o = S\Delta\boldsymbol{\theta}_k\,, \tag{4.14}$$

$$J^o(\boldsymbol{\theta}_{k-1}^o) = SJ(\boldsymbol{\theta}_{k-1}^o)S^\top\,. \tag{4.15}$$

Therefore, $\Delta\boldsymbol{\theta}_k^o$ is a K-dimensional vector and $J^o(\boldsymbol{\theta}_{k-1}^o)$ is a $(K\times K)$-dimensional matrix. To obtain the hypothesis testing framework in (4.12), $\Delta\boldsymbol{\theta}_k, J_0,$ and J_ℓ are replaced by $\Delta\boldsymbol{\theta}_k^o, J_0^o,$ and J_ℓ^o respectively.

4.3 Generalized Likelihood Ratio-Based Detection Scheme

From the previous sections, outage detection is formulated as a problem of distribution change detection under a hypothesis testing framework in Section 4.2.2. In general, under normal conditions, system outputs follow a common distribution with a probability density function f_0. At some unknown time τ, the system condition changes, and the density function changes to f_1. The goal is to design a scheme where an alarm is raised once a monitoring statistic $W(\cdot)$ crosses a pre-defined threshold of c. The two key design aspects are: (1) how to compute the monitoring statistic, $W(\cdot)$ and (2) how to determine the detection threshold, c. The monitoring statistic will be close to zero under a normal condition and

increase unboundedly if a change happens. The detection threshold needs to be specified to meet a particular false alarm rate constraint.

A GLR approach originally proposed by [48] is adopted to design the detection scheme. The scheme repeatedly evaluates the likelihood of a normal condition against the likelihood of an abnormal condition. In the context of power system, bus angle variations are not independent samples since the distribution at time k is influenced by bus angles at time $k-1$ as shown in (4.11). However, $\Delta\boldsymbol{\theta}_k$ can be regarded as a conditionally independent random variable with density function $f_0(\cdot|\boldsymbol{\theta}_{k-1})$ under H_0 in (4.12a) and, after an outage, with density function $f_\ell(\cdot|\boldsymbol{\theta}_{k-1})$ under H_1 in (4.12b). For every new data $\Delta\boldsymbol{\theta}_k$, H_0 is tested against H_1 for some outage scenario $\ell \in \mathcal{L}_o$ using a log-likelihood ratio test statistic. In particular, let

$$Z_k(\ell) = \ln \frac{f_\ell(\Delta\boldsymbol{\theta}_k|\boldsymbol{\theta}_{k-1})}{f_0(\Delta\boldsymbol{\theta}_k|\boldsymbol{\theta}_{k-1})} \tag{4.16}$$

be the log-likelihood ratio of an outage scenario ℓ at time k. $Z_k(\ell)$ is positive if the likelihood of a change is larger than that of a normal condition. Then the test statistic is:

$$G_k = \max\left\{0,\ \max_{1\le i\le k}\max_{\ell\in\mathcal{L}}\sum_{j=i}^{k} Z_j(\ell)\right\}. \tag{4.17}$$

and the GLR detection scheme will raise an alarm at the time:

$$D = \inf\{k \ge 1 : G_k \ge c\}. \tag{4.18}$$

Since the time and location of the outage are not known a priori, they are replaced by their maximum likelihood estimates. Schemes of the form involving searching through the maximum over time ($1 \le i \le k$) and over likelihood ($\sum_{j=i}^{k} Z_j(\ell)$) are referred to as the GLR schemes. Such schemes have optimal properties in terms of their detection performance. Let $E_{H_0}(D)$ be the expectation of time of alarm when there is no outage, i.e., mean time to a false alarm. Suppose c is chosen such that the scheme satisfies a certain false alarm rate, $E_{H_0}(D) \ge \gamma\{1 + o(1)\}$. For conditionally independent data, Lai has proved that the detection rule (4.18) is asymptotically optimal in the sense that among all rules T with $E_{H_0}(T) \ge \gamma\{1 + o(1)\}$, it minimizes the worst-case detection delay

as defined by

$$\overline{E}_{H_1}(T) = \sup_{\tau \geq 1} \operatorname{ess\,sup} E^{(\tau)} \left[(T - \tau + 1)^+ | \boldsymbol{\theta}_1, \cdots, \boldsymbol{\theta}_{\tau-1} \right] , \tag{4.19}$$

as the outage time $\tau \to \infty$ [49].

For the actual online implementation, a recursive formulation of the GLR scheme is used. Note that G_k in (4.17) can be rewritten as

$$\begin{aligned} G_k &= \max \left\{ 0, \max_{\ell \in \mathcal{L}} \max_{1 \leq i \leq k} \sum_{j=i}^{k} Z_j(\ell) \right\} , \\ &= \max_{\ell \in \mathcal{L}} \max \left\{ 0, \max_{1 \leq i \leq k} \sum_{j=i}^{k} Z_j(\ell) \right\} , \\ &= \max_{\ell \in \mathcal{L}} W_{\ell,k} \, . \end{aligned} \tag{4.20}$$

where in the first step the position of the two inner max operators is switched since the overall maximum is not affected [50]. Also, in the last step,

$$W_{\ell,k} = \max \left\{ 0, W_{\ell,k-1} + Z_k(\ell) \right\} , \tag{4.21}$$

an equivalent recursive form of the term $\max\limits_{1 \leq i \leq k} \sum_{j=i}^{k} Z_j(\ell)$ in G_k. Therefore, for every scenario ℓ, just the monitoring statistic W_{k-1} at the previous time step needs to be kept tracked of and the log-likelihood ratio Z_k at the current time step computed. $Z_k(\ell)$ can be found analytically by

$$Z_k(\ell) = \ln |J_\ell| - \ln |J_0| + \frac{1}{2\sigma^2} \Delta \boldsymbol{\theta}_k^T \left[{J_0}^T J_0 - {J_\ell}^T J_\ell \right] \Delta \boldsymbol{\theta}_k \, , \tag{4.22}$$

based on the multivariate Gaussian distribution likelihood function. Using the recursive formulation, the stopping time is

$$D = \inf \left\{ k \geq 1 : \max_{\ell \in \mathcal{L}} W_{\ell,k} \geq c \right\} . \tag{4.23}$$

Intuitively, the threshold is crossed when the evidence against the normal condition, i.e., no outage, has accumulated to a significant level. c is a predefined threshold that controls the balance between the detection delay and the false alarm rate. A smaller c corresponds to a more sensitive scheme that may have a quicker detection but could potentially flag more normal fluctuations as

outages. One advantage of using the GLR approach is that such trade-off can be systematically quantified. Following [26], given a false alarm rate constraint, c could be approximated by

$$c = \ln(ARL_0 \times p)\,, \tag{4.24}$$

where ARL_0 is the average run length to a false alarm of the scheme when no outage occurs. p is the number of PMUs installed. For example, $c = 18.43$ when $ARL_0 = 1$ day with 39 PMUs installed. With this detection delay and false alarm rate trade-off in mind, system operators can choose a desired level of sensitivity, catering to the individual system needs, and implement it in the detection scheme through parameter c and ARL_0. A flowchart summarizing the working of the detection and identification scheme outlined in this section is shown in Fig. 4.2.

4.4 Additional Remarks

4.4.1 Setting up Outage Scenarios

The one-to-one correspondence between the Jacobian and grid topology can be established by looking at how the admittance matrix is constructed in (3.8). $\boldsymbol{Y}_{bus}$ is constructed from the bus incidence matrix A and line admittances. For different outage scenarios, the corresponding column of A needs to be set to 0. For example, to set up the l_{th} line outage, the entries in the l_{th} column of A are set to 0 to get A_ℓ. The corresponding bus admittance matrix $\boldsymbol{Y}_{bus,\ell}$ is obtained by

$$\boldsymbol{Y}_{bus,\ell} = A_\ell \,\mathrm{diag}(\mathbf{y}) A_\ell^\top\,.$$

The Jacobian matrix J_ℓ describing the post-outage system is obtained by (4.4).

For example, a 4-bus power system with five transmission lines might have a bus to branch incidence matrix of

$$A = \begin{bmatrix} 1 & 0 & 1 & 0 & 1 \\ -1 & 1 & 0 & 0 & 0 \\ 0 & -1 & -1 & 1 & 0 \\ 0 & 0 & 0 & -1 & -1 \end{bmatrix}.$$

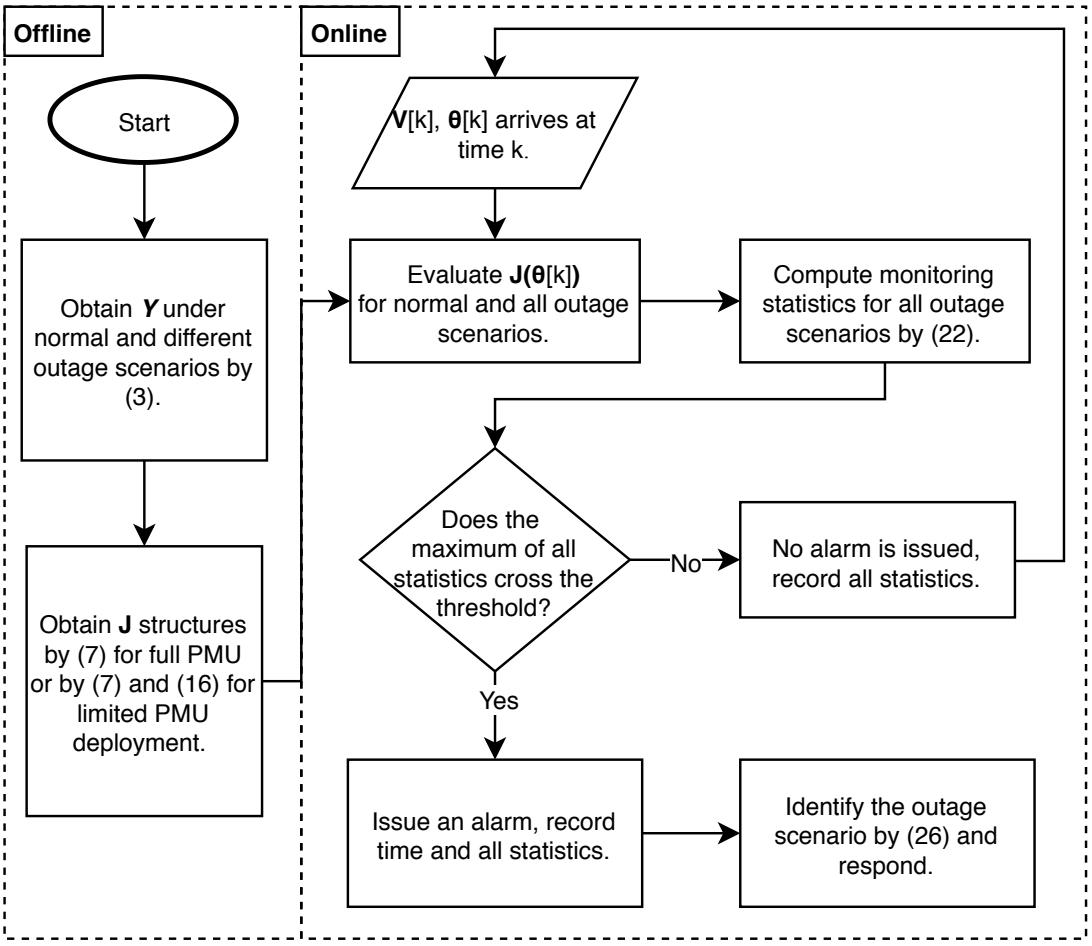

Figure 4.2: *Flowchart summarizing the proposed dynamic outage detection and identification scheme.*

In offline preparation for line 1 outage scenario, the following is obtained:

$$A_{\ell_1} = \begin{bmatrix} 0 & 0 & 1 & 0 & 1 \\ 0 & 1 & 0 & 0 & 0 \\ 0 & -1 & -1 & 1 & 0 \\ 0 & 0 & 0 & -1 & -1 \end{bmatrix}.$$

Subsequently, the corresponding admittance matrix can be obtained as

$$\boldsymbol{Y}_{bus,\ell_1} = A_{\ell_1} \operatorname{diag}(\mathbf{y}) {A_{\ell_1}}^{\top}.$$

Therefore, no simulation or real data is needed to generate the outage scenarios to set up the monitoring scheme during offline preparation. In real applications,

both the bus incidence matrix and line admittances can be obtained based on the network topology and data during the outage-free period. It will then be sufficient to apply the proposed method.

4.4.2 Unobservable Neighbor Buses

For a limited PMU deployment, there may be some inaccuracies in the computed diagonal elements of $J^o(\boldsymbol{\theta}^o_{k-1})$. In particular, if there is no PMU on bus n, a neighbor of bus m, measurements V_n and θ_n would not be available. Therefore, the term, $-\mathrm{V}_m\mathrm{V}_n\mathrm{Y}_{mn}\sin(\theta_m - \theta_n - \alpha_{mn})$, would not be computable and is treated as 0 for the summation in (4.4b). The issue could be alleviated by carefully designing the PMU placement (locations). One possible design rule is to make sure that each observable bus has at least one observable neighbor bus. In general, PMU locations will influence the efficiency of outage detection. It is also of interest to practitioners to find the optimal placement of PMUs so that even with limited PMUs, outages can be detected as quickly as possible. However, the placement problem is beyond the scope of this work, and it will be studied in future research.

4.4.3 Identification of Tripped Lines

Following detection, the actual lines tripped need to be identified so that follow-up, potentially automatic, actions can be taken. Since the likelihoods of every outage scenario are monitored and compared online, one way to locate the tripped line(s) without any extra computation is to identify the scenarios with the top three likelihoods at the time of detection. In particular, following a detection at time D, top-three possible tripped lines can be identified as $\ell_{(1)}, \ell_{(2)}, \text{and } \ell_{(3)}$ such that:

$$W_{\ell_{(1)},D} \geq W_{\ell_{(2)},D} \geq W_{\ell_{(3)},D} \geq W_{\ell,D}\,, \tag{4.25}$$

for all other $\ell \in \mathcal{L}_o$.

4.5 Simulation Study

4.5.1 Simulation Setting

The proposed detection scheme is tested on two IEEE standard test power systems, namely 39-bus New England system [51] and 2383-bus Polish system. System transient responses following an outage are simulated using the open-source dynamic simulation platform COSMIC [43] in which a third-order machine model is used. We conduct extensive single-line outage detection and identification analysis on the 39-bus system by comparing the proposed method to two other methods. Outages on the 2383-bus system are simulated to show that the proposed scheme can be deployed on large-scale systems as well.

The sampling frequency of PMU is assumed to be 30 Hz. For every new simulation, system loads are varied by a random percentage between -5% and 5% from the base-line values. Each simulation runs for 10 seconds, and the line outage takes place at the 3rd second. Active power fluctuations are assumed to be uncorrelated and have homogeneous variances where $\sigma^2 = 0.005$ in (4.12). Artificial noise is added to all sampled bus angle data, $\Delta\boldsymbol{\theta}$, to account for system and measurement noise [52]. The noises are drawn from a normal distribution with mean 0 and standard deviation equivalent to 10% of the average value of sampled $\Delta\theta$ on respective buses. Detection thresholds c in (4.23) corresponding to seven different false alarm rates are obtained by (4.24) and listed in Table 4.1.

Table 4.1: Detection Thresholds Corresponding to Different Systems and False Alarm Rates

Mean Time to	Number of PMUs Installed		
False Alarm (day)	10	39	1000
1/24	13.89	15.25	18.50
1/4	15.68	17.05	20.29
1/2	16.38	17.74	20.98
1	17.07	18.43	21.68
2	17.76	19.12	22.37
7	19.02	20.38	23.62
30	20.47	21.83	25.08

4.5.2 Simulation Results

4.5.2.1 39-Bus New England System

The 39-bus system has 39 buses, 10 generators, and 46 transmission lines. Extensive simulation studies are conducted for the full PMU deployment and limited PMU deployment scenario. For the latter case, PMUs are assumed to be installed on bus 2, 3, 7, 9, 11, 13, 16, 17, 19, and 21. In total, 3000 random simulations of outages at line 1 to 36 are studied, except for line 22 as its outage leads to two separate networks and line 37 to line 46 since they are the only line connecting the generator bus to the system. The proposed method can detect outages instantaneously in most cases with a full PMU deployment. Therefore, only the detection results of a limited PMU deployment are presented.

Table 4.2: Time-step Breakdown of The Detection Scheme For Processing Each New Measurement

Step	Action	Time Required
0	Receive new sample	0
1	Evaluate $\mathbf{J}_0$ and $\mathbf{J}_\ell$ for $\ell \in \mathcal{L}$	1 ms
2	Compute outage statistics $\mathbf{W}_\ell$ for $\ell \in \mathcal{L}$	0.227 ms
3	Check if $\max \mathbf{W}_\ell$ for $\ell \in \mathcal{L}$ exceeds c	0

An outage at line 10 is used to demonstrate the typical working of the detection scheme. Table 4.2 shows a time-step breakdown for the scheme when processing each new measurement. The execution time is obtained by running the algorithm on a personal laptop with a 2.9 GHz Intel Core i5 processor. Note that a new measurement is collected every 33 ms. Fig. 4.3 shows the progression of the individual scenario statistics as well as the overall statistic. After the outage (3rd second), individual statistics start to deviate from zero. The overall monitoring statistic rises quickly, too, since it is the maximum of all individual statistics. The scheme issues an alarm when the overall statistic crosses the threshold at time 3.5 seconds. In this case, the scheme records a detection delay of 0.5 seconds. Among all 35 individual statistics representing different outage scenarios, only

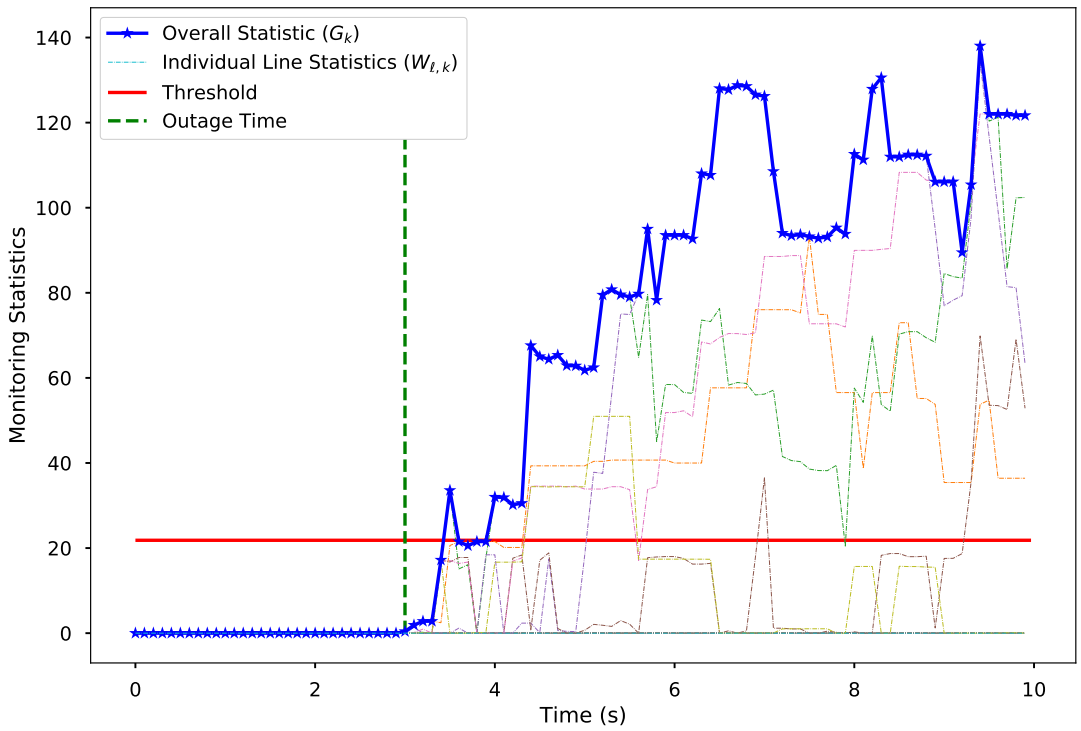

Figure 4.3: *Progression of monitoring statistics for line 10 outage. Individual line statistics are represented by faded dash lines of various colors. The blue solid line is the overall statistic.*

some have values significantly larger than 0, while most of them stay close to 0 as they are deemed as unlikely scenarios by the detection scheme.

Also, since no restriction is placed on the transient stability of the post-outage system, the proposed scheme does not require bounded signals for outage detection, and it works equally well in stable and unstable scenarios. In fact, an outage that creates an unstable system is easier to detect since it produces stronger signals than those that do not. This is illustrated by a separate simulation example included in Appendix A.

Detection Performance Fig. 4.4 shows the empirical distribution of detection delays under seven false alarm rates. A more stringent false alarm rate corresponds to a detection scheme with longer delays on average. For example, the scheme with an $ARL_0 = 1/24$ day detects much more outages within 0.25 seconds than the one with $ARL_0 = 30$ days. These differences are not significant. Hence, the

proposed scheme's performance based on detection delay is not overly sensitive to different false alarm rates.

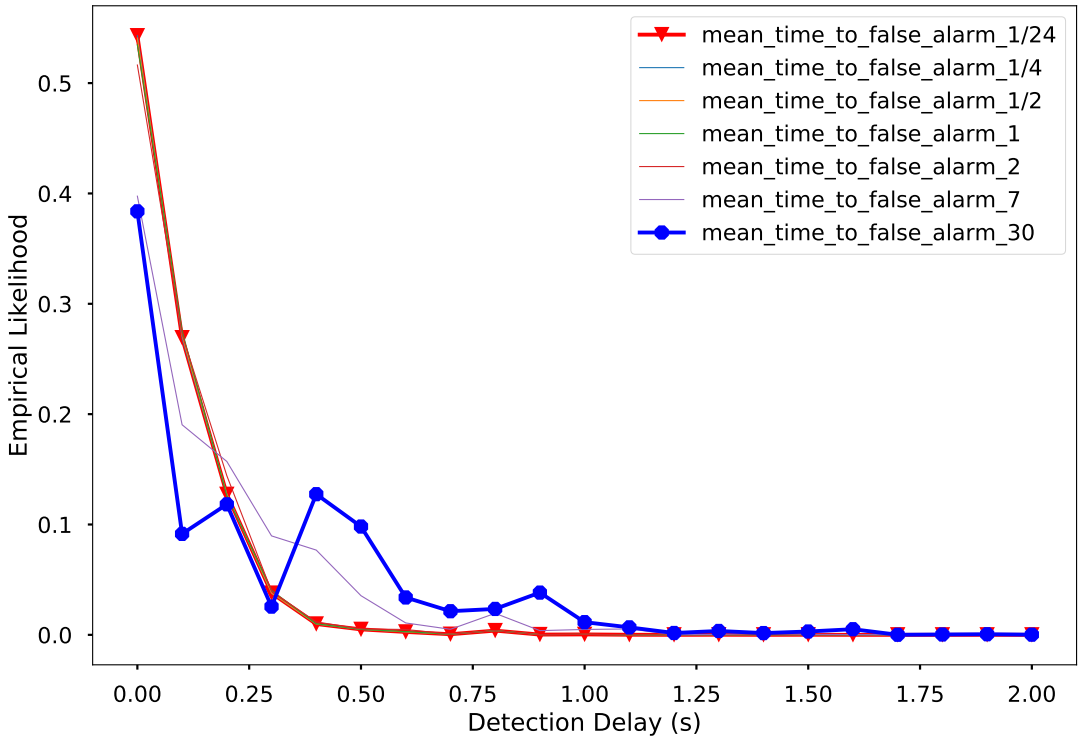

Figure 4.4: *Comparison of the empirical distribution of detection delays in seconds under different false alarm rates. The number in the label is the number of days until a false alarm.*

The detection performance across different line outages is also studied. There are clear variations in terms of detection delay among those detected outages. These variations can be largely attributed to the PMU placement and the grid topology.

For outages with almost zero detection delay, they are lines where either PMUs are installed on both ends of the line, e.g., line 3, 21, and 23, or one PMU is connected to the line, e.g., line 20, 25, and 27. Signals can be readily picked up by nearby PMUs. On the other hand, the absence of PMU nearby may have contributed to the longer detection delays. In particular, there are no PMUs available on either end of line 9, 10, 28, 32, 33, and 34. These outage signals have to be detected by sensors far away from the location. Fig. 4.5 summarizes the comparison.

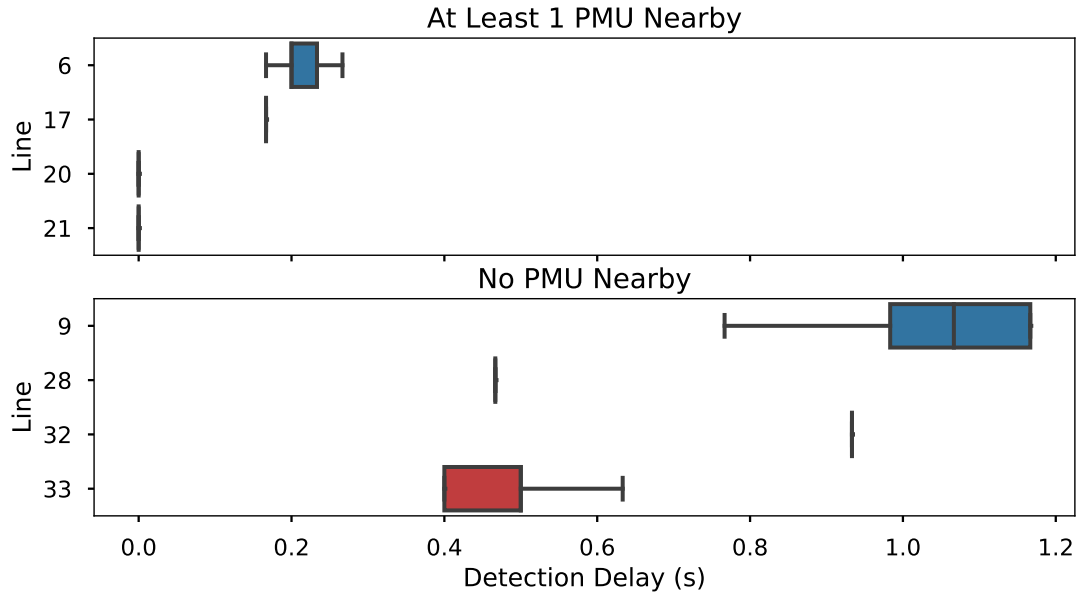

Figure 4.5: *Boxplot of the empirical distributions of detection delay in seconds for lines with at least 1 PMU nearby.*

Another factor is the power grid topology. The scheme recorded shorter delays for line 2, 14, 15, and 30. It is observed that these outages produced severe disturbances. Line 2, 14, and 15 connect to a generator bus, and line 30 connects a subnetwork to the main network. On the other hand, outages at line 5, 11, 13, and 26 produced weaker and shorter disturbances, which are more difficult to detect. Consequently, they recorded longer detection delays. See Fig. 4.6 for the comparison.

Comparison with Other Methods The proposed method's outage detection performance is also compared with two other methods. The line outages considered here are line 26, 27, and 34. Other methods considered here are the static detection method based on the DC power flow model in [26], under a full and limited PMU deployment, and the CUSUM-type central rule based on Ohm's law in [20], with a limited PMU deployment. The placement of 10 PMUs is the same for all methods. For the CUSUM scheme in [20], parameters are chosen to satisfy the same false alarm rates in Table 4.1 based on formula in [53]. The respective detection delays are summarized in Table 4.3. A dash means a missed detection. It can be seen

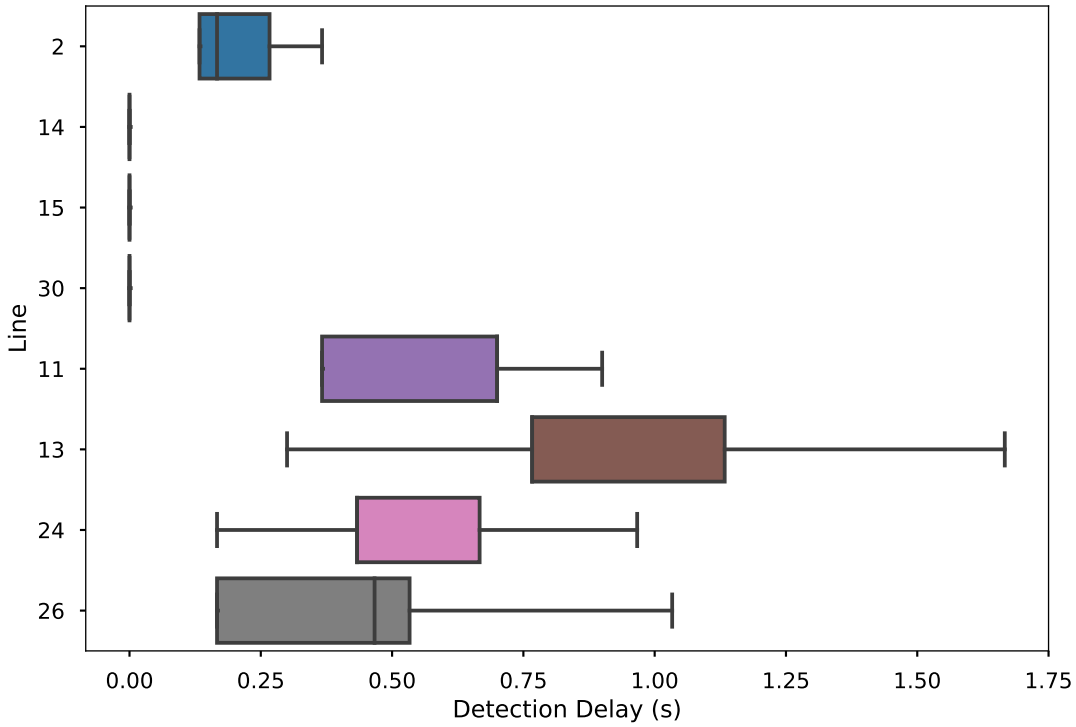

Figure 4.6: *Boxplot of the empirical distributions of detection delay in seconds for lines at different topological locations.*

that the proposed method, "AC - limited", is consistently faster at detecting outages than the other methods.

Identification Performance The identification performance of the proposed scheme is analyzed by comparing the true outage line with the identified line. The results are shown in Fig. 4.7 and Fig. 4.8. True outage lines are listed on the vertical axis, and the lines identified are on the horizontal axis. Cell color represents the empirical likelihood of identification of different lines. Therefore, a perfect identification scheme would have all diagonal cells equal to 1 and 0 everywhere else. As seen from the figure, most lines can be accurately identified under a full PMU deployment. As for the 10-PMU case, around half of the outages can be identified with a high probability. When the scheme misses the true outage line, it often misidentifies the adjacent line as tripped. Systematic biases created by the unavailability of PMUs on certain buses may have contributed to the inaccuracies. This suggests installing more PMUs or inspecting the identified line

Table 4.3: Comparison of Detection Delay (s) of Three Different Line Outages Under Different Detection Schemes

		Mean Time to False Alarm (day)			
Line	Scheme	1/24	2	7	30
26	DC - full	9.9908	9.9908	9.9908	9.9908
	DC - limited	–	–	–	–
	Ohm's Law - limited	2.8150	3.0963	3.1406	3.9333
	AC - limited	0.1001	0.1005	0.3300	0.3489
27	DC - full	4.5398	4.5398	4.5398	4.5398
	DC - limited	–	–	–	–
	Ohm's Law - limited	3.3044	3.5000	3.6900	3.8630
	AC - limited	0.0012	0.0012	0.0026	0.0039
34	DC - full	0.1801	0.1801	0.1801	0.1801
	DC - limited	–	–	–	–
	Ohm's Law - limited	1.5811	2.9250	3.2014	3.6788
	AC - limited	0.0879	0.0879	0.1558	0.4994

and all its neighboring lines could improve the localization accuracy.

4.5.2.2 2383-Bus Polish System

To show that the proposed dynamic detection scheme can be deployed in a system with realistic network size, outages in the 2383-bus system are studied. This test system has 2383 buses and 2896 transmission lines. 1000 PMUs are assumed to be placed at randomly selected locations in the system. Eight different line outages are simulated to test the proposed detection scheme. Detection delay results corresponding to four different false alarm rates are reported in Table 4.4. Considering the size of the system, detecting a single-line outage is much more difficult. Therefore, delays experienced are considerably longer than those in the 39-bus system. There are also several undetected outages.

4.6 Conclusion

This chapter develops a real-time dynamic line outage D&I scheme based on the AC power flow model and GLR scheme. A time-variant small-angle relationship between bus voltage angles and active power injections is derived. The pre- and post-outage statistical models of the angle variations are obtained.

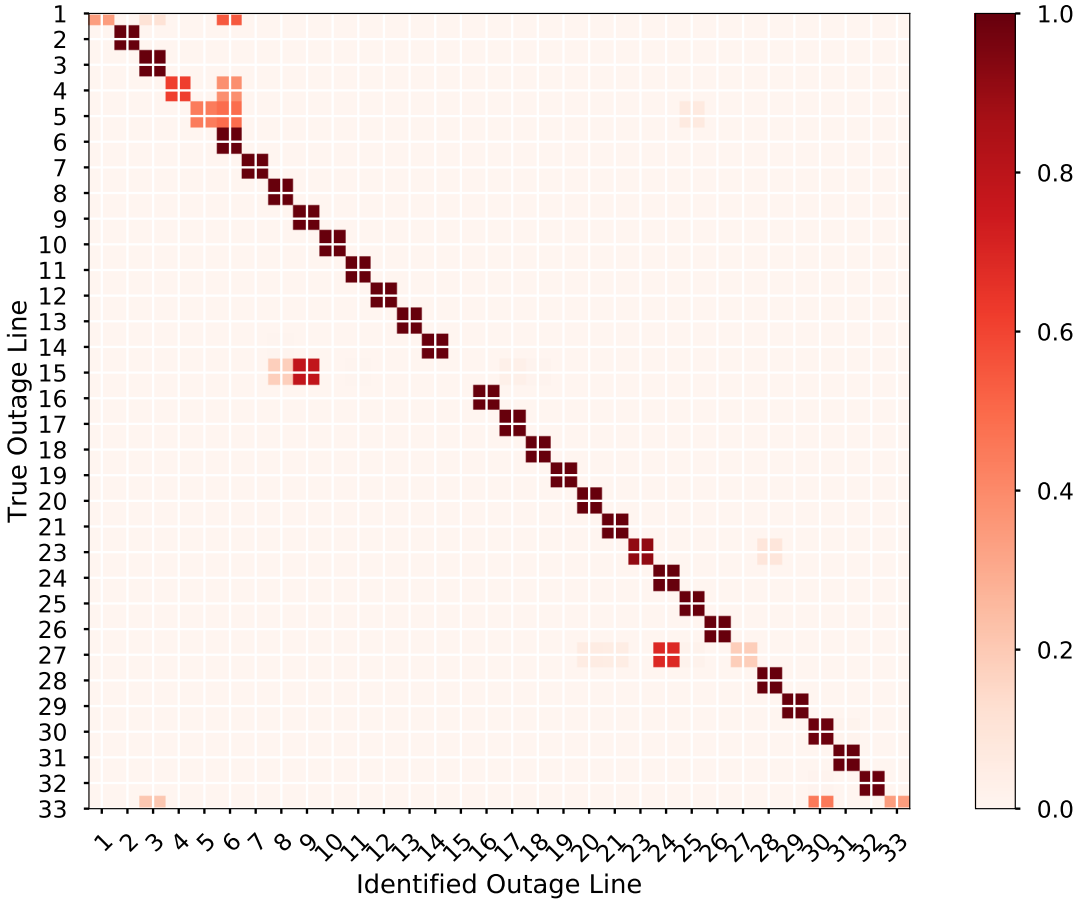

Figure 4.7: *Heat map of the identification accuracy of the proposed method in the 39-bus system with a full PMU deployment.*

Table 4.4: Detection Delay (s) of Eight Different Line Outages in 2383-bus System with 1000 PMUs Deployed

	Mean Time to False Alarm (day)			
Line	1/24	2	7	30
600	4.6667	4.6667	4.6667	4.6667
700	1.3667	1.3667	1.3667	1.3667
750	4.9000	4.9000	4.9000	4.9000
800	1.3667	1.3667	6.7667	6.7667
900	–	–	–	–
1000	–	–	–	–
1050	1.3667	1.3667	1.3667	1.3667
1650	–	–	–	–

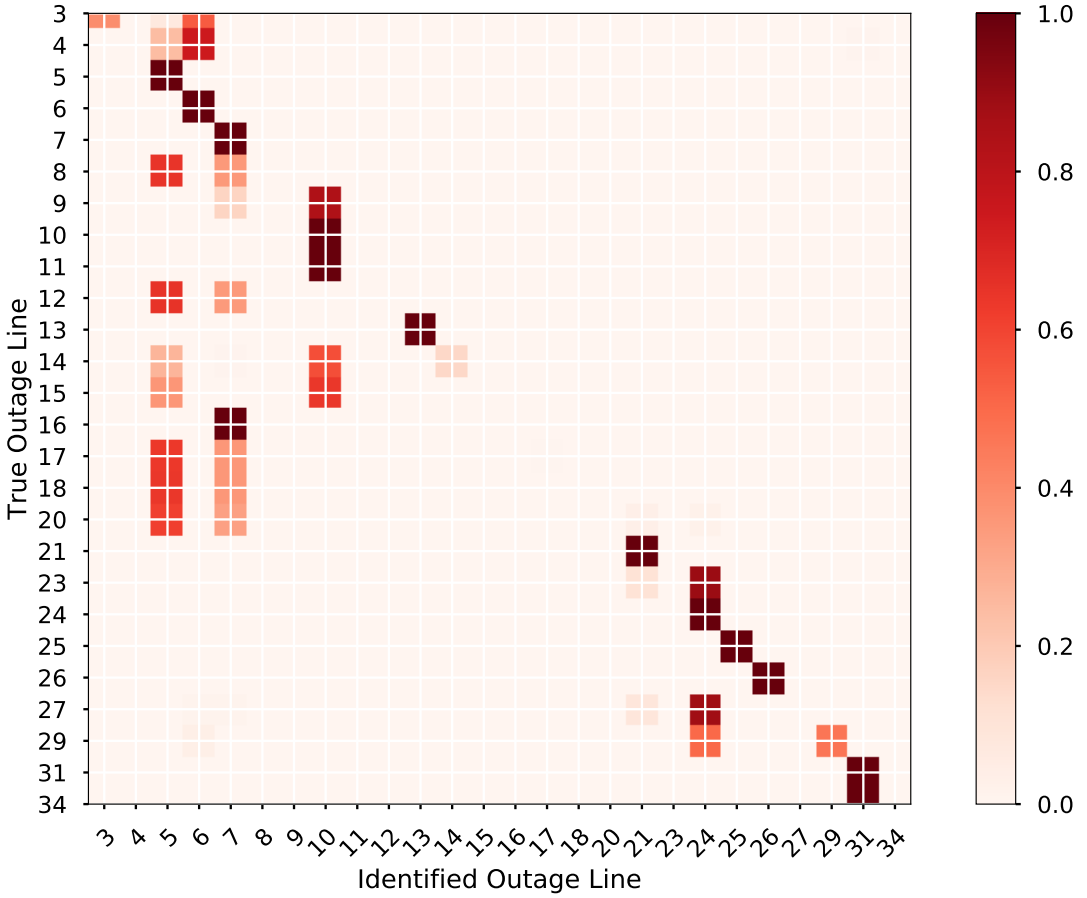

Figure 4.8: *Heat map showing the identification accuracy of the proposed method in the 39-bus system with 10 PMUs deployed.*

The proposed scheme is effective in both detection and identification. It is also scalable, as seen from the results in the 2383-bus system.

For further research, it might be worth investigating the optimal number and placement of a limited number of PMUs. As seen from Section 4.5, there is a varying level of detection delays due to PMU placement. The number of PMUs needed to achieve a certain level of identification accuracy is also worth investigating. In addition, incorporating generator dynamics into the system model might prove useful as the detailed physical model could provide an even better direction for outage detection and identification. This direction of research is pursued in Chapter 5.

Chapter 5

Outage Detection Using Generator and Load Bus Dynamics

5.1 Introduction

A unified detection framework that monitors both generator dynamics and load bus power changes using a limited number of PMUs is proposed in this chapter. System transient dynamics are tracked through nonlinear state estimation via a particle filter (PF). A statistical change detection scheme is constructed by monitoring the PF-predicted system output's compatibility with the expected normal-condition measurement. When an outage happens, a significant reduction in the compatibility triggers an alarm, detecting the outage in the quickest time possible.

The rest of this chapter is organized as follows. A unified outage detection scheme based on nonlinear power system dynamics is formulated in Section 5.2 and Section 5.3. Section 5.4 then describes the PF-based online state estimation necessary for tracking generator dynamics. The proposed scheme's effectiveness and advantages are presented in Section 5.6 using simulation studies. Section 5.7 is the conclusion.

5.2 Power System State-Space Modelling

This section describes a power system model that captures both the generator dynamics and network power flow information in a unified framework. Consider a

power system with M generator buses where $\mathcal{N}_g = \{1, \ldots, M\}$, $N - M$ load buses where $\mathcal{N}_l = \{M+1, \ldots, N\}$, and L transmission lines where $\mathcal{L} = \{1, \ldots, L\}$. The power system is a hybrid dynamic system described by a differential-algebraic model. The second-order generator model, also known as the swing equation [54], is used in this work[1]. For every generator bus $i \in \mathcal{N}_g$, their states are modeled as the differential variables, i.e., $\boldsymbol{X} = [\delta, \omega]^T$ where δ is the rotor angular position in radians with respect to a synchronously rotating reference, and ω is the rotor angular velocity in radians/second. The differential equations governing their dynamics are

$$\dot{\delta}_i = \omega_s \left(\omega_i - 1\right) , \tag{5.1a}$$

$$M_i \dot{\omega}_i = \mathrm{P}_{m,i} - \hat{\mathrm{P}}_{g,i} - D_i \left(\omega_i - 1\right) , \tag{5.1b}$$

where $\dot{\delta}_i$ is the derivative of δ_i with respect to t. ω_s is the synchronous rotor angular velocity such that $\omega_s = 2\pi f_0$ where f_0 is the known synchronous frequency. $\mathrm{P}_{m,i}, M_i$, and D_i denote the mechanical power input, the inertia constant, and the damping factor, respectively. They are assumed known and constant for the duration of this study. The inputs for the model are the generated active power, i.e., $u = \mathrm{P}_g$. Under the classical generator model assumptions, the synchronous machine is represented by a constant internal voltage $\mathrm{E}\angle\delta$ behind its direct axis transient reactance X'_d [54]. Therefore, the active power at generator i is

$$\mathrm{P}_{g,i} = \frac{\mathrm{E}_i \mathrm{V}_i}{\mathrm{X}'_{d,i}} \sin(\delta_i - \theta_i) , \tag{5.2}$$

where θ is the generator bus nodal voltage phase angle. The transient reactance is assumed known and constant, whereas a method will be presented later to adaptively infer the parameter E with online data. Also, denote

$$\hat{\mathrm{P}}_{g,i} = \mathrm{P}_{g,i} + \epsilon_i ,$$

where ϵ is assumed to be a zero-mean Gaussian process with a known variance representing the random fluctuations in electricity load on the bus as well as process noise.

[1] Although the swing equation is used here to model generator rotor dynamics, high-order and more complex models, such as the two-axis model [55], can be used. The detection scheme proposed in this work can be developed similarly.

The outputs of the system model are nodal voltage magnitudes and phase angles which PMUs can measure. More importantly, the algebraic output and generator states have to satisfy an active power balance constraint. The constraint stipulates that the net active power at a bus is the difference between the active power supplied to it by the generator and the load consumed, i.e.,

$$\mathrm{P}_i = \mathrm{P}_{g,i} - \mathrm{P}_{l,i}\,, \tag{5.3}$$

for $i = 1, \ldots, N$, subject to a random demand fluctuation ϵ_i as mentioned above. $\mathrm{P}_{l,i}$ is the load on bus i, P_i is the nodal net active power and

$$\mathrm{P}_i = \mathrm{V}_i \sum_{j=1}^{N} \mathrm{V}_j \mathrm{Y}_{ij} \cos(\theta_i - \theta_j - \alpha_{ij})\,, \tag{5.4}$$

following the AC power flow equation of (3.6a) where $\mathrm{Y}_{ij}e^{j\alpha_{ij}}$ are elements of the bus admittance matrix. Note that for load buses $\mathrm{P}_{g,i} = 0, i \in \mathcal{N}_l$ in (5.3). The total active power generated and load demand of the network are assumed to be balanced as well. This relationship will be the basis for the unified outage detection scheme described in the next section.

Define the discrete counterparts of the system model via a first-order difference discretization by Euler's formula, i.e., let $\delta_{k+1} = \delta_{t_{k+1}}$ for $k = 1, 2, \ldots$, and

$$\dot{\delta}_{t_{k+1}} \approx \frac{\delta_{k+1} - \delta_k}{\Delta t}\,.$$

For PMU devices with a sampling frequency of 30 Hz, $\Delta t = t_{k+1} - t_k = 1/30$ s. Thus, the continuous system of a generator bus i can be approximated by

$$\boldsymbol{X}_{i,k+1} = \begin{bmatrix} \delta_{i,k+1} \\ \omega_{i,k+1} \end{bmatrix} = \begin{bmatrix} \delta_{i,k} + \Delta t \omega_s \left(\omega_{i,k} - 1\right) \\ \omega_{i,k} + \frac{\Delta t}{M_i} q_{i,k} - \epsilon_k \end{bmatrix} \tag{5.5}$$

where

$$q_{i,k} = \mathrm{P}_{m,i} - \mathrm{P}_{g,i,k} - D_i \left(\omega_{i,k} - 1\right)$$

for notational brevity, and

$$\mathrm{P}_{g,i,k} = \frac{\mathrm{E}_i \mathrm{V}_{i,k}}{\mathrm{X}'_{d,i}} \sin(\delta_{i,k} - \theta_{i,k})\,. \tag{5.6}$$

Taking a derivative with respect to time t on both sides of (5.3) and rearranging the terms, then

$$\frac{\partial \mathrm{P}_{l,i}}{\partial t} = \frac{\partial \mathrm{P}_{g,i}}{\partial t} - \frac{\partial \mathrm{P}}{\partial t}\,, \tag{5.7}$$

relating the changes in bus load to the changes in active power generated and transferred from the bus. The discretized relationship is then

$$\Delta \mathrm{P}_{l,i,k} = \Delta \mathrm{P}_{g,i,k} - \Delta \mathrm{P}_{i,k}\,, \tag{5.8}$$

where

$$\Delta \mathrm{P}_{l,i,k} = \mathrm{P}_{l,i,k} - \mathrm{P}_{l,i,k-1}\,,$$

and similarly for the other two terms. Writing the whole system in vector form, we also define the N-dimensional output variable

$$\boldsymbol{Y}_k = \Delta \mathbf{P}_k = \Delta \mathbf{P}_{g,k} - \Delta \mathbf{P}_{l,k}\,, \tag{5.9}$$

where $\Delta \mathbf{P}_{l,k}$ represents the random load fluctuations. $\Delta \mathbf{P}_{l,k}$ is assumed to be a zero-mean Gaussian variable with covariance $\sigma^2 \mathbf{I}$. Note that the entries corresponding to load buses in $\Delta \mathbf{P}_{g,k}$ are all zero.

Through (5.9), the active power changes in both generator and load buses can be monitored. In comparison, detection schemes developed in previous works focus on monitoring changes in net active power, $\Delta \mathbf{P}$, through direct current (DC), e.g., [26], or AC, e.g., [12], power flow equations. Their formulations can be considered as special cases of the proposed unified framework when no generator information is available, e.g., no PMUs are installed on generator buses. However, as shown in simulation studies, having generator power output information helps to detect certain outages when net active power changes are not significant enough to trigger an alarm.

(5.5)-(5.9) define a state-space model (SSM) for the power system that could be summarized in the general form below:

$$\boldsymbol{X}_{k+1} = a(\boldsymbol{X}_k, \boldsymbol{u}_k, \boldsymbol{\epsilon}_k) \;\rightarrow f(\boldsymbol{X}_{k+1}|\boldsymbol{X}_k) \tag{5.10a}$$

$$\boldsymbol{Y}_k = b(\boldsymbol{X}_k, \boldsymbol{u}_k, \boldsymbol{\eta}_k) \;\rightarrow g(\boldsymbol{Y}_k|\boldsymbol{X}_k) \tag{5.10b}$$

The dynamics of the unobservable generator states $\boldsymbol{X}$ are governed by the state transition function $a(\cdot)$ as in (5.5). The output $\boldsymbol{Y}$, computable from PMU measurements, is governed by the output function $b(\cdot)$ as in (5.9). Since $b(\cdot)$ is a nonlinear function of the system states, the power system is a nonlinear dynamic system.

As the transition process is stochastic due to random load fluctuations and measurement errors, the states and outputs can be expressed in a probabilistic way. In particular, we denote the state transition density and output density as

$$f(\boldsymbol{X}_{k+1}|\boldsymbol{X}_k = \boldsymbol{x}_k)$$

and

$$g(\boldsymbol{Y}_k|\boldsymbol{X}_k = \boldsymbol{x}_k)\,,$$

respectively, where $f(\cdot)$ and $g(\cdot)$ are probability density functions (PDFs). These two densities play important roles in the particle filter-based state estimaton described later in the chapter. An important consequence of the SSM is the conditional independence of the states and output due to the Markovian structure. In particular, given $\boldsymbol{X}_k$, $\boldsymbol{X}_{k+1}$ is independent of all other previous states; similarly given $\boldsymbol{X}_k$, $\boldsymbol{Y}_k$ is independent of all other previous states.

5.3 EWMA-Based Outage Detection Scheme

A system-wide detection scheme that utilizes the output of the SSM detailed in the previous section is described here. Under an outage-free scenario, the active power generated, transmitted, and consumed in the network are expected to be balanced with only small random load demand fluctuations. Therefore, $\Delta\mathbf{P}_{l,k}$, which represents the instantaneous changes in power demand, is assumed to be normally distributed with mean zero under the baseline condition:

$$\Delta\mathbf{P}_{l,k} = \Delta\mathbf{P}_{g,k} - \boldsymbol{Y}_k \sim N(\mathbf{0}, \sigma^2\mathbf{I})\,. \tag{5.11}$$

After a line outage, there are two ways that the above relationship will be violated. First, the outage-induced topology change means that the line admittance of the tripped line becomes effectively zero; the bus admittance matrix thus changes

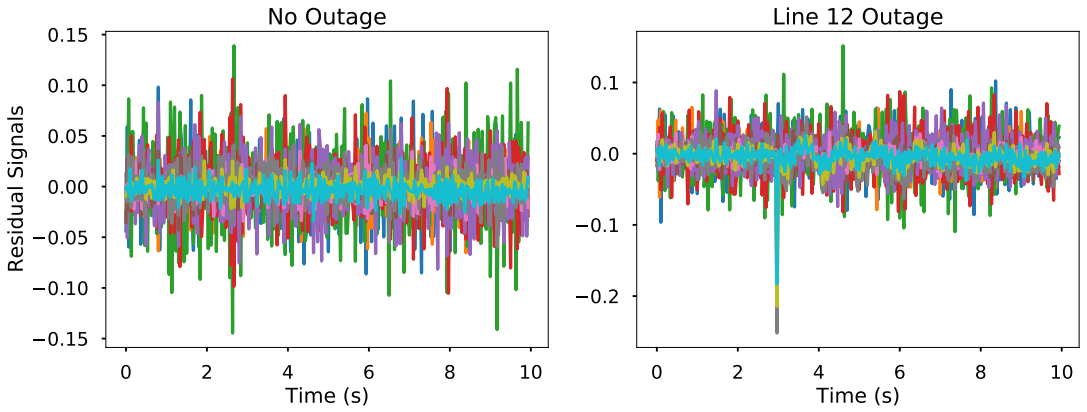

Figure 5.1: *Comparison of the residual signals with no outage and with line 12 outage. A subset of residual signals significantly deviated from the normal mean level and exhibited strong non-Gaussian oscillations after the outage.*

to reflect the post-outage system topology. Therefore, the outage-free AC power flow equation (5.4) used to compute the net active power is no longer valid. Thus $\boldsymbol{Y}_k$ in (5.11) does not represent the actual net active power changes anymore. Second, the outage triggers a period of transient re-balancing in the system where the generators respond to the sudden power imbalance. The immediately affected buses also experience an abrupt change in the net active power due to the outage. As a combination of these effects, the relationship (5.11) will be violated. For example, using data simulated from the IEEE 39-bus test system, Fig. 5.1 shows the signals from a normal system and that with an outage at the third second.

Therefore, the early outage detection problem is formulated as a multivariate process monitoring problem. The multivariate residual signal's significant deviation from the expected distribution indicates an abnormal event, e.g., an outage. For its robustness to non-Gaussian data, superior performance on small to median shifts, and easy of implementation, the multivariate exponentially weighted moving average (MEWMA) control chart, initially developed by [56], is adopted for the detection task. The MEWMA control chart uses an intermediate quantity, $\boldsymbol{Z}_k$, that captures both the current and past signal information from the system. The quantity can be shown to be the weighted average of all past signals with geometrically declining weights. In particular, it can be constructed

with the latest SSM output, $\boldsymbol{Y}_k$, as follows:

$$\boldsymbol{Z}_k = \lambda(\Delta\mathbf{P}_{g,k} - \boldsymbol{Y}_k) + (1-\lambda)\boldsymbol{Z}_{k-1}\,, \tag{5.12}$$

where λ is a pre-defined smoothing parameter that controls the extent of the reliance we would like to put on past information. Also, $0 \leq \lambda \leq 1$ and $\boldsymbol{Z}_0 = \mathbf{0}$. The statistic under monitoring is then constructed similar to that of a Hotelling's T^2 statistic:

$$T_k^2 = \boldsymbol{Z}_k^T \Sigma_{\boldsymbol{Z}_k}^{-1} \boldsymbol{Z}_k\,, \tag{5.13}$$

where the covariance matrix is

$$\Sigma_{\boldsymbol{Z}_k} = \frac{\lambda}{2-\lambda}\left[1-(1-\lambda)^{2k}\right]\sigma^2\mathbf{I}\,.$$

An outage alarm is then triggered when the monitoring statistic crosses a pre-determined threshold, H, chosen to satisfy a certain false alarm rate requirement:

$$D = \inf\{k \geq 1 : T_k^2 \geq H\}\,. \tag{5.14}$$

D is the stopping time of the proposed outage detection scheme. Suppose the onset time of the outage is denoted by t_o, then the difference between the stopping time of the control chart and the onset time is the detection delay, i.e., $D - t_o$. One way of judging the effectiveness of different detection schemes is by comparing their detection delays against various line outage events. An ideal detection scheme is therefore able to detect an outage immediately after it happened, i.e., $D - t_o = 0$.

For MEWMA control charts, it is possible to specify a requirement on the false alarm rate through the selection of λ and H. One way to specify the detection scheme's false alarm rate is through the so-called average run length under zero state (ARL_0), i.e., the average number of signals collected before the above detection threshold is reached under an outage-free scenario. Larger ARL_0s correspond to more lenient false alarm requirements, but possibly longer detection delays. It is also known that small λ values produce control charts more robust against non-Gaussian distributions and have better detection performance for small to medium shifts [53]. Given λ and a false alarm requirement ARL_0,

the detection threshold H can be determined by solving an integral equation of Theorem 2 in [57][2]. The selection of the parameter values and their impact on the detection scheme will be presented in the simulation study section.

5.4 Generator State Estimation via Particle Filtering

In the previous section, a unified framework of real-time system monitoring utilizing post-outage transient dynamics computed from state and algebraic variables, i.e., active power generated and net active power injection, is described. The premise of the unified framework is the availability of accurate state and algebraic variables data. While algebraic variables can be measured by PMUs, generator states are not directly observable. This section shows how the hidden states could be reliably estimated online using a particle filter.

Online state estimation typically involves the inference of the posterior distribution of the hidden states $\boldsymbol{X}_k$ given a collection of output measurements $\boldsymbol{y}_{0:k}$, denoted by $\pi(\boldsymbol{X}_k|\boldsymbol{y}_{0:k})$. This class of marginal state inferences is also known as the filtering problem. When the system can be represented by a linear Gaussian SSM or a finite state-space hidden Markov model, the posterior distribution can be computed in an analytical form using the Kalman technique and Baum-Petrie filter. For systems with nonlinear dynamics and possibly non-Gaussian noises, however, e.g., power systems, the posterior distribution is intractable and cannot be computed in closed form. Extended and unscented Kalman filters have been extensively studied to address the above problem, e.g., [59, 60]. However, these methods' effectiveness becomes questionable when the underlying nonlinearity is substantial or when the posterior distribution is not well-approximated by Gaussian distribution. Instead, PF is increasingly used for this task, e.g., [61], as it handles nonlinearity well and accommodates noise of any distribution with an affordable computational cost [62, 63]. PFs belong to the family of sequential

[2]The equation can be solved using various numerical algorithms or Markov chain approximation, and it be done offline. Interested readers can refer to [58] for a detailed description of the computation procedure required.

Monte Carlo methods where Monte Carlo samples approximate complex posterior distributions, and the distribution information is preserved beyond mean and covariance.

In particular, PF approximates $\pi(\boldsymbol{X}_k|\boldsymbol{y}_{0:k})$ by samples, called particles, obtained via an importance sampling procedure. Each particle is assigned an importance weight proportional to its likelihood of being sampled from the posterior distribution[3]. PF proceeds in a recursive prediction-correction framework. Assuming at time k, the particles and weights obtained from the previous time step are available as:

$$\{(\boldsymbol{x}_{k-1}^i, w_{k-1}^i)\}_{1\leq i\leq n},$$

where n is the number of particles, the posterior distribution at time $k-1$ is approximated by weighted Dirac delta functions as

$$\pi(\boldsymbol{X}_{k-1}|\boldsymbol{y}_{0:k-1}) \approx \sum_{i=1}^{n} w_{k-1}^i \cdot \delta(\boldsymbol{X}_{k-1} - \boldsymbol{x}_{k-1}^i)\,, \tag{5.15}$$

where $\delta(\cdot)$ is the Dirac delta function, and the weights are normalized such that $\sum_{i=1}^n w_{k-1}^i = 1$. The algorithm starts by propagating particles from time $k-1$ to time k through the state transition function in (5.5), i.e., the prediction step. That means, new particles $\{\boldsymbol{x}_k^i\}_{1\leq i\leq n}$ are sampled from the state transition density $f(\boldsymbol{X}_k|\boldsymbol{x}_{k-1}^i)$. The predicted states then have a distribution approximated by

$$\pi(\boldsymbol{X}_k|\boldsymbol{Y}_{0:k-1}) \approx \sum_{i=1}^{n} w_{k-1}^i \cdot \delta(\boldsymbol{X}_k - \boldsymbol{x}_k^i)\,. \tag{5.16}$$

When the new measurement y_k arrives, the above approximation is corrected by updating the particles' weights proportional to their conditional output likelihood to obtain the posterior distribution as

$$\pi(\boldsymbol{X}_k|\boldsymbol{Y}_{0:k}) \approx \sum_{i=1}^{n} w_k^i \cdot \delta(\boldsymbol{X}_k - \boldsymbol{x}_k^i)\,, \tag{5.17}$$

where

$$w_k^i \propto w_{k-1}^i \cdot g(\boldsymbol{y}_k|\boldsymbol{x}_k^i)\,.$$

[3]This type of PF is also known as the bootstrap filter first proposed in [64]. The idea is to use the state transition density as the importance distribution in the importance sampling step. More sophisticated algorithms, such as the guided and auxiliary particle filter could be implemented in the same detection framework proposed here. However, these algorithms are, in general, more difficult to use and interpret. For details, readers can refer to [65].

The intuitive interpretation is that the particles are re-weighted based on their compatibility with the actual system measurement. The approximation of the posterior distribution by these particle-weight pairs is consistent as $n \to +\infty$ at a standard Monte Carlo rate of $\mathcal{O}(n^{-1/2})$ guaranteed by the Central Limit Theorem [65].

A well-known problem of PF is that the weights will become highly degenerate overtime. In particular, the density approximation will be concentrated on a few particles, and all the other particles carry effectively zero weight. A common way to evaluate the extent of this degeneracy is by using the so-called Effective Sample Size (ESS) criterion [66]:

$$\text{ESS} = \left(\sum_{i=1}^{n} \left(w_k^i \right)^2 \right)^{-1} . \tag{5.18}$$

In the extreme case where one particle has the weight of 1 and all others of 0, ESS will be 1. On the other hand, ESS is n when every particle has an equal weight of n^{-1}.

A resampling move can be used to mitigate the degeneracy problem. The central idea is to duplicate particles with higher weights and remove the others, thus focusing computational efforts on regions of higher probability. The systematic resampling method is used in this case as it usually outperforms other resampling algorithms [65]. When ESS falls below a threshold, typically $n/2$, n particles are resampled from the existing ones. The number of offspring, n_k^i, is assigned to each particle $\boldsymbol{x}_k^i$ such that

$$\sum_{i=1}^{n} n_k^i = n \, .$$

The systematic sampling proceeds as follows to select the number of offspring n_k^i. A random number U_1 is drawn from the uniform distribution

$$\mathcal{U} \left[0, n^{-1} \right] .$$

Then a series of ordered numbers are obtained by

$$U_i = U_1 + \frac{i-1}{n} \, ,$$

for $i = 2, \ldots, n$. n_k^i is the number of $U_i \in (\sum_{s=1}^{i-1} w_s, \sum_{s=1}^{i} w_s]$ where $\sum_{s=1}^{0} w_s := 0$ by convention. Finally, resampled particles are each assigned an equal weight n^{-1}

before a new round of prediction-correction recursion begins. The detailed PF algorithm with the resampling move is summarized in Algorithm 1.

5.5 Additional Remarks

5.5.1 Limited PMU Deployment

Many power systems have to work with a limited number of PMUs, i.e., some buses are not equipped with a PMU. The detection scheme proposed here is also applicable in this case since the signal under monitoring, $\boldsymbol{Y}$, can be adjusted to include only buses with PMUs. In particular, $\Delta\mathbf{P}_g$ can include those generator buses with PMUs. $\Delta\mathbf{P}$ can be calculated for load buses with fully observable neighbor buses. The impact of an unobserved neighbor bus on the computation of the bus net active power would be an unknown term, $\mathrm{V}_j\mathrm{Y}_{ij}\cos(\theta_i - \theta_j - \alpha_{ij})$, in the AC power flow equation since the neighbor bus' θ_j and V_j are not available. While this impact can be mitigated through a careful selection of the PMU locations, unlike [26] and [12], the proposed detection scheme is effective when most generator buses are monitored, a result corroborated by the simulation studies in this work, e.g., see Fig. 5.6. Also, the number of generator buses is typically much smaller than the total number of buses.

5.5.2 Unknown System Parameter Estimation

In this work, it is assumed that the system parameters in the power system SSM are known and static; therefore, the PF's state estimation is reliable. In real-world applications, these parameters may be known but slow-varying due to factors like system degradation. While parameter estimation in a non-linear system is generally a difficult problem and outside the scope of this paper, there is a natural extension from the particle filtering framework that can tackle the problem. An online expectation maximization (EM) algorithm based on the particles can be implemented to learn the parameters as data arrives sequentially in real-time. The EM algorithm is an iterative optimization method that finds the maximum likelihood estimates of the parameters in problems where hidden

Algorithm 1 Particle Filter for Generator State Estimation

procedure INITIALIZATION($n, \pi_0(\boldsymbol{X}), \boldsymbol{y}_0$)
  for $i = 1, \ldots, n$ **do**
    Sample $\tilde{\boldsymbol{x}}_0^i \sim \pi_0(\boldsymbol{X})$.
    Compute initial importance weight $\tilde{w}_0^i = g(\boldsymbol{y}_0|\tilde{\boldsymbol{x}}_0^i)$ by output function (5.9).
  end for
  return $\{(\tilde{\boldsymbol{x}}_0^i, \tilde{w}_0^i)\}_{1\leq i\leq n}$
end procedure

procedure FILTERING($n, \{(\tilde{\boldsymbol{x}}_{k-1}^i, w_{k-1}^i)\}_{1\leq i\leq n}, \boldsymbol{y}_k$)
  if ESS $\leq n/2$ **then** ▷ Systematic resampling
    Draw $U_1 \sim \mathcal{U}\left[0, n^{-1}\right]$ and obtain $U_i = U_1 + \frac{i-1}{n}$ for $i = 2, \ldots, n$.
    for $i = 1, \ldots, n$ **do**
      Obtain n_k^i as the number of U_i such that

$$U_i \in \left(\sum_{s=1}^{i-1} w_s, \sum_{s=1}^{i} w_s\right] .$$

      Select n particle indices $j_i \in \{1, \ldots, n\}$ according to n_k^i.
      Set $\boldsymbol{x}_{k-1}^i = \tilde{\boldsymbol{x}}_{k-1}^{j_i}$, and $w_{k-1}^i = 1/n$.
    end for
  else
    Set $\boldsymbol{x}_{k-1}^i = \tilde{\boldsymbol{x}}_{k-1}^i$ for $i = 1, \ldots, n$.
  end if
  for $i = 1, \ldots, n$ **do**
    Predict k_{th} system state by sampling particles via state transition function (5.5): ▷ State prediction

$$\tilde{\boldsymbol{x}}_k^i \sim f(\boldsymbol{X}_k|\boldsymbol{x}_{k-1}^i) .$$

    Update particle weights using current output measurement via output function (5.9): ▷ Weight correction

$$\tilde{w}_k^i = w_k^i \times g(\boldsymbol{y}_k|\tilde{\boldsymbol{x}}_k^i) .$$

  end for
  Normalize weights

$$w_k^i = \frac{\tilde{w}_k^i}{\sum_{k=1}^n \tilde{w}_k^k} , \text{for } i = 1, \ldots, n .$$

  return $\{(\tilde{\boldsymbol{x}}_k^i, w_k^i)\}_{1\leq i\leq n}$
end procedure

variables are present [67]. This basic EM algorithm can be reformulated to perform the estimation online using the so-called sequential Monte Carlo forward smoothing framework when the complete-data density, i.e., $p_\vartheta(\boldsymbol{x}_{0:k}, \boldsymbol{y}_{0:k})$ where ϑ denote the set of unknown parameters, is from the exponential family [68].

5.6 Simulation Study

5.6.1 Simulation Setting

The proposed PF-based outage detection scheme is tested on the IEEE 39-bus 10-machine New England system [51]. System transient responses after an outage are simulated using the open-source dynamic simulation platform COSMIC [43]. The simulation results are assumed to be the true generator states, and corrupted measurements are synthesized from the noise-free simulation data. Ten PMUs are assumed to be installed at bus 19, 20, 22, 23, 25, 33, 34, 35, 36, and 37, covering five generator buses and their connected load buses. Their sampling frequency is assumed to be 30 samples per second. Each simulation runs for 10 seconds, and the outage happens at the third second. A line outage is detected if the monitoring statistic crosses the detection threshold by the end of the simulation. The detection thresholds of all schemes presented are selected by satisfying a false alarm constraint of 1 in 30 days. The global constants are $f_0 = 60$ Hz and $\omega_s = 1.0$ p.u.. For the SSM, state function noise ϵ_k are assumed to be uncorrelated and homogeneous with a standard deviation of $0.01\% \cdot \mathrm{P}_{g,k}$ in (5.5). Output function error $\boldsymbol{\eta}_k$ are assumed to follow a zero-mean Gaussian distribution with a standard deviation of $1\% \cdot (\mathrm{P}_{g,k} - \mathrm{P}_k)$ in (5.9).

5.6.2 Illustrative Outage Detection Example

To illustrate the working of the detection scheme, line 11 outage is used as an example. Fig. 5.2 shows a typical performance of the particle filter used to estimate generator bus states. The rotor angular speed, ω, can be accurately tracked while the rotor angular position, δ, has some biases after the outage. This is acceptable since the focus is on capturing the abnormal changes, i.e., $\Delta\delta$ and in

turn ΔP_g, in response to the outage rather than accurate state estimations. The complete list of state estimation results for all monitored generator buses can be found in Section B.1 of Appendix B. One advantage of the proposed scheme is

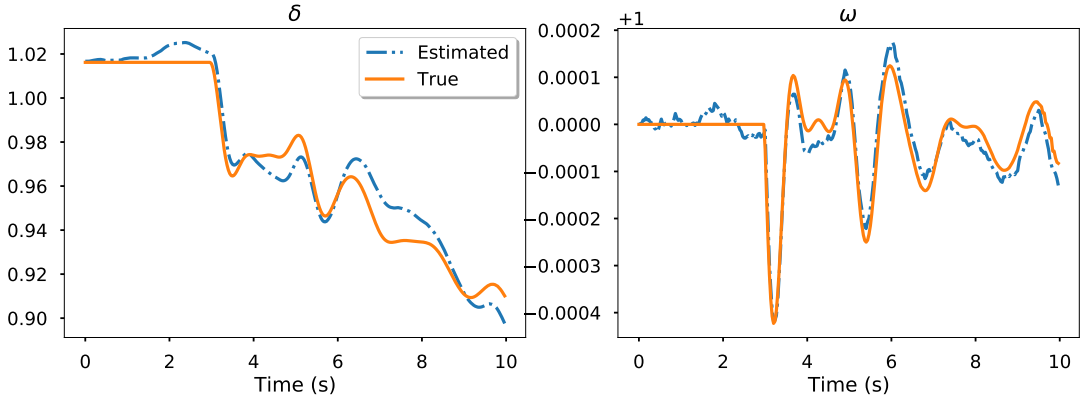

Figure 5.2: *State estimation result of the particle filter on δ and ω of Bus 33. The algorithm can estimate ω accurately, while the estimation of δ has biases after the outage. The changes in δ are sufficiently captured, which are more critical for the detection scheme.*

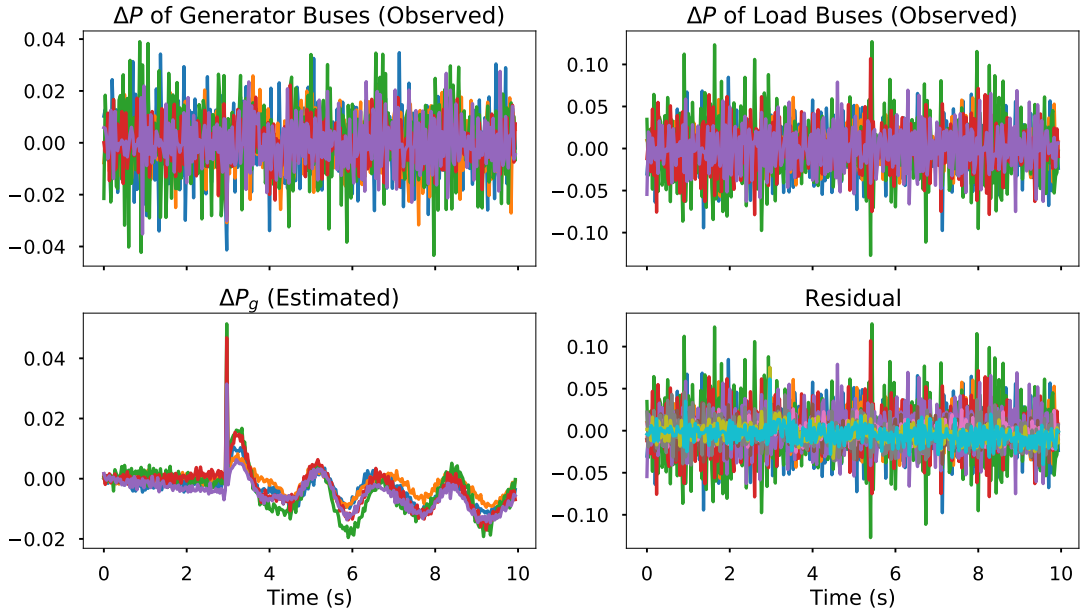

Figure 5.3: *Output signals of the detection scheme for line 11 outage. Each line represents data from a bus equipped with a PMU. Abnormal disturbances in generator rather than load buses contributed to early detection in this case.*

the ability to break down monitored signals and pinpoint the channels leading to

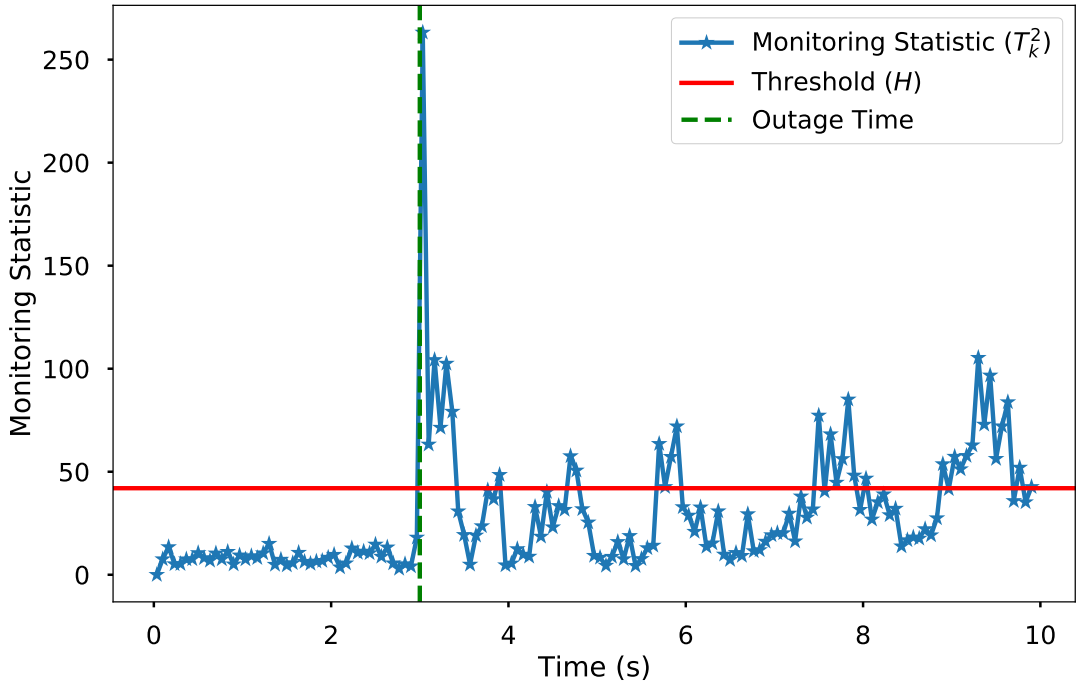

Figure 5.4: *Progression of MEWMA monitoring statistic for detecting line 11 outage. After the outage, the monitoring statistic crosses the detection threshold immediately and remains high afterward. The outage is successfully detected with no detection delay. Points are downsampled to half for clarity*

a detection. Fig. 5.3 shows such a breakdown. The upper two channels are the observable net active power information, and the lower-left one is the estimated generator information. They register different signal strength levels depending on the outage location, e.g., the magnitude of initial shock and the transient oscillation duration. The proposed scheme can detect outages as long as one of them picks up significant changes. It is clear in this case that the signals from PMU measurements do not contribute meaningfully to the detection. Instead, the changes in generated active power on generator buses display significant abnormal fluctuations, leading to the outage detection.

The typical progression of the monitoring statistic, T_k^2, computed via MEWMA from the output signals is shown in Fig. 5.4. Before the outage, the statistic remains close to zero. After the outage at the third second, it increases rapidly and crosses the threshold. Thus, the scheme raises an outage alarm, and no detection delay is incurred. More outage detection and output signal breakdown

examples can be found in Section B.2 of Appendix B. In particular, the results for the scenario of no outage, missed detection, and substantial outage signal are presented.

5.6.3 Results and Discussion

This section presents the result computed from 1000 random simulations of each line outage. It includes the comparison with other state-of-the-art methods, the detection delay over all outage scenarios, the effect of the outage location as well as the impact of the smoothing parameter λ.

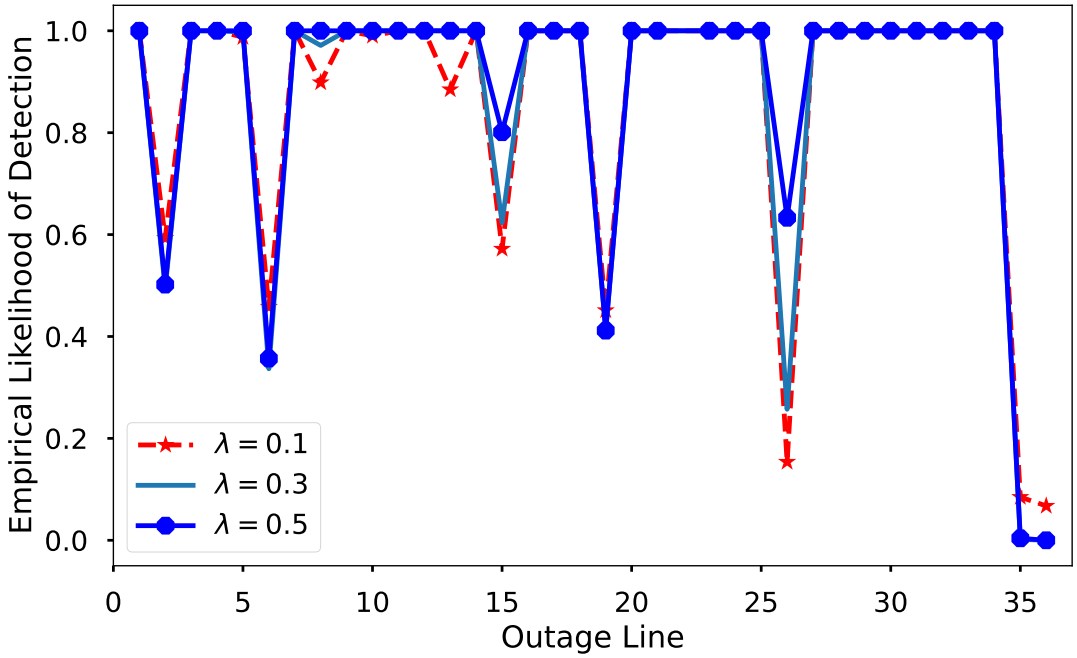

Figure 5.5: *Comparison of the empirical likelihood of detection for all simulated outages under different λs of MEWMA. While 28 out of the 35 line outages can be detected with over 90% likelihood, larger values of λ tend to have a higher detection rate. A small group of outages is difficult to detect regardless of the λ value.*

Detection Rate Fig. 5.5 presents the empirical likelihood of detection for all 35 simulated line outages, which is the percentage of successful detection over 1000 simulations. For both small and large values of λ, the detection scheme can detect 28 out of 35 outages over 90% of the time. In some cases, it can be seen

that larger values of λ tend to have a better detection rate, i.e., line 8, 13, 15, and 26. The reason is that these line outages produce more severe initial shock relative to their after-outage oscillation. Hence, larger values of λ help to capture the immediate shock. Also, a small group of outages is challenging to detect regardless of the λ value, i.e., line 2, 6, 19, 35, and 36. Diagnostic inspection of these cases' output signals reveals that they generally produce weak system disturbances, especially from the generators, hence often not triggering an outage alarm. The weak disturbance might be explained by the fact that these lines are connected to buses that serve zero or small loads.

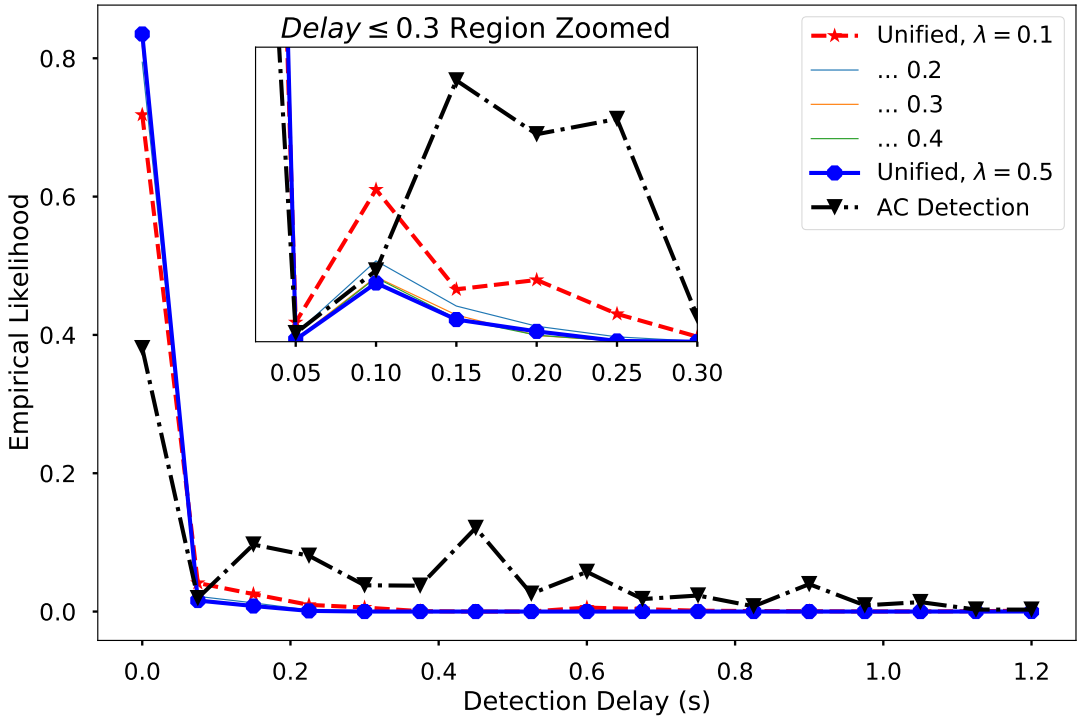

Figure 5.6: *Comparison of the empirical distribution of detection delays in seconds for the proposed unified scheme and the scheme based on AC power flow equations. The proposed scheme has a higher percentage of zero detection delays. It can detect almost all outages within 0.2 seconds, whereas the AC detection scheme does it in 1 second.*

Detection Delay The empirical distribution of the detection delays is presented in Fig. 5.6. The figure shows the results of the proposed scheme with different λ values and the detection scheme based on AC power flow equations from [12].

Intuitively, the scheme is faster at detecting outages when the area under the curve towards the left of the figure is larger. In this case, the proposed scheme has a much higher chance of detecting outages with zero detection delay than the AC scheme. The best-performing scheme ($\lambda = 0.5$) also detects most outages within 0.2 seconds, whereas the AC scheme detects most outages within 1 second.

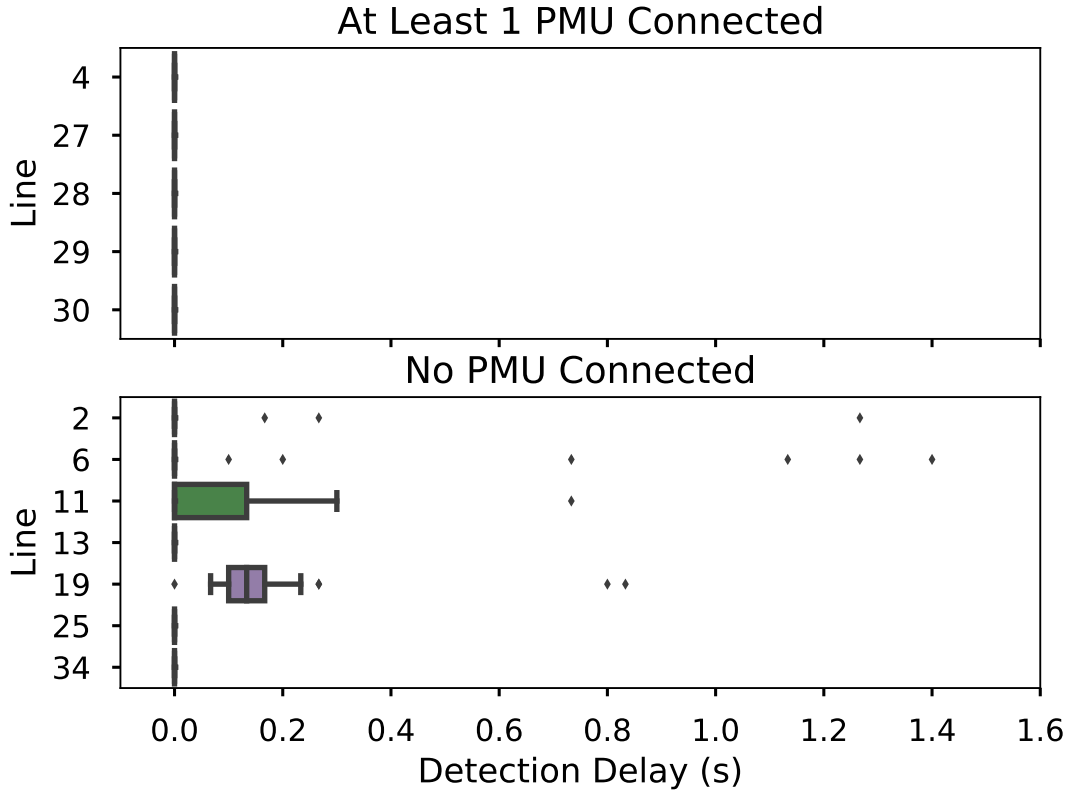

Figure 5.7: *Box plot of the empirical distributions of detection delays in seconds for lines with at least 1 PMU nearby and those without a PMU.*

Effect of Outage Location Relative to the PMUs In some related work and Chapter 4 of this thesis, significant variations of average detection delays for outages at different lines relative to the PMU locations can be observed. Fig. 5.7 shows a comparison of detection delays for outage lines with at least one PMU connected to it versus those with no PMU nearby. Since only ten buses are equipped with PMUs, most lines belong to the second group[4]. While outages at

[4]Only a few lines in the second group are presented due to space constraints. All of those omitted line outages can be detected with zero mean detection delay, except for line 35, and 36,

line 11 and 19 are often detected with 0.1-second delay, most outages are detected immediately regardless of the relative position to the PMUs. Line 11 connects to the slack bus, and its outage creates a minimal disturbance in all three output channels. This result demonstrates the spatial advantage of the proposed method and its robustness to the outage locations.

Table 5.1: Detection Delay (s) Comparison of Different Detection Schemes

	Average Detection Delay[5]			
Line	DC - full	Subspace - full	AC	Unified
2	1.165 (0.006)	2.822 (1.924)	0.283 (0.263)	**0.012** (0.183)
6	–	3.060 (2.011)	0.246 (0.129)	**0.052** (0.463)
11	**0** (0)	3.048 (1.969)	0.602 (0.205)	0.058 (0.077)
15	**0** (0)	2.634 (1.850)	0.005 (0.034)	**0** (0)
19	–	2.836 (2.018)	0.335 (0.378)	**0.160** (0.315)
26	–	2.850 (1.958)	0.385 (0.228)	**0** (0)

Comparison with Other Methods The proposed method's performance is also compared with three other methods in Table 5.1. The chosen outages are, in general, more difficult to detect. The first method for comparison is based on the DC power flow model from [26] and the second based on subspace identification from [18]. Both of them are tested using a full PMU deployment. The third is from the method proposed in Chapter 4 that relies on the AC power flow model where 10 PMUs are assumed to be installed at locations used in [12]. The thresholds for all methods are selected by satisfying a false alarm constraint of 1 in 30 days. The average detection delays and their standard deviations are computed from 1000 random simulations, while a dash means a missed detection. The method proposed, "Unified", is consistently faster at detecting outages than the other methods.

which are often undetected.

[5]One standard deviation appears in ().

5.7 Conclusion

In this chapter, a unified framework of online transmission line outage detection is proposed. The framework utilizes information from both generator machine states and load bus algebraic variables. The signals are obtained through nonlinear state estimation of particle filters and direct measurements of PMUs. They are effectively used for outage monitoring and detection by MEWMA control charts while meeting a particular false alarm criterion. The approach is shown to be quicker at detecting outages and more robust to a priori unknown outage locations under a limited PMU deployment through an extensive simulation study. Further research can be done to improve the detection scheme's effectiveness by investigating the optimal installation location of limited PMUs given a network of power stations. Also, it is observed that a group of lines is consistently challenging to detect regardless of the detection schemes or parameter designs used. More work needs to be done in this area so that these detection blind spots could be reduced.

Chapter 6

Multiple-line Outage Identification via Sparse Regression

6.1 Introduction

Rapid disruption detection and accurate localization are needed to facilitate the recovery of power systems following a disruption, e.g., line outage. The previous two chapters detail two frameworks of detecting line outages as fast as possible. In this chapter, the problem of identifying true outage lines after a detection alarm has been raised is investigated.

There are two main challenges to accurate outage identification. The first is limited observability. One must consider a limited PMU deployment in the system when designing an outage identification scheme [11]. The proposed scheme, therefore, has to maximize its performance under the constraint of limited observability. The second challenge is the identification scheme's scalability, giving the inherent combinatorial nature of potential outage locations. For example, the search space consists of 2^L outage location combinations for a system with L transmission lines.

This chapter describes a new framework of multiple-line outage identification based on power system sensitivity analysis and sparse regression methods considering line diagnosabilities. A signature map of line outages based on AC power flow sensitivity analysis is built in advance using readily available system topology and parameter information. The outage identification problem is then formulated

into an underdetermined sparse regression problem that accommodates any a priori unknown number of simultaneous line outages. Crucially, clusters of lines whose outages are indistinguishable under a given PMU placement are identified and augmented with the initial result to improve identification accuracy.

The contributions of this chapter's research work can be summarized in three aspects: (1) This work improves the state-of-the-art multiple-line outage identification performance under limited PMU deployment; (2) The novel sparse regression formulation accommodates an unknown number of outage lines and is robust with noisy data; (3) A new way to account for indistinguishable outages is proposed using minimal diagnosable clusters, significantly improving overall identification accuracy.

The rest of this chapter is organized as follows. The basis for outage identification is the post-outage voltage angle signature and is derived in Section 6.2. A multiple-line outage identification scheme is then described in Section 6.3. Section 6.5 demonstrates the effectiveness of the proposed scheme compared to existing ones. The conclusion and future research directions are summarized in Section 6.6.

6.2 Phase Angle Signature of Outages

Each outage is different. Machine learning-based approaches let algorithms learn the difference through clever training and generalizable data. Physics-informed approaches, e.g., the proposed method, leverage physical laws governing power systems to find out the difference instead. In general, two questions need to be answered to build an effective physics-informed outage identification scheme: (1) How to quantify the impact of each line outage on nodal bus state variables? (2) Given the characterization, how to identify the most probable outage lines out of all possible ones? This section addresses the first question through sensitive analysis of the AC power flow model. In the next section, an efficient and robust identification scheme is developed.

6.2.1 Power Flow Model

Consider a power system with N buses and L transmission lines where $\mathcal{N} = \{1, 2, \ldots, N\}$ and $\mathcal{L} = \{1, 2, \ldots, L\}$. The AC power flow model of (3.6) is the governing equation between active and reactive power injection (P, Q) and voltage phasor (V$\angle\theta$) at each bus. V_m and θ_m are assumed to be observable if bus m has a PMU. Let $\mathbf{P}$, $\boldsymbol{\theta}$, and $\mathbf{V}$ represent the vectors of active power injections, voltage angles, and magnitudes at all buses[1]. A sensitivity analysis on power injections by linearization of the active power flow equation (3.6a) around a pre-outage steady-state operating point yields the following partial differential equation:

$$\Delta\mathbf{P} \approx J_1 \Delta\boldsymbol{\theta} + J_2 \Delta\mathbf{V}\,, \tag{6.1}$$

where J_1, J_2 are two submatrices of the AC power flow Jacobian with

$$J_1 = \frac{\partial \mathbf{P}}{\partial \boldsymbol{\theta}}\,, J_2 = \frac{\partial \mathbf{P}}{\partial \mathbf{V}}\,. \tag{6.2}$$

Let

$$\Delta\mathbf{P} = \mathbf{P}' - \mathbf{P}\,,$$

where $\mathbf{P}$ and $\mathbf{P}'$ denote pre- and post-outage bus power injections and similarly define

$$\Delta\boldsymbol{\theta} = \boldsymbol{\theta}' - \boldsymbol{\theta}\,.$$

In the usual operating range of relatively small angles, power systems exhibit much stronger interdependence between $\mathbf{P}$ and $\boldsymbol{\theta}$ as compared to $\mathbf{P}$ and $\mathbf{V}$ [44]. Therefore, it is sufficient to focus on the relationship between real power injection and voltage phase angle, i.e., J_1, in the remainder of this chapter[2]. Redefining J_1 as J, the off-diagonal and diagonal elements of J can be derived from (3.6a) and are detailed in (4.4). Therefore, an AC power flow-based relationship is established between instantaneous real power injection changes and voltage phase angle changes as

$$\Delta\mathbf{P} = J\Delta\boldsymbol{\theta}\,.$$

[1]By convention, bus 1 is assumed to be the reference bus whose voltage phase angle is set to 0° and magnitude to 1.0 per unit (p.u.).

[2]The same set of analysis can applied to reactive power and voltage magnitude as well, which is omitted here. Some details about power system linearization are also skipped as the formulation is standard. Interested reader can refer to Section II of [12].

Inverting the Jacobian matrix, the relationship can be written as:

$$\Delta\boldsymbol{\theta} = J^{-1}\Delta\mathbf{P}\,. \tag{6.3}$$

Therefore, given a unit change of real power injections, J^{-1} in (6.3) quantifies the associated impact on system-wide bus voltage angles.

6.2.2 Outage Signature Map

We can break down the $\Delta\mathbf{P}$ term in (6.3) in order to establish a "dictionary" of phase angle changes specific to each line outage. Under the DC assumptions specified in Section 4.2.1 of Chapter 3, a neat way to characterize the impact of an outage at line l carrying power $\tilde{p}_l$ from bus i to j is a real power injection of p_l at bus i and withdrawal of $-p_l$ at bus j [69]. The constant p_l can be determined by

$$p_l = \frac{-\tilde{p}_l}{1 + PTDF_{l,i,j}}\,,$$

where $PTDF_{l,i,j}$ is the so-called power transfer distribution factor that depends on the pre-outage power flow on line l, the sending bus location i, and the receiving bus location j [70]. The factor is a sensitivity measure of how a change in a line's status affects the flows on other lines in the system. Equivalently, the change in real power injection due to an outage at line l can be written as:

$$\Delta\mathbf{P} = p_l \cdot \mathbf{a}_l\,,$$

where $\mathbf{a}_l$ is an N-vector of zeros except with 1 at the i_{th} and -1 at the j_{th} position. In general, the expected change in phase angles due to all outages at line $l, l \in \mathcal{L}$ can be obtained. Let

$$\boldsymbol{p} = [p_1, p_2, \ldots, p_L]^\top$$

denote the vector of power transfers of all transmission lines. Then by putting the p_l and m_l for all transmission lines together, an angle signature map of all line outages can be written in matrix form:

$$\begin{aligned}[\Delta\boldsymbol{\theta}] &= J^{-1}\begin{bmatrix} p_1\mathbf{a}_1 & p_2\mathbf{a}_2 & \cdots & p_L\mathbf{a}_L \end{bmatrix} \\ &= J^{-1}\begin{bmatrix} \mathbf{a}_1 & \mathbf{a}_2 & \cdots & \mathbf{a}_L \end{bmatrix}\operatorname{diag}(\boldsymbol{p}) \\ &= J^{-1}A\operatorname{diag}(\boldsymbol{p})\,, \end{aligned} \tag{6.4}$$

where A is the $N \times L$ bus to branch incidence matrix defined in Section 3.1 with columns corresponding to lines and rows to buses. $\text{diag}(\boldsymbol{p})$ is the diagonal matrix with individual line power transfer p_l on the diagonal.

In a realistic setting of limited PMU deployment, it is assumed that there are fewer PMUs than buses and transmission lines, i.e., $K \leq N$ and $K \leq L$. Define a bus selection matrix $S \in \{0,1\}^{K \times N}$ that selects rows of buses with PMUs, the observable phase angle impact from all line outages is

$$\begin{aligned}[\Delta\boldsymbol{\theta}]_I &= SJ^{-1}A\,\text{diag}(\boldsymbol{p}) \\ &= F\,\text{diag}(\boldsymbol{p})\,, \end{aligned} \tag{6.5}$$

where F is defined by

$$F = SJ^{-1}A\,. \tag{6.6}$$

Therefore, F is a $K \times L$ outage signature map determined by PMU locations, system operating states, and topology. Each column of F, i.e., $F_l, \ell \in \mathcal{L}$ represents the incremental effect of line l outage on all bus voltage angles captured by PMUs. Fig. 6.1 shows an example of F for 19 PMUs randomly placed on the New England 39-bus system, using J^{-1} obtained from steady-state bus voltages. The signature map captures the varying degree of impact each line outage has on PMU-equipped buses. Outages of some lines might not be uniquely identified because they create similar phase angle responses, e.g., line 10 and 11, line 32 and 33. The map also suggests that some line outages create a minimal impact that might be indistinguishable from normal conditions, e.g., line 37 or line 41. While distinctive signatures from the map should help identify outage lines, indistinguishable line outages must be addressed to exploit the signature map information fully.

6.3 Outage Identification Scheme

After a single- or multiple-line outage, the signature map developed in the previous section provides a basis for accurate outage identification. The outage event is assumed to be detected quickly using a detection scheme, e.g., of [12] or [15]. The multiple-line outage identification problem is first formulated as a

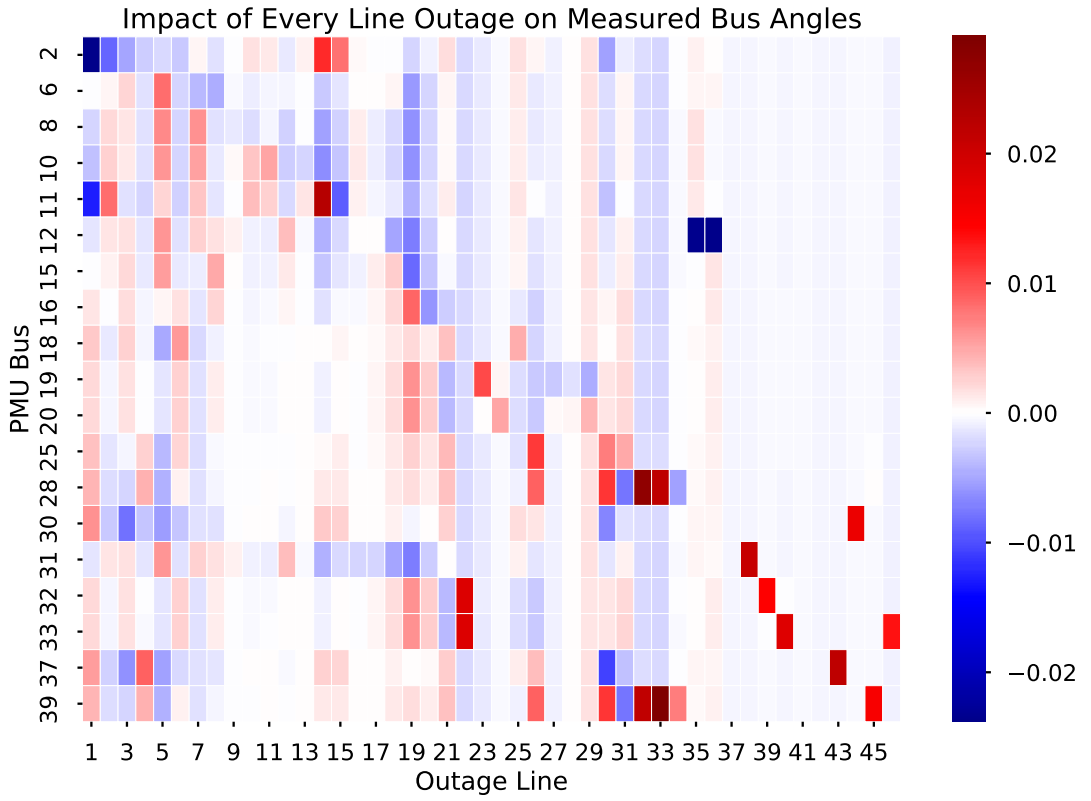

Figure 6.1: *An example of the* 19×46 *signature map constructed using a random placement of 19 PMUs in the New England 39-bus system with 46 transmission lines. Each column corresponds to a single line outage and its incremental impact on PMU-equipped bus voltage phase angles.*

sparse regression problem. Then, a method to address indistinguishable outages is proposed to further improve the outage line identification accuracy.

6.3.1 Identification by Sparse Regression

Suppose an outage of s line happen at $\{l_i, i = 1, \ldots, s, i \in \mathcal{L}\}$ and the size is relatively small, i.e., $s \ll L$. Let $\boldsymbol{\beta}$ be an L-vector with all zeros except at $\boldsymbol{\beta}_{l_i}$ with value p_{l_i} for $i = 1, \ldots, s$. If the outage model in Section 6.2 holds, then

$$\begin{aligned} \Delta\boldsymbol{\theta} &= SJ^{-1}(\mathbf{a}_{l_1}p_{l_1} + \cdots + \mathbf{a}_{l_s}p_{l_s}) + \boldsymbol{\epsilon} \\ &= SJ^{-1}A\boldsymbol{\beta} + \boldsymbol{\epsilon} \\ &= F\boldsymbol{\beta} + \boldsymbol{\epsilon}\,, \end{aligned} \tag{6.7}$$

where $\boldsymbol{\epsilon}$ is a Gaussian noise term with mean zero and known variance $\sigma^2\mathbf{I}_{K\times K}$, representing the measurement error of K PMUs. Hence, non-zero entries, or support, of the power transfer vector $\boldsymbol{\beta}$ reveal true outage locations. Given the signature map F and PMU measurements $\Delta\boldsymbol{\theta}$, $\boldsymbol{\beta}$ can be estimated from the above relationship by minimizing the squared-error loss, subject to the outage size constraint as

$$\begin{aligned} &\min_{\boldsymbol{\beta}\in\mathbb{R}^L} \|\Delta\boldsymbol{\theta} - F\boldsymbol{\beta}\|_2^2 \,, \\ &\text{s.t. } \|\boldsymbol{\beta}\|_0 = s \,, \end{aligned} \tag{6.8}$$

where $\|\cdot\|_2^2$ is the square of the ℓ_2 norm and $\|\cdot\|_0$ is the number of non-zero entries of a vector. However, as the location of the non-zero entries are not known a priori, the above formulation presents a challenging combinatorial optimization problem. Methods such as exhaustive search, forward-stepwise regression or mix integer optimization could be used to solve the problem [71]. However, compared to shrinkage method, in particular, lasso, they are computationally more intensive, thus not suitable for real-time application in realistic power systems [72].

Lasso was originally proposed in [73] and has since been used in various applications for ease of implementation, robustness to noise, and the ability to shrink some coefficients to exactly zero, thus recovering true support of the vector. Lasso solves a relaxed version of the problem in (6.8) by replacing the ℓ_0 constraint with an ℓ_1 constraint:

$$\begin{aligned} &\min_{\boldsymbol{\beta}\in\mathbb{R}^L} \|\Delta\boldsymbol{\theta} - F\boldsymbol{\beta}\|_2^2 \,, \\ &\text{s.t. } \|\boldsymbol{\beta}\|_1 \leq s \,, \end{aligned} \tag{6.9}$$

and equivalently in Lagrangian form:

$$\min_{\boldsymbol{\beta}\in\mathbb{R}^L} \left\{ \|\Delta\boldsymbol{\theta} - F\boldsymbol{\beta}\|_2^2 + \lambda\|\boldsymbol{\beta}\|_1 \right\}, \tag{6.10}$$

where $\|\cdot\|$ is the ℓ_1 norm and λ is a regularization parameter that has a one-to-one correspondence to s for solutions of (6.9) and (6.10). Larger values of λ impose stronger regularization on $\boldsymbol{\beta}$, whereas if $\lambda = 0$, the lasso solution $\hat{\boldsymbol{\beta}}$ is the same

as the least squares estimate. According to [74], given a fixed F, there exists a finite sequence,

$$\lambda_0 > \lambda_1 > \cdots > \lambda_Q = 0\,, \tag{6.11}$$

such that (1) for all $\lambda > \lambda_0$, $\hat{\boldsymbol{\beta}} = \mathbf{0}$, (2) the support of $\hat{\boldsymbol{\beta}}$ does not change with λ for $\lambda_q < \lambda < \lambda_{q+1}\,, q = 0, \ldots, Q-1$. These λ_q's are called transition points as the support in lasso solution changes at each λ_q. Often, λ is selected according to some parameter tuning scheme, e.g., cross validation, such that the resultant regression model achieves best prediction accuracy. However, the objective of this research work is to uncover the true support of $\boldsymbol{\beta}$, which might change for each instance of outage. Thus, lasso solutions at various transition points need to be obtained each time an outage is detected to ascertain the location, and in effect the number, of outage lines.

Least angle regression (LARS), originally proposed by [75], with lasso modification is an efficient algorithm that computes the entire lasso path with a complexity of least squares regression. Briefly, starting with coefficients of zero, LARS identifies the first variable as the one most correlated with the response, e.g., $\Delta\boldsymbol{\theta}$. As the coefficients of the active variables move toward their least squares estimates, a new variable becomes active when its correlation with the residual "catches up" with the active set. These changes happen at the transitions points of (6.11) and variables enter one at a time [75]. The process is stopped after Q steps and in general $Q = \min\{K-1, L\}$ for standardized data unless otherwise specified.

Assuming $\Delta\boldsymbol{\theta}$, its mean $\Delta\bar{\boldsymbol{\theta}}$, signature map F, and the maximum number of non-zero entries Q are provided, LARS can produce a sequence of regularization parameters λ^q and the associated lasso solution $\boldsymbol{\beta}^q$ to (6.10) as described in Algorithm 2. Indices of significantly non-zero entries of $\boldsymbol{\beta}^Q$ are then identified as potential outage locations. Fig. 6.2 shows an example of the lasso path computed using LARS for a double-line outage event. The final $\boldsymbol{\beta}$ has five non-zero coefficients after five transitions. The scheme correctly identifies line 17 and 25 as they have significantly non-zero estimated coefficients compared to the others. The third-highest coefficient corresponds to line 38 which is a

Algorithm 2 Least Angle Regression with Lasso Modification

Input: $\Delta\boldsymbol{\theta}, \Delta\bar{\boldsymbol{\theta}}, F, Q$

Output: Lasso solution path $\{\lambda_q, \boldsymbol{\beta}^q\}_{q=0}^{Q}$

1: Standardize columns of F to mean zero and unit ℓ_2 norm. Set $\boldsymbol{\beta}^0 = (\beta_1, \beta_2, \ldots, \beta_L) = \mathbf{0}$. Let $r_0 = \Delta\boldsymbol{\theta} - \Delta\bar{\boldsymbol{\theta}}$.

2: Get first active column:

$$j = \arg\max_{i \in \mathcal{L}} |\langle r_0, F_i \rangle| .$$

Let $\lambda_0 = |\langle r_0, F_j \rangle|$. Define $\mathcal{A} = \{j\}$ and $F_{\mathcal{A}}$ as the active set and signature matrix with columns from the set.

3: **for** $q = 1, 2, \ldots, Q$ **do**

4: Get current least-squares direction: $\delta = \frac{1}{\lambda_{q-1}}(F_{\mathcal{A}}^{\top} F_{\mathcal{A}})^{-1} F_{\mathcal{A}}^{\top} r_{q-1}$. Define L-vector $\mathbf{u}$ such that $\mathbf{u}_{\mathcal{A}} = \delta$ and zero everywhere else.

5: Move coefficients toward least-squares estimate: $\boldsymbol{\beta}(\lambda) = \boldsymbol{\beta}^{q-1} + (\lambda_{q-1} - \lambda)\mathbf{u}$, for $0 < \lambda \leq \lambda_{q-1}$ while maintaining $r(\lambda) = \Delta\boldsymbol{\theta} - F\boldsymbol{\beta}(\lambda)$. Drop any element of $\mathcal{A}$ if the corresponding coefficient crosses 0 and recompute the least-squares estimate.

6: Identify the largest λ at which $|\langle r(\lambda), F_l \rangle| = \lambda$ for $l \notin \mathcal{A}$. Let $\lambda_q = \lambda$, the new transition point.

7: Suppose the new active column has index j. Update $\mathcal{A} = \mathcal{A} \cup j$, $\boldsymbol{\beta}^q = \boldsymbol{\beta}(\lambda_q) + (\lambda_{q-1} - \lambda_q)\mathbf{u}$, and $r_q = \Delta\boldsymbol{\theta} - F\boldsymbol{\beta}^q$.

8: **end for**

9: Return the sequence $\{\lambda_q, \boldsymbol{\beta}^q\}_0^Q$.

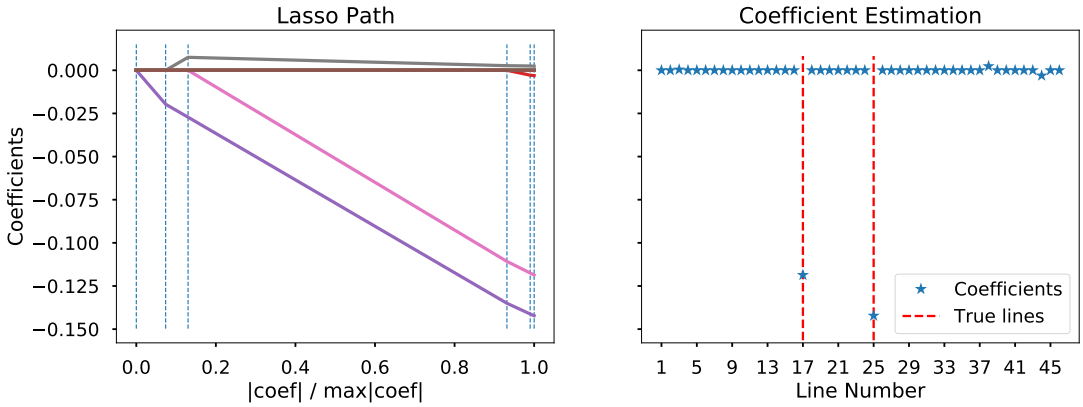

Figure 6.2: *Lasso path via LARS illustration for double-line outage at line 17 and 25. Complete lasso regularization path is shown on the left and coefficient estimation after five candidates entered the model on the right.*

neighbor of line 17 that likely produces similar outage response. It enters the model before line 17 does. However its coefficient is overtaken by that of line 17 as they increase towards the least squares solution, giving the correct final identification result.

6.3.2 Indistinguishable Line Outages

As seen from the signature map of Fig. 6.1, some outages create highly similar responses from the system, i.e.,

$$F_i \approx F_j$$

for some $i, j \in \mathcal{L}$. In general, this ambiguity problem is commonly encountered in realistic systems [13]. One reason is that some line outages do indeed create similar responses due to a combination of topological positions and pre-outage power flow carried. On the other hand, a limited PMU deployment might mean distinctive signatures of some outages are not observable. Intuitively, the second situation is more pronounced as the PMU budget decreases. It is also well-known that with a group of highly correlated predictors, the lasso formulation of (6.10) tends to select one from the group and does not care which one to select [76]. In the extreme case where $F_i = F_j$ for some $i, j \in \mathcal{L}$ and $\hat{\boldsymbol{\beta}}$ is the lasso solution, it can be shown that $\hat{\beta}_i \hat{\beta}_j \geq 0$ and $\hat{\boldsymbol{\beta}}^*$ is another solution of (6.10) where

$$\hat{\beta}_k^* = \begin{cases} \hat{\beta}_k \,, k \neq i, k \neq j \\ (\hat{\beta}_i^* + \hat{\beta}_j^*) r \,, k = i \\ (\hat{\beta}_i^* + \hat{\beta}_j^*)(1-r) \,, k = j \,, \end{cases} \tag{6.12}$$

for some $r \in [0, 1]$ and $k \in \mathcal{L}$. Therefore, lasso might not have a unique solution when predictors are highly correlated.

In the context of the identification problem under study, the true outage line, e.g., i, might not be correctly identified if $F_i \approx F_j$, and equivalently their correlation is close to 1,

$$\begin{aligned} \text{corr}(p_i F_i, p_j F_j) &= \text{corr}(F_i, F_j) \\ &\approx 1 \end{aligned}$$

for some $i, j \in \mathcal{L}$. This work proposes to group transmission lines into minimal diagnosable clusters (MDCs) to address this ambiguity problem. Each MDC contains lines that, given a fixed PMU placement, produce responses that the proposed lasso formulation could not distinguish with a high probability. Concretely, a MDC is defined as a group of lines whose observable outage effects have pairwise correlations higher than a pre-defined threshold ρ^*. Therefore, the MDC of line i is

$$g_i = \{i\} \cup \{j : \text{corr}(F_i, F_j) \geq \rho^*\}, \tag{6.13}$$

for $j \in \mathcal{L} \setminus i$. The collection of MDCs for all transmission lines is

$$G_F = \{g_1, g_2, \ldots, g_L\}. \tag{6.14}$$

Fig. 6.3 shows a heatmap of the correlation between each column of F of the previously mentioned 19-PMU placement on 39-bus system. Only correlations higher than 0.9 are plotted. It can be seem that some groups of lines have close to correlation of 1, e.g., line 1 and 2, line 32, 33, and 34.

Also, the diagnosability of a system with given PMU locations can be characterized by the proportion of single-element MDCs,

$$V(\rho^*) = \left(\sum_{i=1}^{L} \mathbf{1}(|g_i| = 1) \right) / L,$$

where $\mathbf{1}(\cdot)$ is indicator function and $|g|$ counts the number of elements in the set g. Intuitively, a smaller ρ^* corresponds to a more relaxed correlation requirement to enter the MDC, therefore in general decreases $V(\rho^*)$ and vice versa. With MDCs constructed offline, they can augment the lasso solution in real-time outage identification. Suppose $L_o = \{l_i^*, i = 1, \ldots, s\}$ are identified by lasso as outage lines. The augmented solution set would be

$$L_o^* = \{g_{l_1^*} \cup g_{l_2^*} \cup \cdots \cup g_{l_s^*}\}. \tag{6.15}$$

With MDC augmentation, outage identification accuracy is improved, however, potentially at the expense of identification precision. The trade-off is influenced by both the correlation threshold ρ^* and the diagnosability of the system. Note that if every MDC of the identified lines contain only a single element, i.e., the

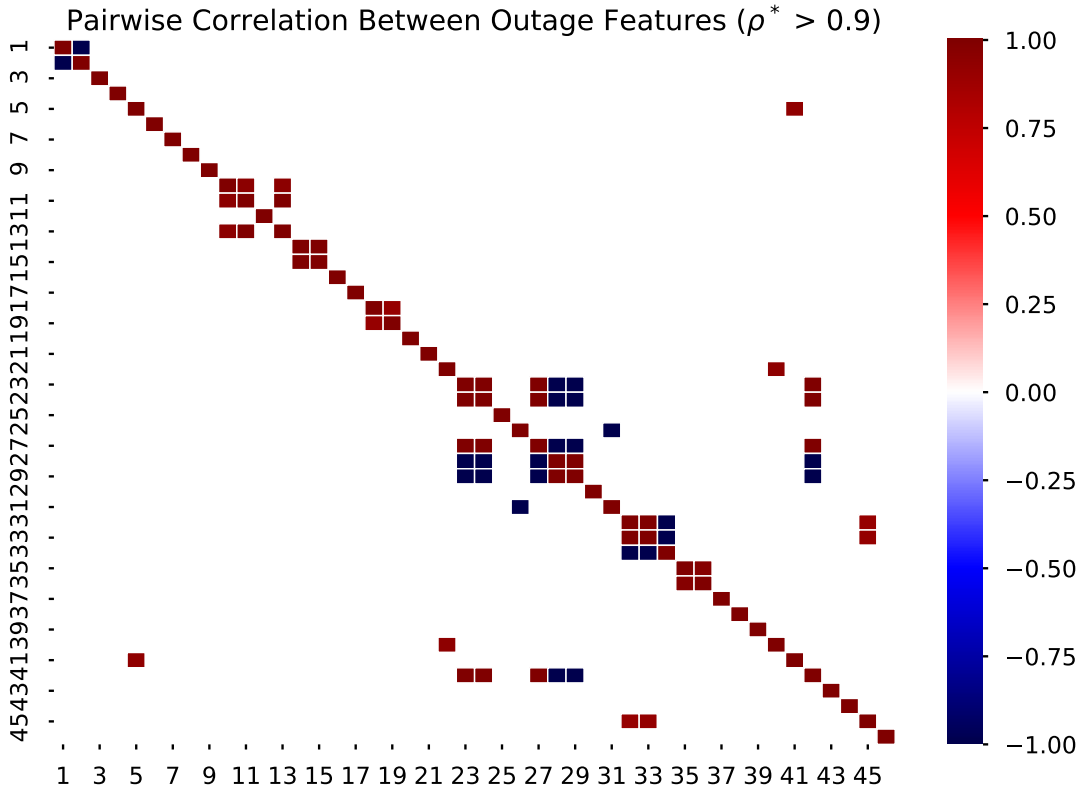

Figure 6.3: *Heatmap of pairwise correlation between columns of the signature map constructed from a random placement of 19 PMUs on the 39-bus system. Only correlations higher than 0.9 are plotted.*

line itself, then $L_o^* = L_o$. The impact of the correlation threshold on identification accuracy-precision trade-off is investigated further in simulation study of Section 6.5.

To end this section, Fig. 6.4 presents a summary of the proposed identification scheme. The scheme is split into an offline and online part. Preparation work of step one to three could be done offline since they only require quasi-steady-state information and baseline system parameters. Once the signature map and MDCs are constructed, they could be used in real-time monitoring operations as in step four to six.

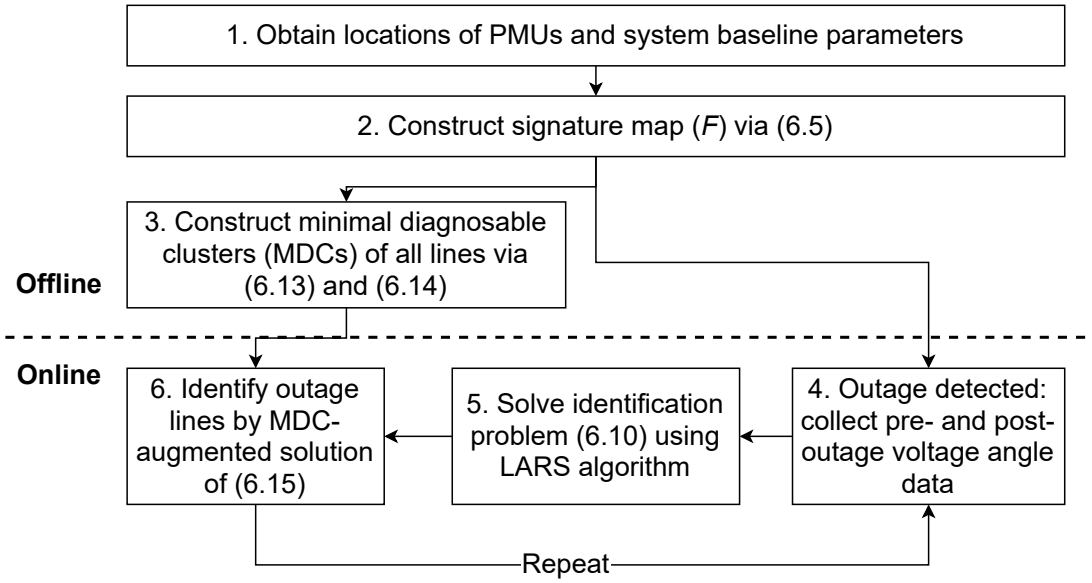

Figure 6.4: *Framework of the proposed line outage identification scheme. Preparation steps one to three can be performed offline while outage identification steps four to six can be carried out during real-time monitoring operations.*

6.4 Additional Remarks

6.4.1 Comparison with Close Works

The idea of constructing expected angle change based on power injection to identify outage lines is not new [13, 14, 23]. Separately, authors in [40] and [42] have also formulated outage identification as a sparse vector recovery problem. However, the proposed method is different in the following aspects: 1) All except [14] have relied on the simplified DC power flow model by assuming a flat voltage profile and approximately identical phase angles. The outage signature map is derived from the AC power flow model, reflecting the heterogeneous operating condition of power systems. 2) All except [13] do not consider the impact of indistinguishable outage events on identification performance. Whereas Wu *et al.* conduct an online search for indistinguishable outage locations, the proposed MDCs are constructed in advance and incur no extra computation during real-time identification. 3) Enriquez *et al.* use both voltage and current phasor for identification, while the proposed method only requires voltage measurements

[14]. Performance of a sparse regression-based [40] and an AC power flow-based method [14] are compared in the simulation study.

6.4.2 Optimal PMU Placement

While outside the scope of this work, it has been observed that the locations of the PMUs influence the identification accuracy [77]. Intuitively, the signature map constructed in Section 6.2.2 suggests that an optimal PMU placement should capture as much distinctive outage impact as possible in order to reduce ambiguities in identification. Pairwise correlation between columns of the design matrix of an underdetermined sparse regression problem is closely related to the study of signal reconstruction in compressive sensing. In particular, the condition on the design matrix that guarantees the recovery of the unknown coefficient vector is a function of the maximum of all pairwise absolute correlations [78]. This suggests that F could be optimized in some way regarding its pairwise column correlations to improve the diagnosability of all line outages. Using a genetic algorithm, an optimal placement of 19 PMUs, i.e., 50% coverage, is generated and the correlation heatmap of the corresponding signature map is shown in Section C.1 of Appendix C. Highly correlated pairs of outage lines are significantly reduced compared to the random placement.

6.5 Simulation Study

6.5.1 Simulation Setting

The proposed identification scheme is tested on the IEEE 39-bus New England test system [51]. System transient responses following an outage are simulated using the open-source simulation package COSMIC [43], in which a third-order machine model and AC power flow model are used. The sampling frequency of a PMU is assumed to be 30 samples per second. For each simulation run, system loads are varied by a random percentage between -5% and 5% from the base-line values. The total duration of a run is 10 seconds; the outage takes place at the 3rd second. Pre- and post-outage voltage phase angles are obtained at the 1st and

10th second. Artificial noise is added to all sampled angle data, $\Delta\boldsymbol{\theta}$, to account for system and measurement noise. They are drawn from a Gaussian distribution with mean $\mathbf{0}$ and standard deviation of 5% of the pre-outage $\Delta\boldsymbol{\theta}$ on respective buses.

Simulated single-line outages include line 1 to 36 except line 21 as it creates two islands. Double-line outages include 100 random pairs of lines from line 1 to 46 that does not create separate islands. Given a list of identified and true outage lines, L_o and L_{true}, identification performance is assessed by Accuracy (A),

$$A(L_o, L_{true}, a) := \frac{\sum_i \mathbf{1}(|L_{o,i} \cap L_{true,i}| = a)}{|L_{true}|}\,. \tag{6.16}$$

Therefore, the accuracy of single-line outage identification of a scheme is $A(L_o, L_{true}, 1)$. Similarly, the "half-correct" and "all-correct" accuracy of double-line outage is $A(L_o, L_{true}, 1)$ and $A(L_o, L_{true}, 2)$. Accuracy with MDC augmentation for each scenario is obtained by replacing L_o with L_o^*, the augmented identification set defined in (6.15).

6.5.2 Illustrative Outage Identification Example

Using the same example of a double-line outage at line 17 and 25, Fig. 6.5 demonstrates limited observability (top) and the estimation of $\Delta\boldsymbol{\theta}$ by each method (bottom). The angle change estimation is obtained using recovered power transfer coefficient $\hat{\boldsymbol{\beta}}$, i.e., $\Delta\hat{\boldsymbol{\theta}} = F\hat{\boldsymbol{\beta}}$. Limited deployment of PMUs means some bus angles are not observed. This is illustrated in the top figure where some signatures of the outage are missed. If unobserved locations contain all the distinctive signatures of that outage, distinguishing it from the others would be challenging. Therefore, characterizing and exploiting line diagnosabilities through MDCs are necessary to overcome this challenge.

The bottom figure shows a comparison of $\Delta\hat{\boldsymbol{\theta}}$ by three methods under comparison. Columns of F corresponding to the outage lines identified by each method are used. The AC power flow-based methods are clearly better at reconstructing the angle changes than the DC one. Notice that the DC estimation has more "flat" angles than the other two, thus fewer details to distinguish it from other outages. While variable selection accuracy rather than estimation accuracy is the

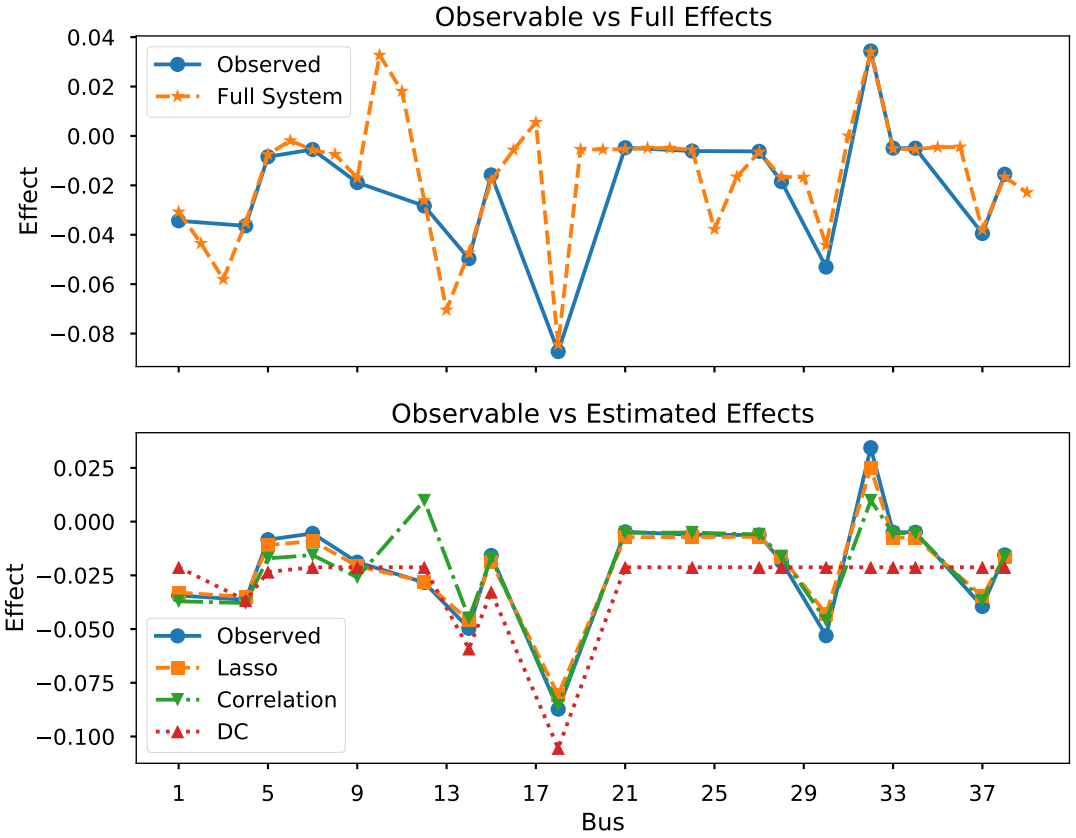

Figure 6.5: *Full, observed, and estimated outage impact on bus voltage phase angles after a double-line outage at line 17 and 25. 19 out of 39 buses are equipped with PMUs. The top figure shows observed noisy data with true and complete system states. The bottom figure compares the estimated phase angles changes from three methods against the observed states.*

focus, this figure nevertheless demonstrates the superior performance of the AC power flow model at capturing a more nuanced outage impact.

6.5.3 Average Identification Performance

The average performance of each identification scheme is reported based on 200 simulation runs over all the single- and double-line outages. Random noises and random PMU placements of a 25% or 50% PMU coverage are used in each run. Two existing methods are compared, namely "DC" for the DC power flow-based method in [40] and "Corr" for the AC power flow-based method in [14]. Performance gain with MDC augmentation of (6.15) is also reported under the

name "...+MDC".

6.5.3.1 Single-line Outage

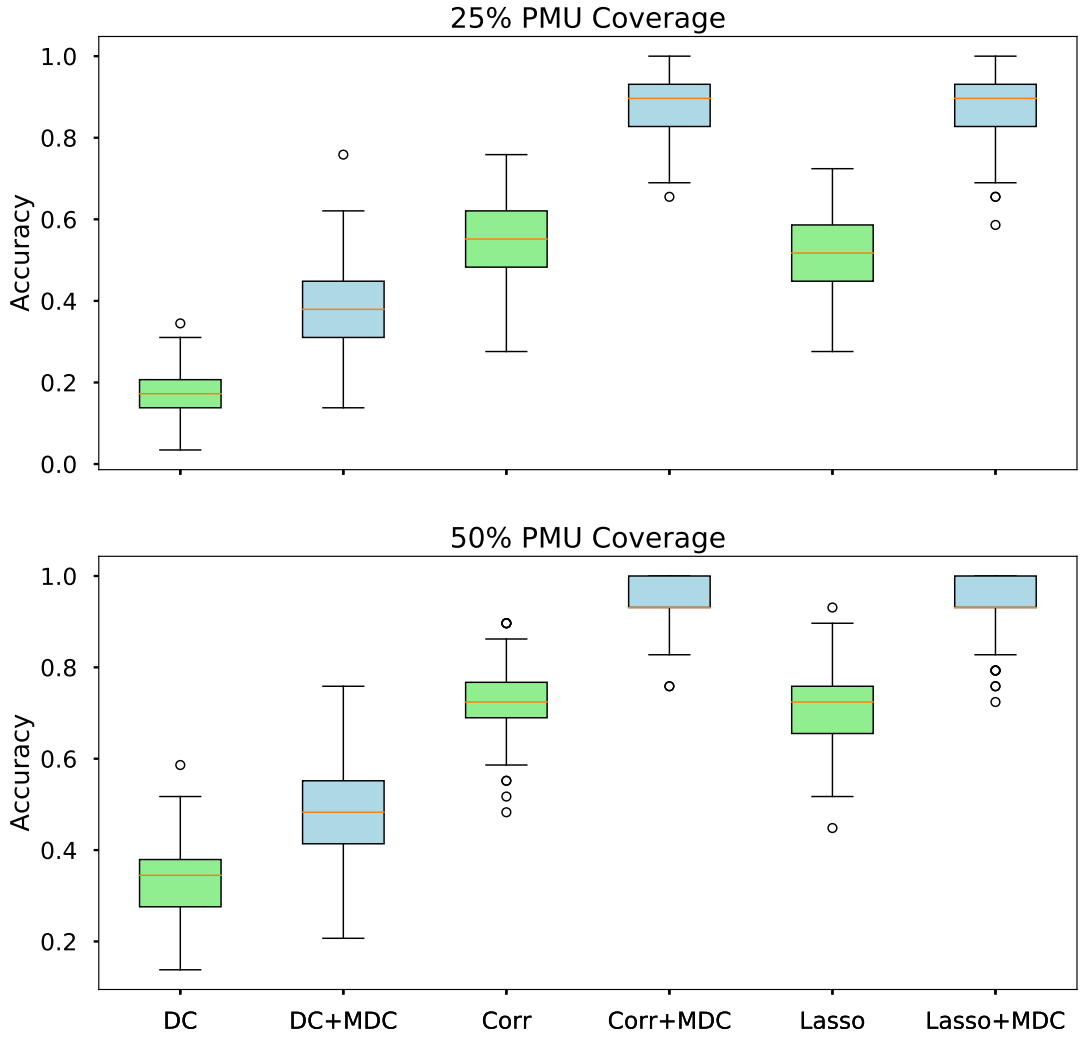

Figure 6.6: *Box-plots of single-line outage identification results for DC-based, correlation-based, and the proposed method. Results are based on 200 random simulation runs under 25% (top) and 50% (bottom) PMU coverage in the New England 39-bus system. Each method has two sets of results: accuracy of the original identification and of that augmented with MDCs.*

Fig. 6.6 shows the identification results for the single-line outage. With or without MDC augmentation, the correlation-based method and the proposed method consistently outperform the DC-based method in both cases of PMU coverage. The former two are roughly always 40% more accurate than the DC-

based method. The correlation-based method achieves an almost identical result with the proposed method regardless of MDC augmentation or PMU coverage. This is expected since the proposed method identifies the first variable as the one most correlated with the response, an identical procedure as the correlation-based method.

When PMU coverage is increased from 25% to 50%, improvements in identification accuracy across all methods are observed as expected. Under 25% coverage, the proposed method is 52% and 86% accurate (median), without and with MDC augmentation. With 50% coverage, the performance is 72% and 93%. Lastly, augmenting original solutions with their MDCs improves accuracy across methods and PMU coverage. Roughly speaking, MDC augmentation improves accuracy by 30% for the 25% coverage and 20% for the 50% coverage. Notably, the two AC-based methods reach 93% identification accuracy under 50% coverage with MDCs. The decrease in accuracy improvement for better-observed system might be because they tend to have more distinguishable outages. The single-line outage identification results for 75% PMU coverage of all methods are reported in Section C.2 of Appendix C.

6.5.3.2 Double-line Outage

Fig. 6.7 shows the identification results for the double-line outage under 50% PMU coverage. The proposed method consistently outperforms the other two methods, especially in the "all correct" case. The DC-based method performs worst in both categories. The correlation-based method is not as accurate beyond the identification of the first line. The reason might be that the proposed formulation treats $\boldsymbol{p}'$ as an unknown vector. It is systematically estimated from data by lasso. However, the correlation-based method treats it as a fixed vector of line reactance. Inaccuracy in the model might then lead to inaccurate identification of multiple outage lines. Again, augmenting solutions with MDCs improve accuracy for all methods, especially in the "all correct" category. Overall, the proposed method with MDC augmentation (Lasso+MDC) achieves the best performance. It can identify 80% of the simulated double-line outages under 50% PMU coverage. The double-line outage identification results for all methods

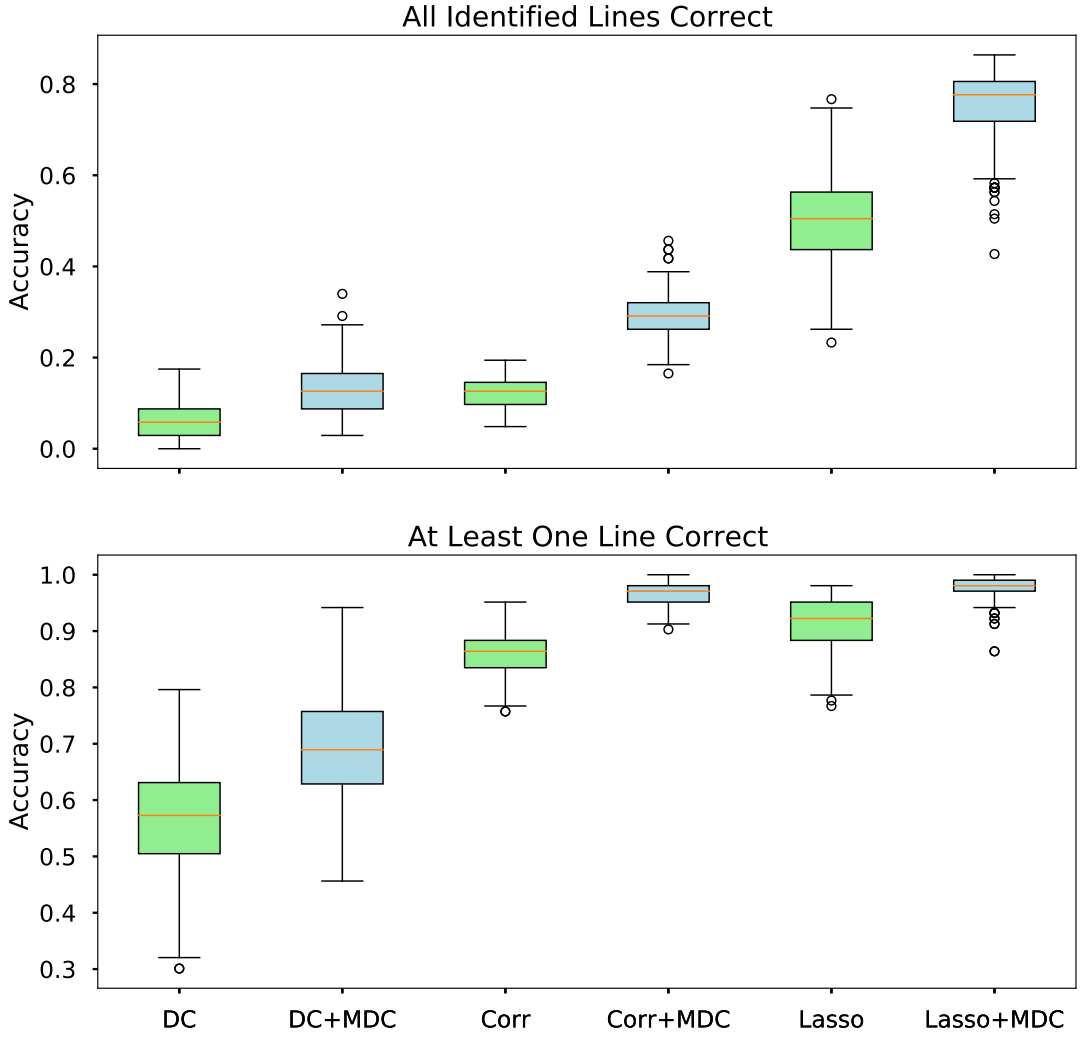

Figure 6.7: *Box-plots of double-line outage identification results for DC-based, correlation-based, and the proposed method. "All correct" (top) and "half correct" (bottom) results are based on 200 random simulation runs under 50% PMU coverage in the New England 39-bus system. Each method has two sets of results: accuracy of the original identification and of that augmented with MDCs.*

Table 6.1: Impact of Minimal Diagnosable Cluster Threshold on Identification Precision-Accuracy Trade-off Using Lasso+MDC With 50% PMU Coverage

Threshold (ρ^*)	Single-element MDC[3] (%)	Single-line	Double-line
0.80	0.34 (0.06)	0.94 (0.06)	0.69 (0.08)
0.84	0.42 (0.06)	0.94 (0.05)	0.69 (0.07)
0.88	0.49 (0.07)	0.95 (0.05)	0.69 (0.08)
0.93	0.55 (0.06)	0.93 (0.06)	0.67 (0.09)
0.95	0.58 (0.06)	0.93 (0.07)	0.66 (0.09)
0.98	0.62 (0.06)	0.92 (0.06)	0.66 (0.09)
0.99	0.68 (0.07)	0.89 (0.07)	0.61 (0.09)

under 25% and 75% PMU coverage are reported in Section C.2 of Appendix C.

6.5.3.3 Effect of Minimal Diagnosable Cluster

Table 6.1 shows the trade-off between identification precision and accuracy by varying the MDC threshold ρ^* in (6.13) with 50% PMU coverage. As expected, the proportion of single-element MDC, $V(\rho^*)$, increases as the threshold approaches 1. In particular, a threshold of $\rho^* = 0.8$ leads to 34% MDCs with a single element. That proportion increases to 68% when $\rho^* = 0.99$. The good news is, a tighter requirement on MDC does not lead to much decrease in single- and double-line outage identification accuracy using the proposed method, from 94% to 89% and 69% to 61%, respectively. Similar results are observed under 25% and 75% PMU coverage, which are presented in Section C.2 of Appendix C.

Therefore, augmenting solutions with MDCs could substantially improve identification accuracy while sacrificing identification precision moderately. The result also suggests that recognizing the most highly correlated line outages, e.g., setting $\rho^* \geq 0.95$, is enough to reap the benefit of MDC augmentation. Nevertheless, there is a trade-off between accuracy and precision. The threshold could be determined jointly with decision-makers' other considerations, e.g., resources available or criticality of the system.

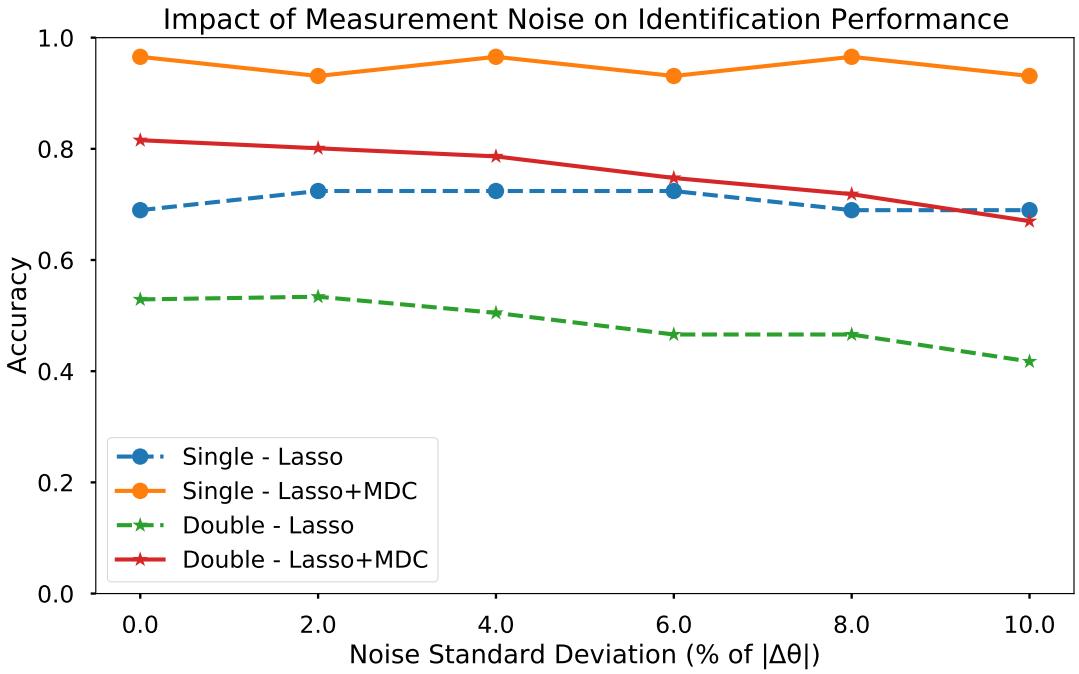

Figure 6.8: *Impact of measurement noise on identification performance of the proposed method with 50% PMU coverage. Performance using data with noise standard deviation varying from 0% to 10% of* $|\Delta\boldsymbol{\theta}|$ *is reported by median accuracy of single- and double-line outages using Lasso and Lasso+MDC.*

6.5.3.4 Effect of Measurement Noise

The performance of the proposed method concerning measurement noise is also reported in Fig. 6.8 under 50% PMU coverage. The performance is largely robust to measurement noise. The accuracy for single-line identification shows no apparent difference as the noise level increases. There is a moderate decrease in accuracy for double-line outage identification as the noise level increases to 10%. Lasso formulation is known to be robust to noise [72]. Results from the simulation study corroborate this. The impact of the measurement noise levels with 25% and 75% PMU coverage is reported in Section C.2 of Appendix C.

[3]One standard deviation appears in ().

6.6 Conclusion

In this chapter, a novel framework of real-time multiple-line outage identification with limited PMU deployment is studied. AC power flow model is utilized to construct a signature map that encodes voltage phase angle signatures of each line outage. Identification is then formulated into an underdetermined sparse regression problem solved by lasso. Minimal diagnosable clusters are proposed to improve identification accuracy further. Single-line and double-line outages simulated on the New England 39-bus system with 25% and 50% PMU deployment are used to study the proposed method's performance. The proposed method has better identification accuracy under all simulation settings, especially for double-line outages. The robustness of the method is also demonstrated using varying levels of noisy data. Finally, the merit of exploiting line diagnosability through minimal diagnosable clusters is also shown. The MDCs significantly improve identification accuracy by trading off a small amount of precision.

The problem of post-outage system parameter recovery is not considered in this work. In general, online updating of system parameters under partial observability remains a challenging but important task worth investigating. Also, the problem of optimal PMU placement can be pursued. As mentioned in the additional remark, the locations of the PMUs affect the network's diagnosability through pairwise correlations. In addition, the optimal PMU solution under one set of system operating states might be sub-optimal when the system states change. Optimal PMU placement for outage identification under different operating states remains a challenge worth investigating.

Chapter 7

Conclusion

Motivated by the need to improve real-time situational awareness of power system operators and the emergence of the PMU technology, this thesis sets out to develop advanced data analytic methods to detect and identify transmission line outages in real-time.

7.1 Contributions

In Chapter 4, a novel line outage detection scheme is proposed based on the power flow model and generalized likelihood ratio testing. The power flow model is used as the basis for predicting post-outage angle deviations. The control chart constructed based on the GLR procedure can detect any outages quickly while controlling for the false alarm rate. Notably, the proposed method can capture system dynamics since it retains the time-variant and nonlinear nature of the power system. An extensive simulation study suggests that the method performs well for outage detection, where most outages can be detected with less than one second of delay. However, longer delays are observed for outage lines with no nearby PMU sensors, prompting the need for research into a more robust detection scheme.

Chapter 5 extends the research in the previous chapter by proposing a unified detection framework that monitors both generator dynamics and load bus dynamics. The unified framework consists of a particle filter-based nonlinear state estimator and a MEWMA-based control chart. The simulation study using the IEEE 39-bus system shows that the inclusion of generator dynamics makes detection faster and more robust to a priori unknown outage locations. In particular,

80% of the simulated outages can be detected, and most of them are detected by 0.2 seconds after the event.

Although encouraging results are seen from the previous two chapters, they do not address another critical and practical question regarding line outage awareness - identification. Assuming an outage detection alarm has been raised, Chapter 6 proposes a novel method to accurately identify a priori unknown number of outage lines using limited PMU sensors. This work draws inspiration from sensitivity analysis of the AC power flow model and advances in underdetermined sparse regression methods. The use of lasso formulation and the LARS algorithm, in particular, overcomes the inherent combinatorial challenge of the line identification problem. Compared to the state-of-the-art in multiple-line outage identification, the proposed method achieves over 90% and 80% accuracy for single- and double-line outage identification.

The guiding principle to this thesis' approach to addressing the outage detection and identification problem is deep integration between statistical monitoring and diagnostic methods and power system physical modeling. Through three chapters of work, it is demonstrated that the AC power flow model, although nonlinear and more complex than the DC version commonly used, can provide a significant advantage in both detection and identification. Still, the performance is achieved by combining the physical model with careful application of methods outside the traditional domain of power system research, e.g., statistical quality control and data mining. As PMU technology takes a central role in the modernization drive of power grids across the world, real-time outage detection and identification methods developed in this thesis can contribute to a more reliable and resilient power system.

7.2 Limitations

There are several limitations in the studies conducted in this thesis. Although important, the optimal placement of PMU sensors is not investigated in depth in all of our studies. Also, given the size of a power system, the minimum number of PMUs required to achieve a certain level of detection and identification percentage

is not investigated. On the other hand, the emerging issue of PMU data quality is also not addressed in this thesis. In all three studies, the PMU data is assumed to be corrupted with only normal sensor errors and random load fluctuations. Bad PMU data due to sensor error or maliciously injected false data could impact the effectiveness of the detection and identification schemes proposed in this thesis. Also, the concept of minimal diagnosable cluster of lines proposed in the third study is an approximation of the distinctiveness between outages. They are limited to linear correlations between a pair of transmission lines. More general definition of similarity and diagnosability between an arbitrary number of lines could be proposed.

7.3 Future Research Directions

Three future research directions stemming from this thesis are worth pursuing: (1) The first concerns the optimal placement of limited PMUs in a network that maximizes detection speed, detection rate, and identification accuracy. Firstly, although increasing the number of PMUs leads, in general, to an increased performance in terms of detection speed, rate, and identification accuracy, the performance gain seems to diminish quickly as more PMUs become available. One could wish to study the minimum number of PMUs needed to achieve a certain level of detection speed, rate, or identification accuracy. Secondly, for fast outage detection without using generator state dynamics, e.g., the proposed method in Chapter 4, a scattered and spread out set of PMU locations tend to achieve better detection speed compared to a set of concentrated locations. On the other hand, for the proposed method in Chapter 5, it requires PMUs to be installed on both generator and load buses. PMU location optimization in this case has to accommodate this requirement. For example, the optimization problem might need to be divided into two subproblems, one for generator bus PMUs and one for load bus PMUs. Lastly, as seen in Chapter 6, the placement of PMUs influences the diagnosability of the system, suggesting the potential reward of a carefully considered placement. For example, PMUs can be located in a way such that the orthogonality of the columns in the phase angle signature matrix

are maximized. (2) The second area of future research is active diagnostics for indistinguishable line outages. The problem of ambiguous outage lines has been observed in previous research and this thesis. Until now, most research efforts have focused on passively analyzing power system data to ascertain the location of outage lines. However, for the group of line outages that might be difficult to distinguish from one another, proactive identification methods might be needed. For example, targeted system inputs can be employed to specifically find out the most probably outage line among a group of highly similar candidate lines. (3) Lastly, more research can be done in the area of optimal post-disruption recovery for power systems. With contingencies like line outages detected and identified, system operators need to coordinate recovery actions to minimize the potential impact while considering various constraints. Also, uncertainties in resources available and repair duration of line outages need to be factored in when designing a recovery strategy. The ability to recover efficiently following a disruption is a critical aspect of resilient power systems.

Bibliography

[1] J. Ellis, D. Fisher, T. Longstaff, L. Pesante, and R. Pethia, "Report to the president's commission on critical infrastructure protection." Carnegie-Mellon Univ Pittsburgh PA Software Engineering Inst, Tech. Rep., 1997.

[2] S. D. Guikema, "Natural disaster risk analysis for critical infrastructure systems: An approach based on statistical learning theory", *Reliability Engineering & System Safety*, vol. 94, no. 4, pp. 855–860, 2009.

[3] M. Amin, "Challenges in reliability, security, efficiency, and resilience of energy infrastructure: Toward smart self-healing electric power grid", in *2008 IEEE Power and energy society general meeting-conversion and delivery of electrical energy in the 21st century*, IEEE, 2008, pp. 1–5.

[4] J. Seymour and T. Horsley, "The seven types of power problems", *APC, USA*, 2005.

[5] M. Kezunovic, L. Xie, and S. Grijalva, "The role of big data in improving power system operation and protection", in *2013 IREP Symposium Bulk Power System Dynamics and Control-IX Optimization, Security and Control of the Emerging Power Grid*, IEEE, 2013, pp. 1–9.

[6] F. Aminifar, M. Fotuhi-Firuzabad, A. Safdarian, A. Davoudi, and M. Shahidehpour, "Synchrophasor measurement technology in power systems: panorama and state-of-the-art", *IEEE Access*, vol. 2, pp. 1607–1628, 2014.

[7] FERC and NAERC, "Arizona-Southern California outages on September 8, 2011: Causes and recommendations", Tech. Rep., 2012.

[8] F. Milano, "Power System Modelling and Scripting", Springer Science & Business Media, 2010.

[9] M. Pignati, M. Popovic, S. Barreto, R. Cherkaoui, G. D. Flores, J.-Y. Le Boudec, M. Mohiuddin, M. Paolone, P. Romano, S. Sarri, *et al.*, "Real-time state estimation of the epfl-campus medium-voltage grid by using pmus", in *2015 IEEE Power & Energy Society Innovative Smart Grid Technologies Conference*, IEEE, 2015, pp. 1–5.

[10] M. Panteli and P. Mancarella, "The grid: Stronger, bigger, smarter?: Presenting a conceptual framework of power system resilience", *IEEE Power and Energy Magazine*, vol. 13, no. 3, pp. 58–66, May 2015.

[11] F. Aminifar, M. Fotuhi-Firuzabad, A. Safdarian, A. Davoudi, and M. Shahidehpour, "Synchrophasor measurement technology in power systems: Panorama and state-of-the-art", *IEEE Access*, vol. 2, pp. 1607–1628, 2014.

[12] X. Yang, N. Chen, and C. Zhai, "A control chart approach to power system line outage detection under transient dynamics", *IEEE Transactions on Power Systems*, vol. 36, no. 1, pp. 127–135, 2021.

[13] J. Wu, J. Xiong, and Y. Shi, "Efficient location identification of multiple line outages with limited pmus in smart grids", *IEEE Transactions on Power Systems*, vol. 30, no. 4, pp. 1659–1668, 2015.

[14] N. Costilla-Enríquez, C. R. Fuerte-Esquivel, and V. J. Gutiérrez-Martínez, "A sensitivity-based approach for the detection of multiple-line outages using phasor measurements", *IEEE Transactions on Power Systems*, vol. 34, no. 5, pp. 3697–3705, 2019.

[15] X. Yang, N. Chen, and C. Zhai, "Dynamic power systems line outage detection using particle filter and partially observed states", 2021. arXiv: 2107.06754 [eess.SY].

[16] L. Xie, Y. Chen, and P. R. Kumar, "Dimensionality reduction of synchrophasor data for early event detection: Linearized analysis", *IEEE Transactions on Power Systems*, vol. 29, no. 6, pp. 2784–2794, 2014.

[17] M. Rafferty, X. Liu, D. M. Laverty, and S. McLoone, "Real-time multiple event detection and classification using moving window PCA", *IEEE Transactions on Smart Grid*, vol. 7, no. 5, pp. 2537–2548, 2016.

[18] S. Hosur and D. Duan, "Subspace-driven output-only based change-point detection in power systems", *IEEE Transactions on Power Systems*, vol. 34, no. 2, pp. 1068–1076, 2019.

[19] M. Jamei, A. Scaglione, C. Roberts, E. Stewart, S. Peisert, C. McParland, and A. McEachern, "Automated anomaly detection in distribution grids using upmu measurements", in *Proceedings of the 50th Hawaii International Conference on System Sciences*, 2017, pp. 3184–3193.

[20] ——, "Anomaly detection using optimally placed μPMU sensors in distribution grids", *IEEE Transactions on Power Systems*, vol. 33, no. 4, pp. 3611–3623, 2017.

[21] O. Ardakanian, Y. Yuan, R. Dobbe, A. von Meier, S. Low, and C. Tomlin, "Event detection and localization in distribution grids with phasor measurement units", in *2017 IEEE Power & Energy Society General Meeting*, IEEE, 2017, pp. 1–5.

[22] O. Ardakanian, V. W. Wong, R. Dobbe, S. H. Low, A. von Meier, C. J. Tomlin, and Y. Yuan, "On identification of distribution grids", *IEEE Transactions on Control of Network Systems*, vol. 6, no. 3, pp. 950–960, 2019.

[23] J. E. Tate and T. J. Overbye, "Line outage detection using phasor angle measurements", *IEEE Transactions on Power Systems*, vol. 23, no. 4, pp. 1644–1652, 2008.

[24] J. E. Tate and T. J. Overbye, "Double line outage detection using phasor angle measurements", in *2009 IEEE Power & Energy Society General Meeting*, IEEE, 2009, pp. 1–5.

[25] Z. Dai and J. E. Tate, "Line outage identification based on ac power flow and synchronized measurements", in *2020 IEEE Power & Energy Society General Meeting (PESGM)*, IEEE, 2020, pp. 1–5.

[26] Y. C. Chen, T. Banerjee, A. D. Dominguez-Garcia, and V. V. Veeravalli, "Quickest line outage detection and identification", *IEEE Transactions on Power Systems*, vol. 31, no. 1, pp. 749–758, 2016.

[27] G. Rovatsos, X. Jiang, A. D. Dominguez-Garcia, and V. V. Veeravalli, "Statistical power system line outage detection under transient dynamics", *IEEE Transactions on Signal Processing*, vol. 65, no. 11, pp. 2787–2797, 2017.

[28] M. Babakmehr, M. G. Simões, M. B. Wakin, and F. Harirchi, "Compressive sensing-based topology identification for smart grids", *IEEE Transactions on Industrial Informatics*, vol. 12, no. 2, pp. 532–543, 2016.

[29] M. Babakmehr, M. G. Simoes, A. Al-Durra, F. Harirchi, and Q. Han, "Application of compressive sensing for distributed and structured power line outage detection in smart grids", in *2015 American Control Conference (ACC)*, IEEE, 2015, pp. 3682–3689.

[30] J. D. Glover, M. S. Sarma, and T. Overbye, "Power System Analysis & Design, SI Version", Cengage Learning, 2012.

[31] Q. Huang, L. Shao, and N. Li, "Dynamic detection of transmission line outages using Hidden Markov Models", *IEEE Transactions on Power Systems*, vol. 31, no. 3, pp. 2026–2033, 2016.

[32] W. Pan, Y. Yuan, H. Sandberg, J. Gonçalves, and G. B. Stan, "Online fault diagnosis for nonlinear power systems", *Automatica*, vol. 55, pp. 27–36, 2015.

[33] C. Yang, Z. H. Guan, Z. W. Liu, J. Chen, M. Chi, and G. L. Zheng, "Wide-area multiple line-outages detection in power complex networks", *International Journal of Electrical Power and Energy Systems*, vol. 79, pp. 132–141, 2016.

[34] J. Yu, Y. Weng, and R. Rajagopal, "PaToPa: A data-driven parameter and topology joint estimation framework in distribution grids", *IEEE Transactions on Power Systems*, vol. 33, no. 4, pp. 4335–4347, 2018.

[35] ——, "PaToPaEM: A data-driven parameter and topology joint estimation framework for time-varying system in distribution grids", *IEEE Transactions on Power Systems*, vol. 34, no. 3, pp. 1682–1692, 2019.

[36] M. Garcia, T. Catanach, S. Vander Wiel, R. Bent, and E. Lawrence, "Line outage localization using phasor measurement data in transient state", *IEEE Transactions on Power Systems*, vol. 31, no. 4, pp. 3019–3027, 2016.

[37] T. Kim and S. J. Wright, "PMU placement for line outage identification via multinomial logistic regression", *IEEE Transactions on Smart Grid*, vol. 9, no. 1, pp. 122–131, 2018.

[38] W. Li, D. Deka, M. Chertkov, and M. Wang, "Real-time faulted line localization and pmu placement in power systems through convolutional neural networks", *IEEE Transactions on Power Systems*, vol. 34, no. 6, pp. 4640–4651, 2019.

[39] Y. Zhao, J. Chen, and H. V. Poor, "A learning-to-infer method for real-time power grid multi-line outage identification", *IEEE Transactions on Smart Grid*, vol. 11, no. 1, pp. 555–564, 2020.

[40] H. Zhu and G. B. Giannakis, "Sparse overcomplete representations for efficient identification of power line outages", *IEEE Transactions on Power Systems*, vol. 27, no. 4, pp. 2215–2224, 2012.

[41] R. Emami and A. Abur, "External system line outage identification using phasor measurement units", *IEEE Transactions on Power Systems*, vol. 28, no. 2, pp. 1035–1040, 2013.

[42] J. C. Chen, W. T. Li, C. K. Wen, J. H. Teng, and P. Ting, "Efficient identification method for power line outages in the smart power grid", *IEEE Transactions on Power Systems*, vol. 29, no. 4, pp. 1788–1800, 2014.

[43] J. Song, E. Cotilla-Sanchez, G. Ghanavati, and P. D. H. Hines, "Dynamic modeling of cascading failure in power systems", *IEEE Transactions on Power Systems*, vol. 31, no. 3, pp. 2085–2095, 2016.

[44] P. Murty, "Power Systems Analysis", Butterworth-Heinemann, 2017.

[45] P. Anderson and A. Bose, "Stability simulation of wind turbine systems", *IEEE Transactions on Power Apparatus and Systems*, no. 12, pp. 3791–3795, 1983.

[46] R. Kaye and F. Wu, "Analysis of linearized decoupled power flow approximations for steady-state security assessment", *IEEE Transactions on Circuits and Systems*, vol. 31, no. 7, pp. 623–636, 1984.

[47] D. R. Cox, "The Theory of Stochastic Processes", Routledge, 2017.

[48] G. Lorden *et al.*, "Procedures for reacting to a change in distribution", *The Annals of Mathematical Statistics*, vol. 42, no. 6, pp. 1897–1908, 1971.

[49] T. L. Lai, "Information bounds and quick detection of parameter changes in stochastic systems", *IEEE Transactions on Information Theory*, vol. 44, no. 7, pp. 2917–2929, 1998.

[50] Y. Mei, "Efficient scalable schemes for monitoring a large number of data streams", *Biometrika*, vol. 97, no. 2, pp. 419–433, 2010.

[51] T. Athay, R. Podmore, and S. Virmani, "A practical method for the direct analysis of transient stability", *IEEE Transactions on Power Apparatus and Systems*, no. 2, pp. 573–584, 1979.

[52] M. Brown, M. Biswal, S. Brahma, S. J. Ranade, and H. Cao, "Characterizing and quantifying noise in PMU data", in *IEEE Power and Energy Society General Meeting*, 2016, pp. 1–5.

[53] D. C. Montgomery, "Introduction to Statistical Quality Control", John Wiley & Sons, 2007.

[54] P. Kundur, N. J. Balu, and M. G. Lauby, "Power system stability and control", McGraw-Hill New York, 1994.

[55] P. W. Sauer, M. A. Pai, and J. H. Chow, "Power system dynamics and stability: with synchrophasor measurement and power system toolbox", John Wiley & Sons, 2017.

[56] C. A. Lowry, W. H. Woodall, C. W. Champ, and S. E. Rigdon, "A multivariate exponentially weighted moving average control chart", *Technometrics*, vol. 34, no. 1, pp. 46–53, 1992.

[57] S. E. Rigdon, "An integral equation for the in-control average run length of a multivariate exponentially weighted moving average control chart", *Journal of Statistical computation and simulation*, vol. 52, no. 4, pp. 351–365, 1995.

[58] S. Knoth, "Arl numerics for mewma charts", *Journal of Quality Technology*, vol. 49, no. 1, pp. 78–89, 2017.

[59] J. Zhao, M. Netto, and L. Mili, "A robust iterated extended kalman filter for power system dynamic state estimation", *IEEE Transactions on Power Systems*, vol. 32, no. 4, pp. 3205–3216, 2017.

[60] S. Wang, W. Gao, and A. P. Meliopoulos, "An alternative method for power system dynamic state estimation based on unscented transform", *IEEE Transactions on Power Systems*, vol. 27, no. 2, pp. 942–950, 2012.

[61] Y. Cui and R. Kavasseri, "A particle filter for dynamic state estimation in multi-machine systems with detailed models", *IEEE Transactions on Power Systems*, vol. 30, no. 6, pp. 3377–3385, 2015.

[62] V. Kadirkamanathan, P. Li, M. H. Jaward, and S. G. Fabri, "Particle filtering-based fault detection in non-linear stochastic systems", *International Journal of Systems Science*, vol. 33, no. 4, pp. 259–265, 2002.

[63] O. Cappé, S. J. Godsill, and E. Moulines, "An overview of existing methods and recent advances in sequential monte carlo", *Proceedings of the IEEE*, vol. 95, no. 5, pp. 899–924, 2007.

[64] N. J. Gordon, D. J. Salmond, and A. F. Smith, "Novel approach to nonlinear/non-gaussian Bayesian state estimation", *IEE Proceedings, Part F: Radar and Signal Processing*, vol. 140, no. 2, pp. 107–113, 1993.

[65] A. Doucet and A. M. Johansen, "A tutorial on particle filtering and smoothing: Fifteen years later", *Handbook of nonlinear filtering*, vol. 12, no. 656-704, p. 3, 2009.

[66] J. S. Liu, "Monte Carlo strategies in scientific computing", Springer Science & Business Media, 2008.

[67] A. P. Dempster, N. M. Laird, and D. B. Rubin, "Maximum likelihood from incomplete data via the em algorithm", *Journal of the Royal Statistical Society: Series B (Methodological)*, vol. 39, no. 1, pp. 1–22, 1977.

[68] S. Yildirim, S. S. Singh, and A. Doucet, "An online expectation–maximization algorithm for changepoint models", *Journal of Computational and Graphical Statistics*, vol. 22, no. 4, pp. 906–926, 2013.

[69] A. J. Wood, B. F. Wollenberg, and G. B. Sheblé, "Power generation, operation, and control", John Wiley & Sons, 2013.

[70] M. Liu and G. Gross, "Role of distribution factors in congestion revenue rights applications", *IEEE Transactions on Power Systems*, vol. 19, no. 2, pp. 802–810, 2004.

[71] D. Bertsimas, J. Pauphilet, and B. Van Parys, "Sparse regression: Scalable algorithms and empirical performance", *Statistical Science*, vol. 35, no. 4, pp. 555–578, 2020.

[72] T. Hastie, R. Tibshirani, and R. Tibshirani, "Best subset, forward stepwise or lasso? analysis and recommendations based on extensive comparisons", *Statistical Science*, vol. 35, no. 4, pp. 579–592, 2020.

[73] R. Tibshirani, "Regression shrinkage and selection via the lasso", *Journal of the Royal Statistical Society: Series B (Methodological)*, vol. 58, no. 1, pp. 267–288, 1996.

[74] H. Zou, T. Hastie, and R. Tibshirani, "On the "degrees of freedom" of the lasso", *The Annals of Statistics*, vol. 35, no. 5, pp. 2173–2192, 2007.

[75] B. Efron, T. Hastie, I. Johnstone, and R. Tibshirani, "Least angle regression", *The Annals of statistics*, vol. 32, no. 2, pp. 407–499, 2004.

[76] H. Zou and T. Hastie, "Regularization and variable selection via the elastic net", *Journal of the royal statistical society: series B (statistical methodology)*, vol. 67, no. 2, pp. 301–320, 2005.

[77] X. Yang, N. Chen, and C. Zhai, "Optimal placement of limited pmus for transmission line outage detection and identification", in *2020 International Conference on Probabilistic Methods Applied to Power Systems (PMAPS)*, IEEE, 2020, pp. 1–6.

[78] K. Bastani, Z. Kong, W. Huang, and Y. Zhou, "Compressive sensing–based optimal sensor placement and fault diagnosis for multi-station assembly processes", *IIE Transactions*, vol. 48, no. 5, pp. 462–474, 2016.

Appendix A

Unstable Post-Outage System

A simulation example is shown here to illustrate the working of the detection scheme proposed in Chapter 4 when the outage creates an unstable and transient system. In the 39-bus system, line 37 outage creates large disturbances throughout the system, as shown in Figure A.1. From the onset of the outage to the end of the simulation, voltage phase angles at most buses show no significant sign of stabilization. The detection scheme is able to detect the outage immediately, as shown in Figure A.2. In this case, the monitoring statistic records a significantly large value, indicating that the strength of the signals is strong.

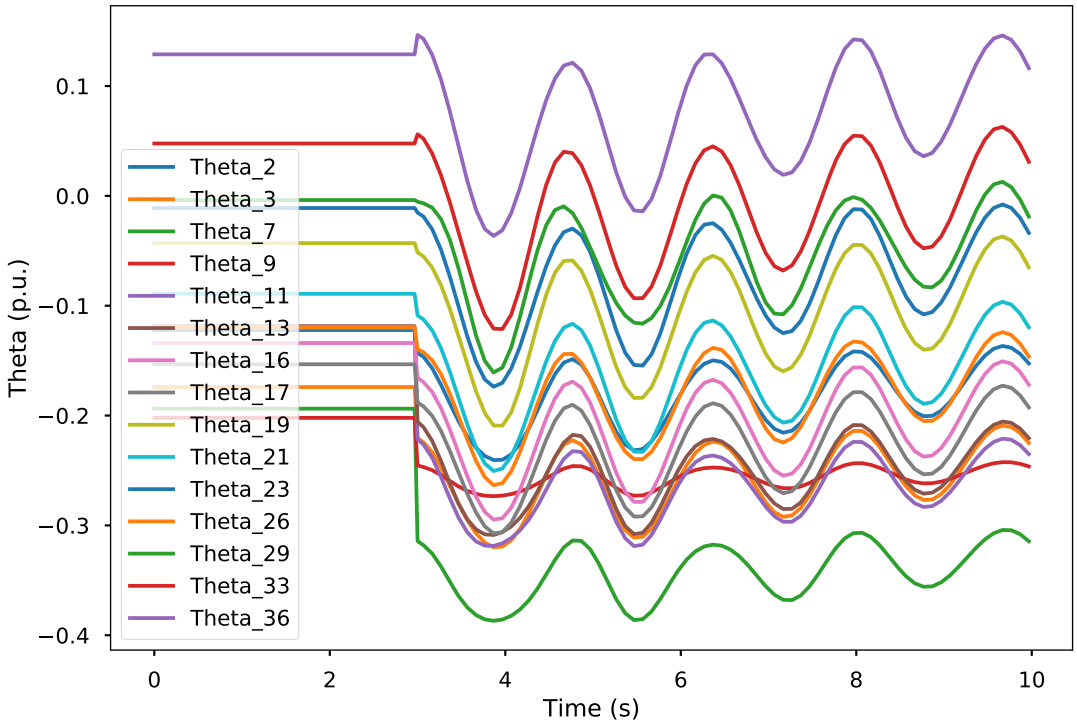

Figure A.1: *The progression of bus voltage phase angles after the outage of line 37. Each line represents the voltage phase angles from one of the buses.*

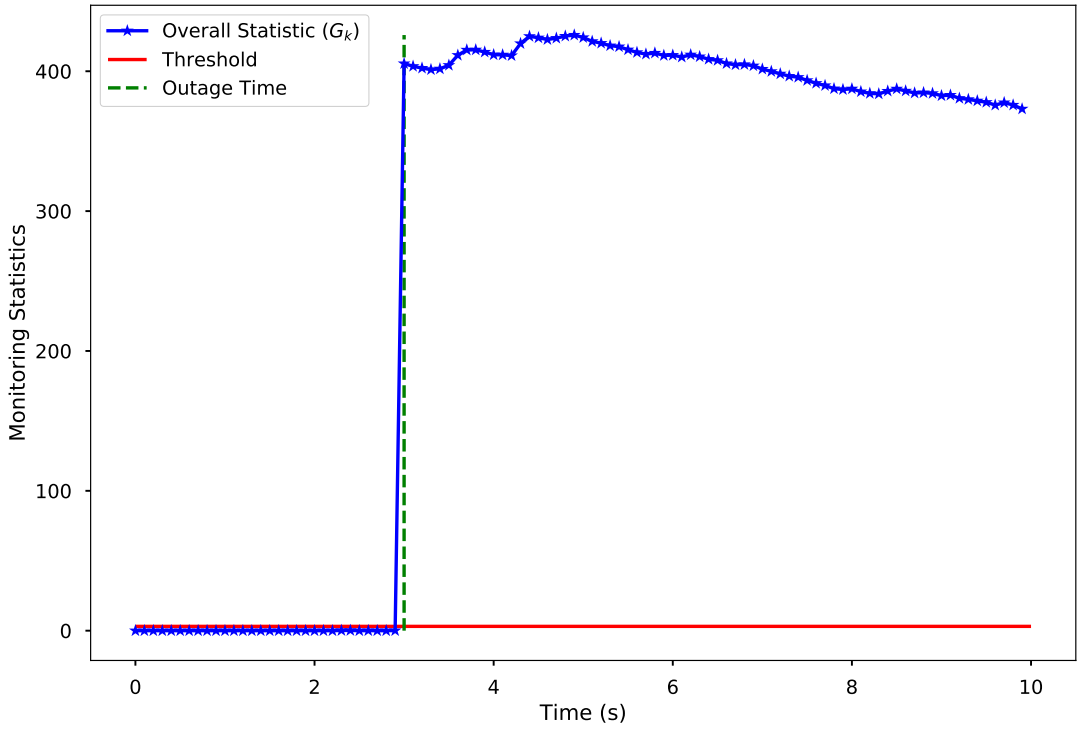

Figure A.2: *The progression of the monitoring statistic for line 37 outage.*

Appendix B

Additional Simulation Results

Additional state estimation and outage detection results from the method proposed in Chapter 5 are reported here.

B.1 Additional Generator State Estimation Results

An example of line 18 outage is illustrated in Section 5.6.2 with generator state estimation using the particle filter. The complete list of state estimation results for all the other monitored generator buses, i.e., Bus 34, 35, 36, and 37, are shown in Fig. B.1 to Fig. B.4.

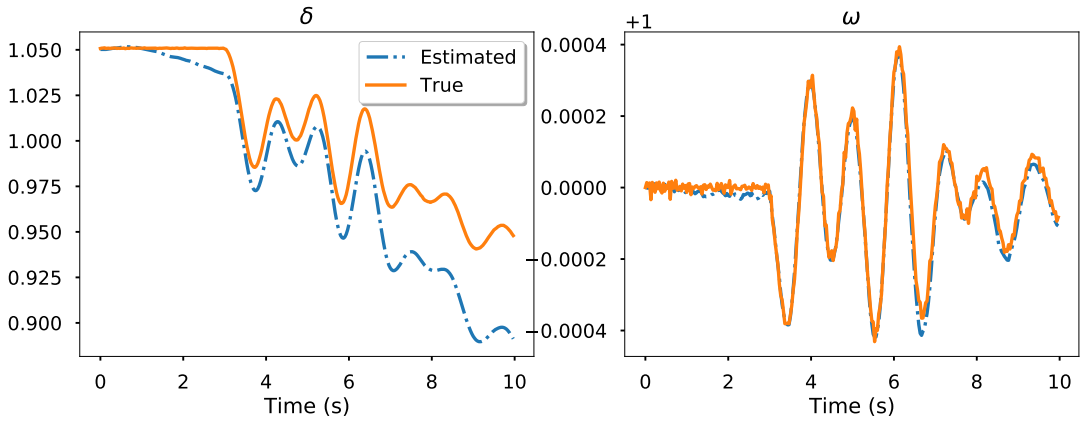

Figure B.1: *State estimation result of the particle filter on δ and ω of Bus 34.*

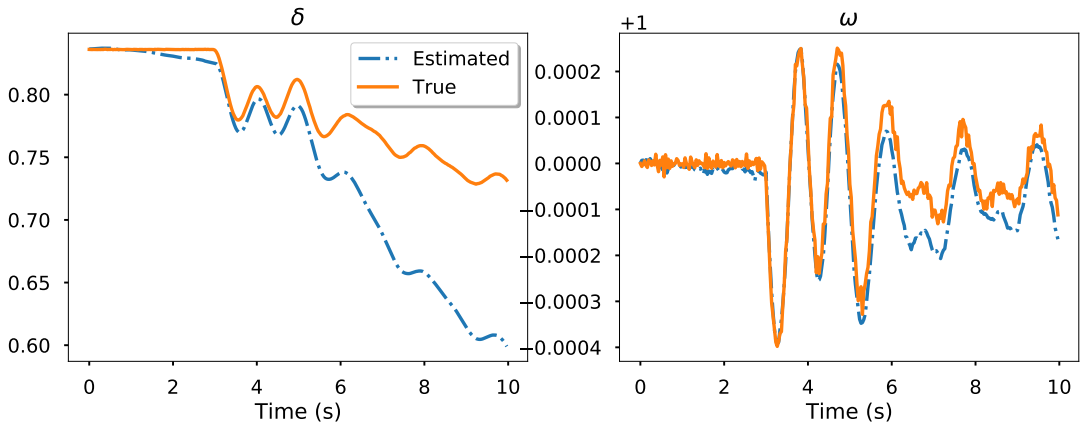

Figure B.2: *State estimation result of the particle filter on δ and ω of Bus 35.*

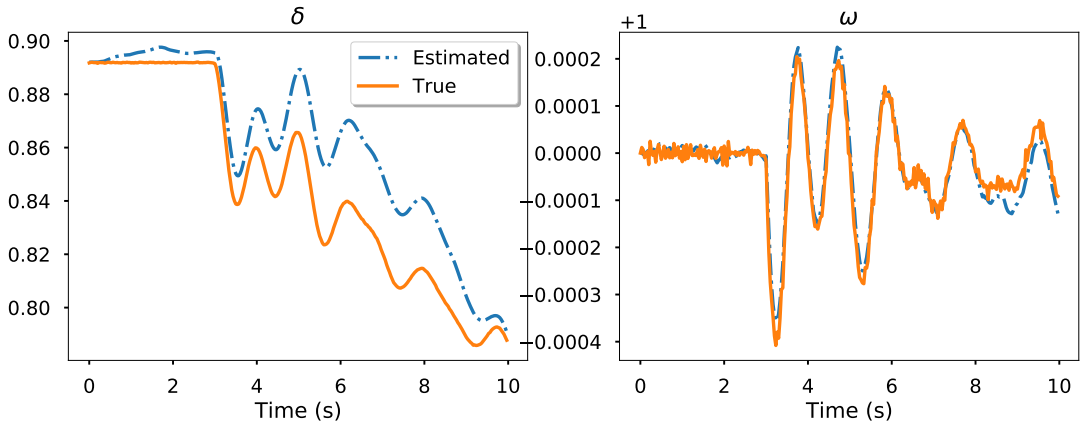

Figure B.3: *State estimation result of the particle filter on δ and ω of Bus 36.*

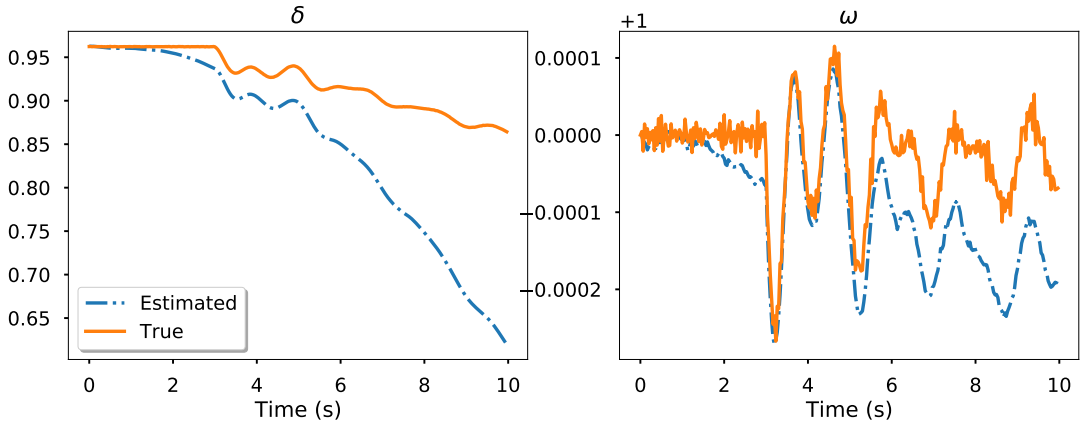

Figure B.4: *State estimation result of the particle filter on δ and ω of Bus 37.*

B.2 Additional Outage Detection Results

Additional line outage detection results are shown here. Fig. B.5 and Fig. B.6 show the output signal breakdown and monitoring statistic progression under the outage-free scenario, i.e., zero line outage is simulated. Fig. B.7 and Fig. B.8 show the output signal breakdown and monitoring statistic progression for line 6 outage. The outage impact on the power grid is mild and short-lived, triggering insignificant increase in the monitoring statistic. Fig. B.9 and Fig. B.10 show the output signal breakdown and monitoring statistic progression for line 34 outage. The observed impact of this outage is significant and triggers a large and sustained increase in the monitoring statistic.

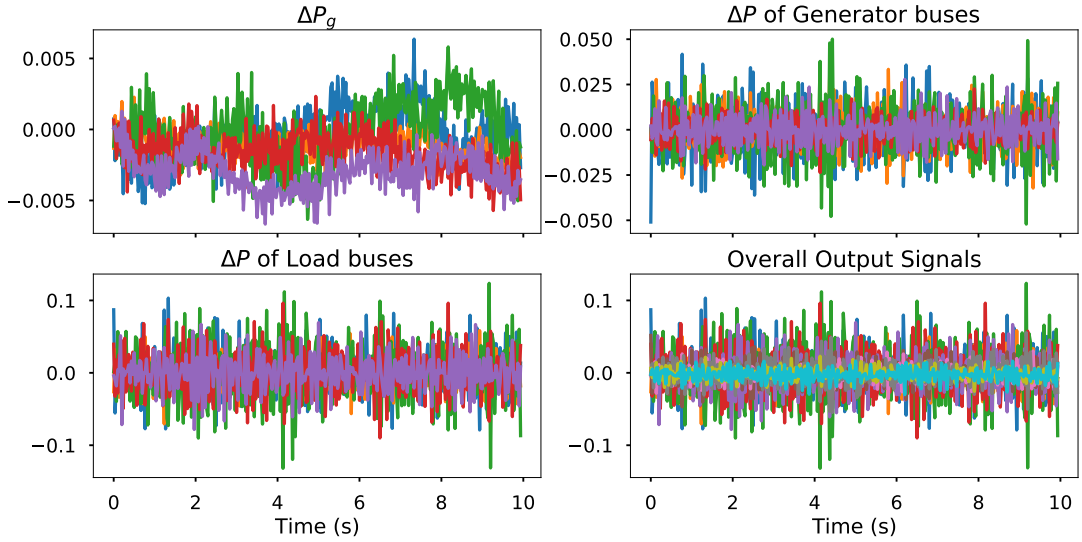

Figure B.5: *Output signals of the detection scheme under outage-free condition and the breakdown by components.*

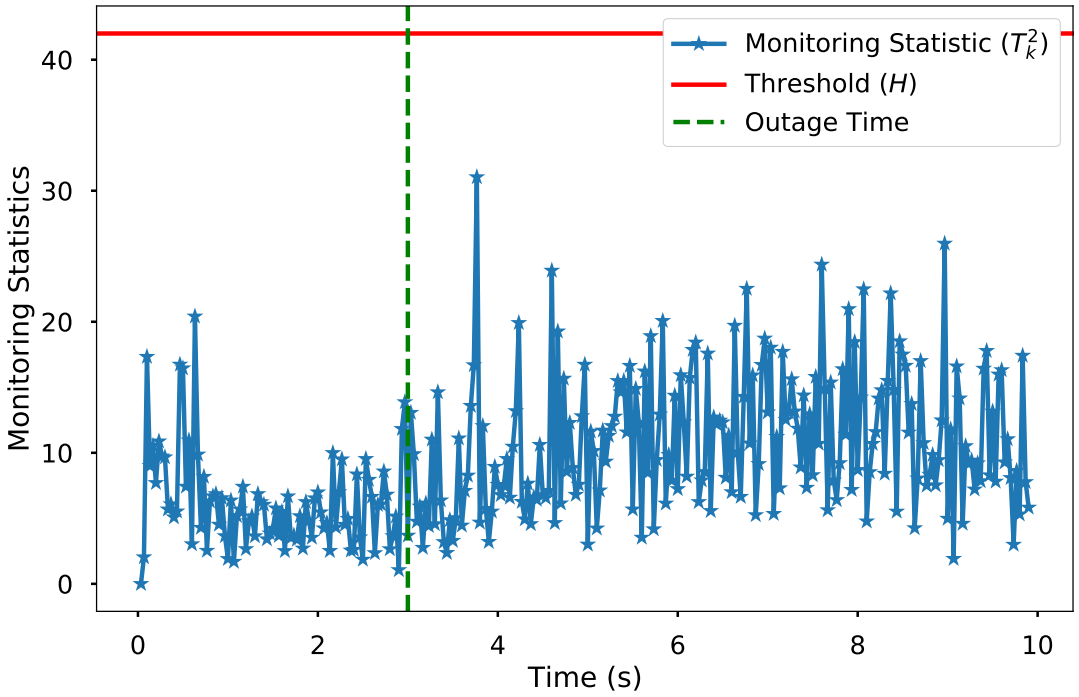

Figure B.6: *Progression of MEWMA monitoring statistic for the outage-free scenario.*

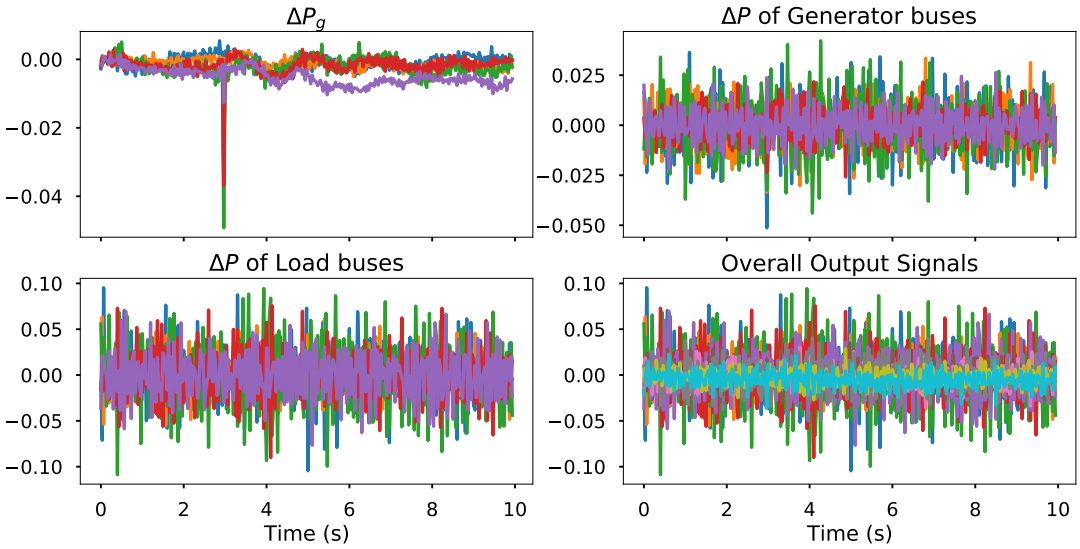

Figure B.7: *Output signals of the detection scheme for line 6 outage and the breakdown by components.*

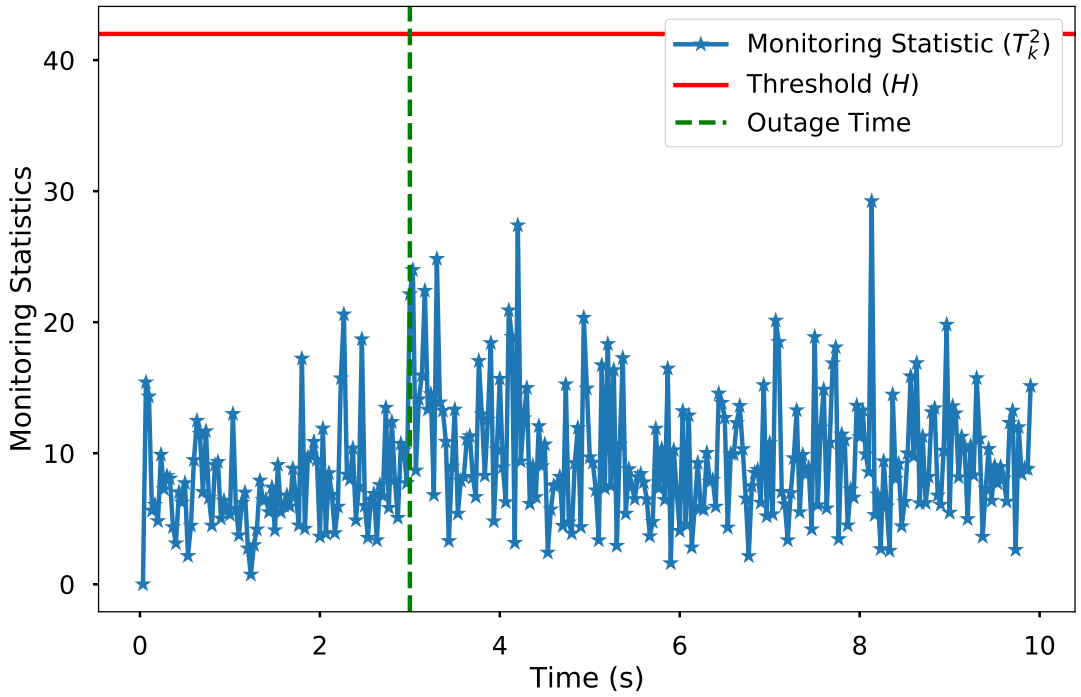

Figure B.8: *Progression of MEWMA monitoring statistic for detecting line 6 outage.*

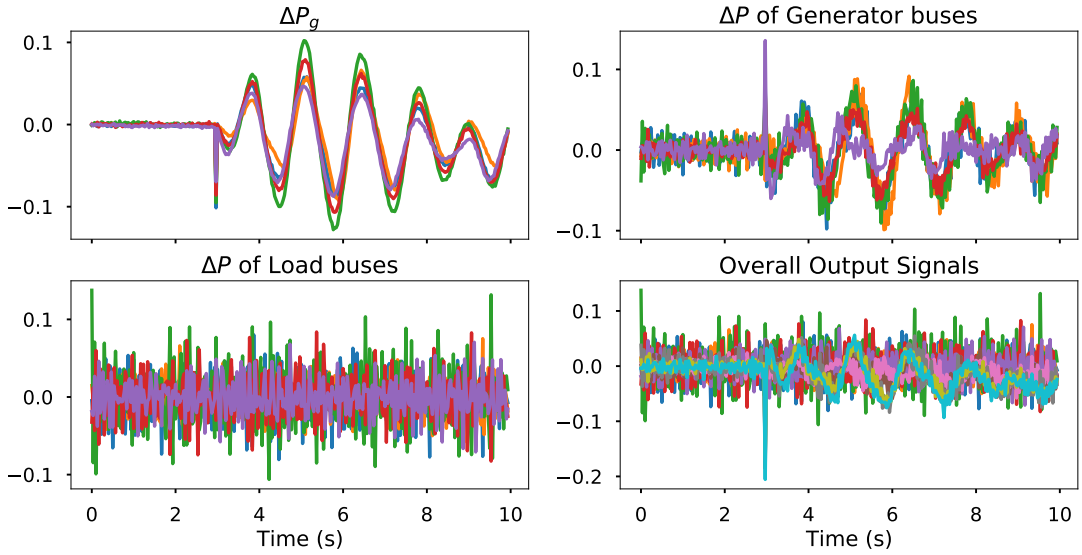

Figure B.9: *Output signals of the detection scheme for line 34 outage and the breakdown by components.*

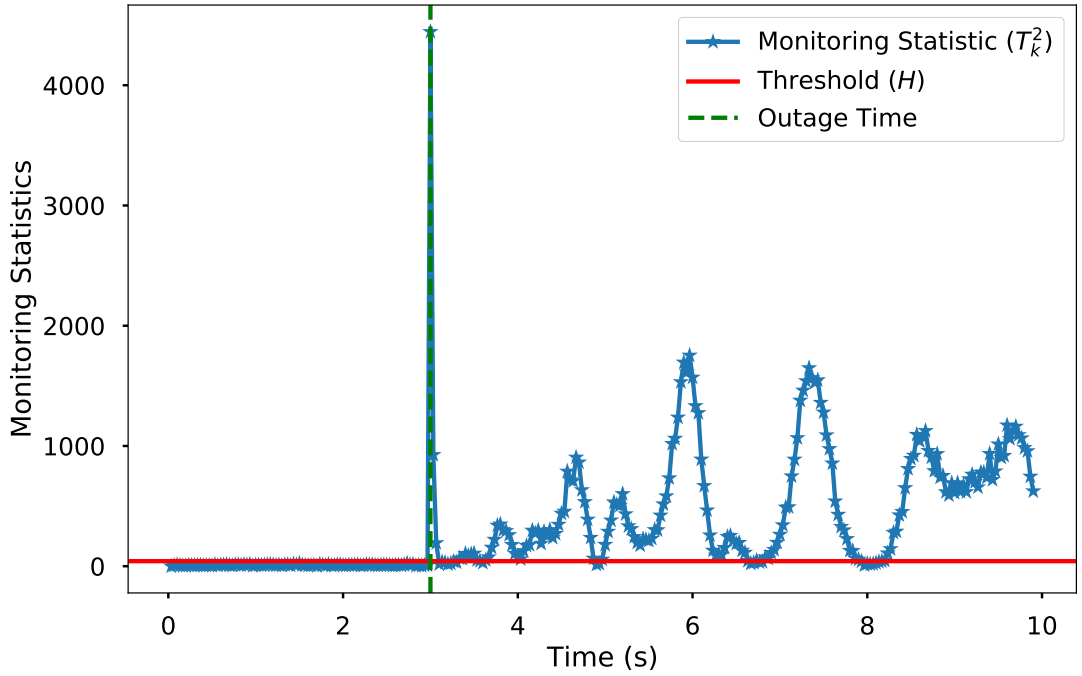

Figure B.10: *Progression of MEWMA monitoring statistic for detecting line 34 outage.*

Appendix C

PMU Placement and Additional Identification Results

C.1 Genetic Algorithm-generated PMU Placement

The pairwise correlation heatmap of the signature map based on the genetic algorithm-generated optimal PMU placement is shown in Fig. C.1. It can be observed that the number of lines with high pairwise correlation has significantly reduced compared to that of a random PMU placement shown in Fig. 6.3.

C.2 Additional Identification Results

Additional results of the proposed method's identification performance are reported here.

C.2.1 Average Performance

The average identification performance of the proposed method and other methods under comparison for single-line outages with 75% PMU coverage is shown in Fig. C.2.

The average identification performance of the proposed method and other methods under comparison for double-line outages with 25% PMU coverage is shown in Fig. C.3 and 75% PMU coverage in Fig. C.4.

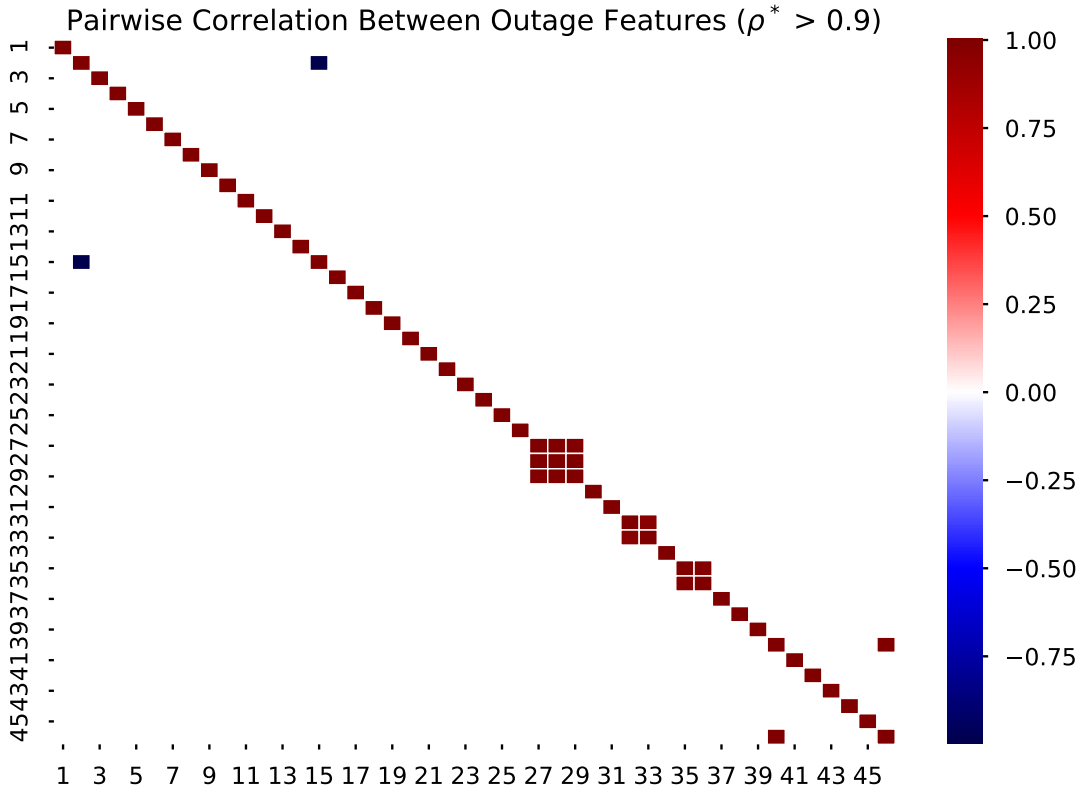

Figure C.1: *Heatmap of pairwise correlation between columns of the signature map constructed from an optimal placement of 19 PMUs on the 39-bus system. The placement is generated by minimizing the average mutual coherence of the signature map using a genetic algorithm. Only correlations higher than 0.9 are plotted.*

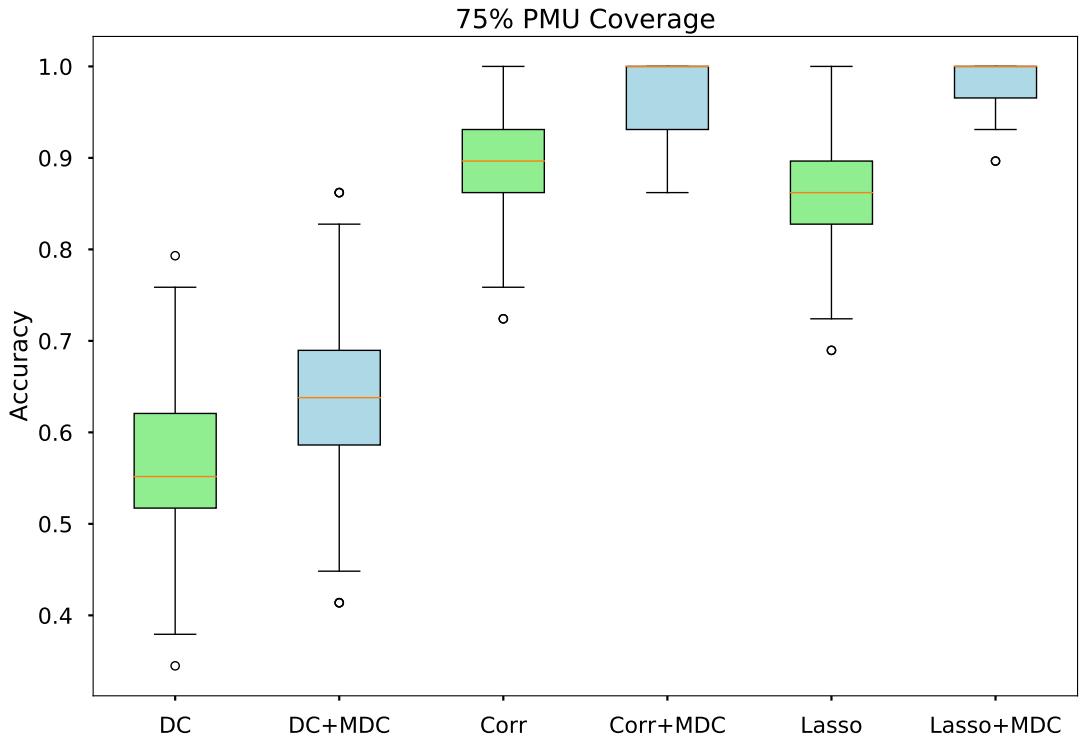

Figure C.2: *Box-plots of single-line outage identification results for DC-based, correlation-based, and the proposed method. Results are based on 200 random simulation runs under a 75% PMU coverage in the New England 39-bus system. Each method has two sets of results: accuracy of the original identification and of that augmented with MDCs.*

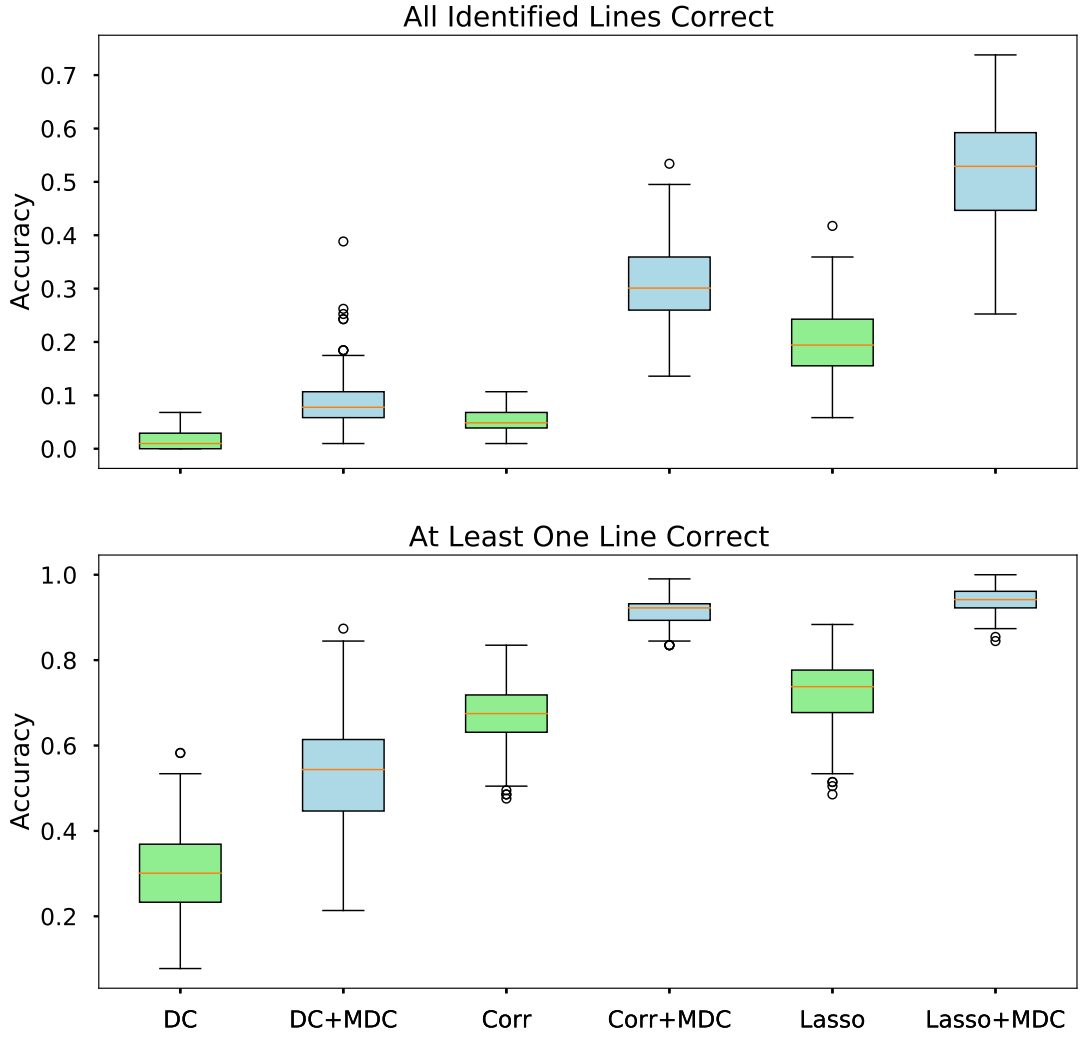

Figure C.3: *Box-plots of double-line outage identification results for DC-based, correlation-based, and the proposed method. "All correct" (top) and "half correct" (bottom) results are based on 200 random simulation runs under a 25% PMU coverage in the New England 39-bus system. Each method has two sets of results: accuracy of the original identification and of that augmented with MDCs.*

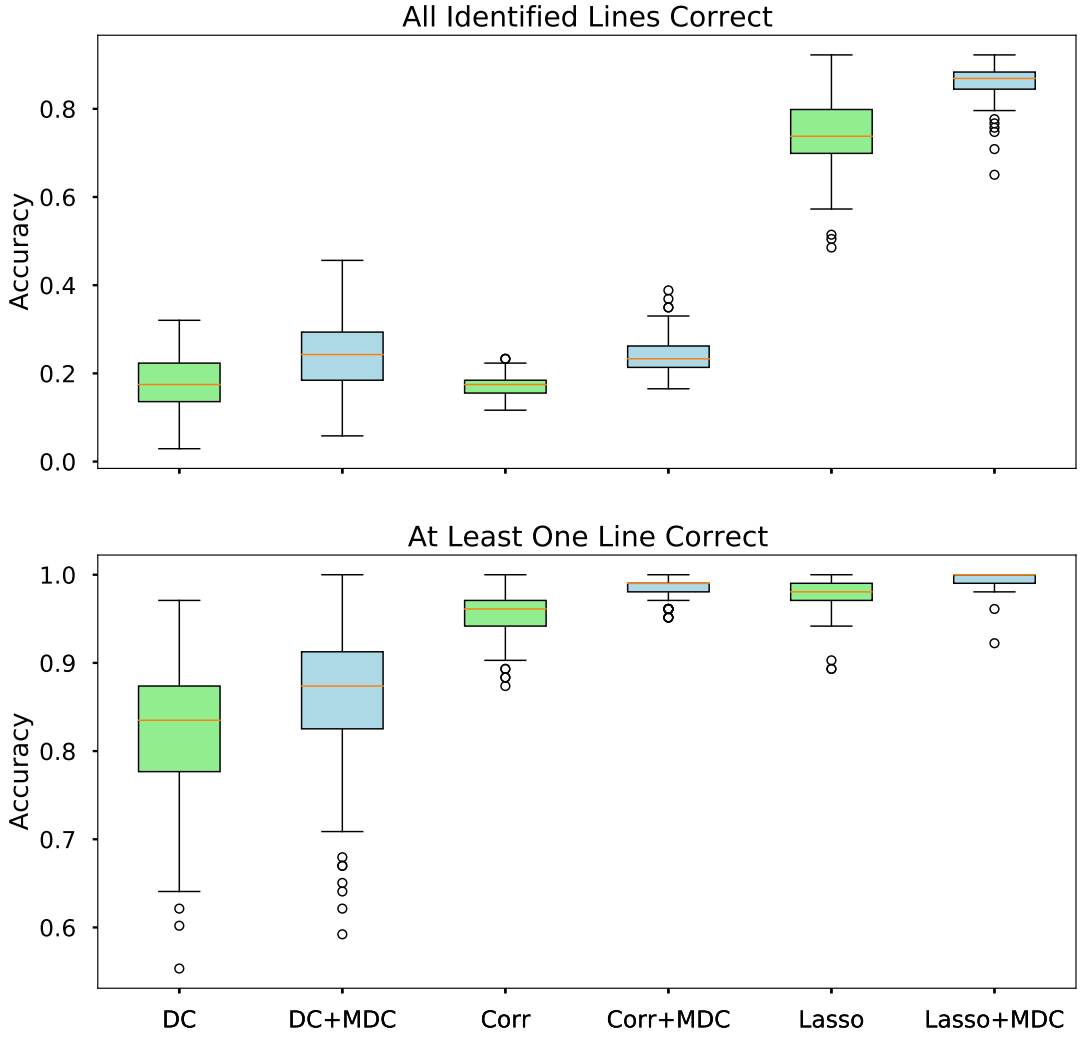

Figure C.4: *Box-plots of double-line outage identification results for DC-based, correlation-based, and the proposed method. "All correct" (top) and "half correct" (bottom) results are based on 200 random simulation runs under a 75% PMU coverage in the New England 39-bus system. Each method has two sets of results: accuracy of the original identification and of that augmented with MDCs.*

C.2.2 Effect of Minimal Diagnosable Cluster

The impact of the MDC correlation threshold on the outage identification accuracy and the proportion of single-element MDCs is reported in Table C.1 for 25% PMU coverage and in Table C.2 for 75% PMU coverage.

Table C.1: Impact of Minimal Diagnosable Cluster Threshold on Identification Precision-Accuracy Trade-off Using Lasso+MDC Under 25% PMU Coverage

Threshold (ρ^*)	Single-element MDC (%)	Single-line	Double-line
0.80	0.12 (0.04)	0.88 (0.09)	0.54 (0.09)
0.84	0.17 (0.05)	0.89 (0.08)	0.50 (0.09)
0.88	0.23 (0.05)	0.87 (0.08)	0.46 (0.09)
0.93	0.31 (0.06)	0.85 (0.08)	0.41 (0.09)
0.95	0.35 (0.06)	0.86 (0.09)	0.41 (0.11)
0.98	0.39 (0.06)	0.84 (0.09)	0.38 (0.11)
0.99	0.49 (0.07)	0.78 (0.09)	0.29 (0.10)

Table C.2: Impact of Minimal Diagnosable Cluster Threshold on Identification Precision-Accuracy Trade-off Using Lasso+MDC Under 75% PMU Coverage

Threshold (ρ^*)	Single-element MDC (%)	Single-line	Double-line
0.80	0.57 (0.05)	0.98 (0.03)	0.79 (0.06)
0.84	0.62 (0.06)	0.99 (0.03)	0.79 (0.03)
0.88	0.71 (0.06)	0.98 (0.03)	0.79 (0.04)
0.93	0.77 (0.06)	0.98 (0.03)	0.79 (0.05)
0.95	0.78 (0.06)	0.97 (0.03)	0.79 (0.04)
0.98	0.84 (0.06)	0.96 (0.02)	0.78 (0.04)
0.99	0.86 (0.06)	0.95 (0.03)	0.76 (0.05)

C.2.3 Effect of Measurement Noise

The performance of the proposed method under different measurement noise levels is reported in Fig. C.5 for 25% PMU coverage and in Fig. C.6 for 75% PMU coverage.

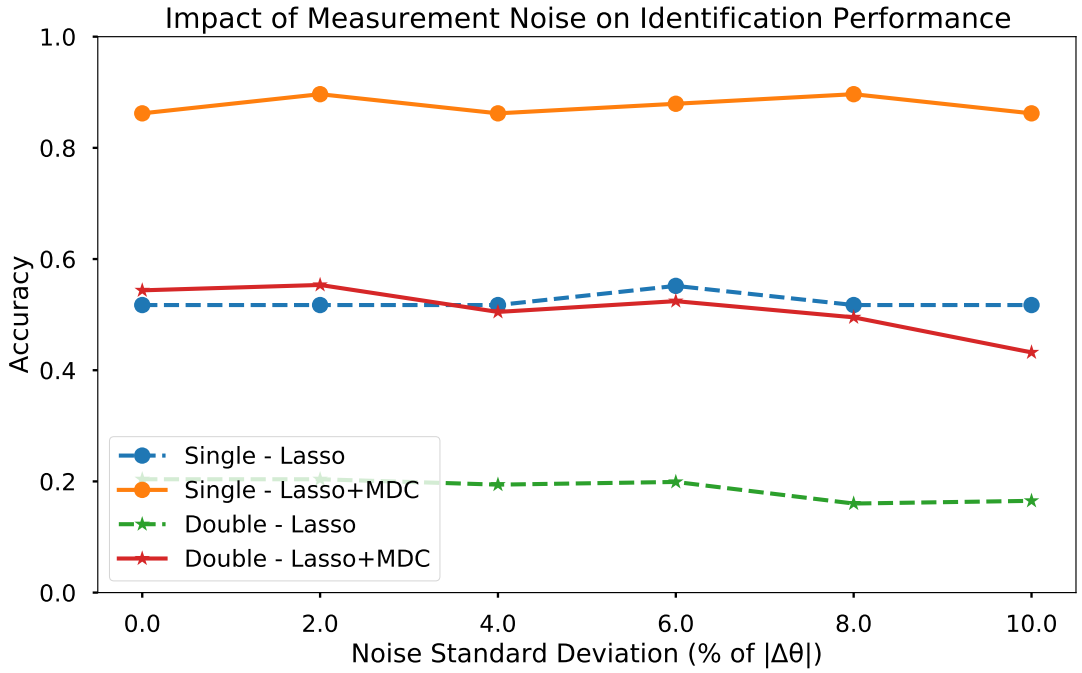

Figure C.5: *Impact of measurement noise on identification performance of the proposed method under a 25% PMU coverage. Performance using data with noise standard deviation varying from 0% to 10% of $|\Delta\boldsymbol{\theta}|$ is reported by median accuracy of single- and double-line outages using Lasso and Lasso+MDC.*

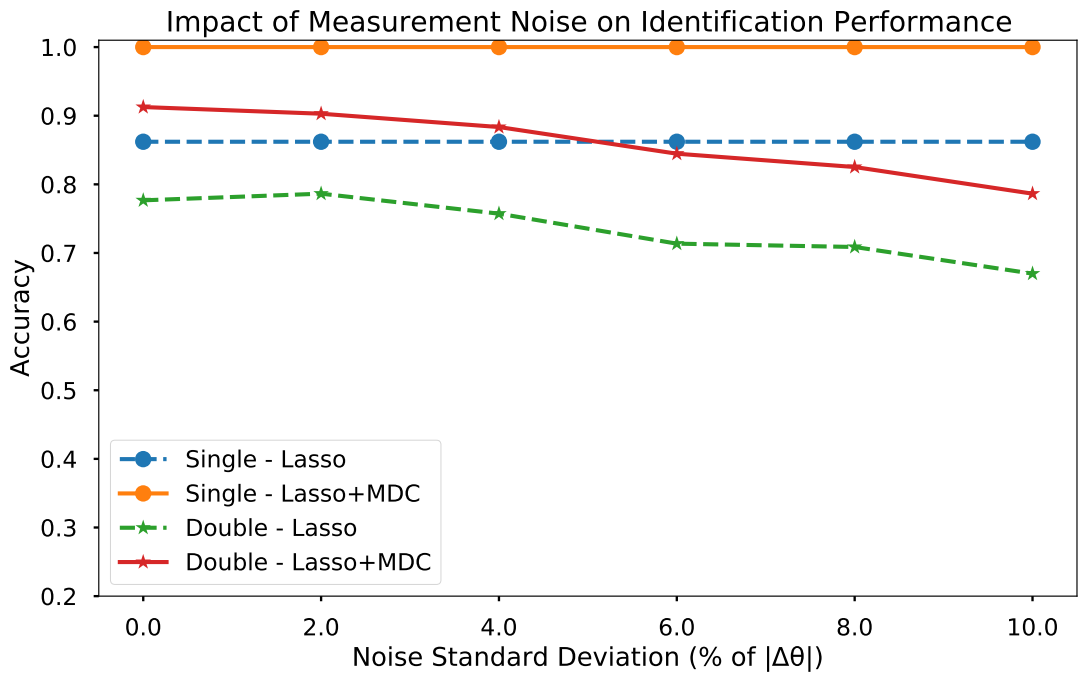

Figure C.6: *Impact of measurement noise on identification performance of the proposed method under a 75% PMU coverage. Performance using data with noise standard deviation varying from 0% to 10% of* $|\Delta\boldsymbol{\theta}|$ *is reported by median accuracy of single- and double-line outages using Lasso and Lasso+MDC.*